
Expedition 323 summary¹

Expedition 323 Scientists²

Chapter contents

Abstract	1
Introduction	2
Background	3
Scientific objectives	6
Summary of expedition results	7
References	15
Figures	19
Tables	51

Abstract

Paleoclimate and paleoceanographic studies present opportunities to study the dynamics of the climate system by examining how it responds to external forcing (e.g., greenhouse gas and solar radiation changes) and how its interacting components generate climate oscillations and abrupt changes. Of note is the amplified recent warming of the high latitudes in the Northern Hemisphere, which is presumably related to sea ice albedo feedback and teleconnections to other regions; both the behavior of sea ice–climate interactions and the role of large-scale atmospheric and oceanic circulation in climate change can be studied with geologic records of past climate change in the Bering Sea.

Over the last 5 m.y., global climate has evolved from being warm with only small Northern Hemisphere glaciers to being cold with major Northern Hemisphere glaciations every 100–40 k.y. The ultimate reasons for this major transition are unknown. In addition, climate cycles on orbital and millennial timescales characterize the variability found in most continuous paleoceanographic records. Although regional environmental cycles and trends reflected in the sediment have been documented in some regions, the mechanisms by which they propagate globally are not understood. Possible mechanisms responsible for both the long-term evolution of global climate as well as the generation of high-frequency climate oscillations involve processes such as intermediate water ventilation and sea ice formation in the North Pacific. However, the paucity of data in critical regions of the Pacific such as the Bering Sea has prevented an evaluation of the role of North Pacific Intermediate Water (NPIW) has the potential to be influenced by dense water forming in the Bering Sea and because changes in sea ice distribution have potential far-field impacts, the Bering Sea may be critically involved in major climate changes. Thus, drilling in the Bering Sea may help answer questions not only about the global extent of climate trends and oscillations but also about the mechanisms that produce them.

In addition to having important sedimentary records of past climate change, the Bering Sea is a region of relatively high surface productivity, elevated intermediate-water and deepwater nutrient concentrations, and microbially mediated biogeochemical cycling. Thus, Integrated Ocean Drilling Program (IODP) Expedition 323 was also dedicated to examining for the first time seafloor

¹Expedition 323 Scientists, 2011. Expedition 323 summary. In Takahashi, K., Ravelo, A.C., Alvarez Zarikian, C.A., and the Expedition 323 Scientists, *Proc. IODP, 323*: Tokyo (Integrated Ocean Drilling Program Management International, Inc.). doi:10.2204/iodp.proc.323.101.2011

²[Expedition 323 Scientists' addresses.](#)



biomass and microbial processes in high-productivity regions.

The major objectives of Expedition 323 in the Bering Sea are

1. To elucidate a detailed evolutionary history of climate and surface-ocean conditions since the earliest Pliocene in the Bering Sea, where amplified high-resolution changes in climatic signals are recorded;
2. To shed light on temporal changes in the origin and intensity of NPIW and possibly deeper water mass formation in the Bering Sea;
3. To characterize the history of continental glaciation, river discharges, and sea ice formation in order to investigate the link between the continental and oceanic conditions of the Bering Sea and adjacent land areas;
4. To investigate, through comparison to pelagic records, linkages between ocean/climate processes that occur in the more sensitive marginal sea environment of the Bering Sea and those that occur in the North Pacific and/or globally. This objective includes an evaluation of how the ocean/climate history of the Bering Strait gateway region may have affected North Pacific and global conditions; and
5. To constrain global models of seafloor biomass and microbial respiration by quantifying seafloor cell abundance and pore water chemistry in an extremely high productivity region of the ocean. We also aim to determine how seafloor community composition is influenced by high productivity in the overlying water column.

During Expedition 323 in the Bering Sea, 5741 m of sediment (97.4% recovery) was drilled at seven sites covering three different areas: Umnak Plateau, proximal to where the modern Alaskan Stream enters the Bering Sea; Bowers Ridge, in the open waters of the Bering Sea and also proximal to the glacial Alaskan Stream entry; and the Bering Sea shelf region, proximal to the modern sea ice extent. Four deep holes that range in depth from 600 to 745 m below seafloor (mbsf) and generally span 1.9–5 Ma in age were drilled. Some basement of older age was recovered at one site (U1342). The water depths of the drill sites range from 818 to 3174 m in order to characterize past vertical water mass distribution and circulation. The highlights of our findings include the following:

1. An understanding of the long-term evolution of surface water mass distribution during the past 5 m.y., including the southward expansion of seasonal sea ice to Bowers Ridge between 3.0 and 2.5 Ma and the intensification of seasonal sea ice at both Bowers Ridge and the Bering slope at ~1.0 Ma (the mid-Pleistocene Transition);

2. The characterization of intermediate-water and deepwater masses, including evidence from benthic foraminifers and sediment laminations, for episodes of low-oxygen conditions in the Bering Sea in the last 5 m.y.;
3. The terrigenous and biogenic sedimentary history of the Bering Sea, including evidence for strong climatological and sea level control of siliciclastic deposition at all sites. Records of lithostratigraphic variations indicate that Bering Sea environmental conditions were strongly linked to global climate change; this is apparent both in long-term, million year trends and in orbital, millennial, and shorter oscillations within the lithostratigraphic records generated at sea; and
4. A large range of inferred microbial activity with notable site-to-site variations, including significant activity as deep as 700 mbsf at the Bering slope sites, and, in contrast, low rates of microbially mediated sulfate reduction at Bowers Ridge.

Introduction

The rate and regional expression of recent global warming is difficult to understand and even more difficult to predict because of the complex nature of the climate system, whose components interact nonlinearly with various time lags. Paleoclimate and paleoceanographic studies present opportunities to study climate system dynamics by examining how they respond to external forcing (e.g., greenhouse gas and solar radiation changes) and how they generate internal variability due to interacting Earth-system processes. Of note is the amplified recent warming of the high latitudes in the Northern Hemisphere (Solomon et al., 2007), which is presumably related to sea ice albedo feedback and teleconnections to other regions; both the behavior of sea ice–climate interactions and the role of large-scale atmospheric and oceanic circulation in climate change can be studied with geologic records of past climate changes in the Bering Sea.

Prior to Integrated Ocean Drilling Program (IODP) Expedition 323, little was known about the sedimentology and climate history of the Bering Sea outside of a few piston core studies (e.g., Cook et al., 2005; Okazaki et al., 2005; Tanaka and Takahashi, 2005; Takahashi et al., 2005) and Deep Sea Drilling Project (DSDP) Sites 188 and 185 (Scholl and Creager, 1973), which were drilled in 1971 with old drilling technology and poor recovery. Past studies using piston cores in the Bering Sea indicate that although current conditions in the Bering Sea promote seasonal sea ice formation, during the Last Glacial Maximum (LGM), conditions sustained perennial or nearly pe-

rennial sea ice cover (Katsuki and Takahashi, 2005), attesting to the potential usefulness of sedimentary records in the Bering Sea in examining sea ice distribution. In paleoceanographic studies in the North Pacific, the Bering and Okhotsk seas have been implicated as sources of dense, oxygenated intermediate water that possibly impacted oceanic and climate conditions throughout the Pacific on glacial–interglacial (e.g., Gorbarenko, 1996; Matsumoto et al., 2002) and millennial (e.g., Hendy and Kennett, 2003) timescales. In addition, changes in Bering Sea conditions could be related to sea level and circulation changes, which alter flow through small straits that connect the Bering Sea to the Arctic Ocean to the north and to the Pacific Ocean to the south. The lack of Bering Sea material has so far prevented the evaluation of these and other ideas.

Seven sites whose terrigenous and biogenic components capture the spatial and temporal evolution of the Bering Sea through the Pliocene and Pleistocene were successfully drilled during Expedition 323 (Fig. F1; Tables T1, T2). Additionally, a rich archive of information was collected regarding the role of microbes on biogeochemical cycles in ultra-high-productivity environments; the postdepositional processes that impact the geochemical, lithologic, and physical properties of sediment; and the chemistry of pore waters. This expedition summary presents background on the environmental setting and important scientific questions in the Bering Sea, followed by highlights of the scientific findings of Expedition 323.

Background

Geological and physical setting

With an area of 2.29×10^6 km² and a volume of 3.75×10^6 km³, the Bering Sea is the third largest marginal sea in the world, surpassed only by the Mediterranean and South China seas (Hood, 1983). Approximately one-half of the Bering Sea is a shallow (0–200 m) neritic environment, with the majority of the continental shelf spanning the eastern side of the basin off Alaska from Bristol Bay to the Bering Strait (Fig. F1). The northern continental shelf is seasonally ice covered, but little ice forms over the deep southwest areas. In addition to the shelf regions, two significant topographic highs have better CaCO₃ preservation than the deep basins: Shirshov Ridge, which extends south of the Koryak Range in eastern Siberia along 170°E and separates the southwestern part of the Bering Sea into Komandorski Basin (to the west) and Aleutian Basin (to the east); and Bowers Ridge, which extends 300 km north from the

Aleutian Island arc (Fig. F1). The Aleutian Basin is a vast plain 3800–3900 m deep, with occasional gradually sloping depressions as deep as 4151 m (Hood, 1983).

Three major rivers flow into the Bering Sea: the Kuskokwim and Yukon rivers drain central Alaska, and the Anadyr River drains eastern Siberia (Fig. F1). The Yukon is the longest of the three rivers and supplies the largest discharge into the Bering Sea. Its discharge peaks in August because of meltwater and is about equal to that of the Mississippi. It has a mean annual flow of 5×10^3 m³/s, which is about two-thirds the annual flow of the Columbia River (Hood, 1983).

Today, a substantial amount of water is transported in and out of the Bering Sea across the Aleutian Island arc and the Bering Strait through passes (Stabeno et al., 1999) (Figs. F1, F2, F3). Water mass exchange with the Pacific through the Aleutian Islands, such as through the Kamchatka Strait, is significant, linking Bering Sea conditions to Pacific climate. The Alaskan Stream, an extension of the Alaskan Current, flows westward along the Aleutian Islands and enters the Bering Sea mainly through the Amchitka Strait and to some extent through the Near Strait, west of Attu Island in the eastern Aleutian Islands (Fig. F1). A part of the Subarctic Current also joins the Alaskan Stream, resulting in a combined volume transport of 11 Sv (Ohtani, 1965).

Bottom and intermediate water in the Bering Sea originates in the North Pacific. After flowing into the Bering Sea, it is slightly modified by the mixing of relatively fresh, warm water with very small amounts of bottom water formed within the Bering Sea today (Warner and Roden, 1995). Nutrient concentrations of North Pacific origin are high compared to all other regions in the global oceans; this explains the very low oxygen concentrations in the Bering Sea today (Fig. F4). The oxygen and nutrient composition of these waters is further modified by the denitrification (Lehmann et al., 2005) and respiration of organic matter in the water column (Nedashkovskiy and Sapozhnikov, 1999). Respiration and the development of an oxygen minimum zone (OMZ) is particularly intense at water depths of ~1000 m (Fig. F4).

Much of the Pacific water that enters the Bering Sea is matched by outflow through the Aleutian Islands. The most significant outflow is through the Kamchatka Strait, which has a maximum depth of 4420 m (Stabeno et al., 1999) (Figs. F1, F3). If some component of North Pacific Intermediate Water (NPIW) or deep water formed in the Bering Sea in past times, particularly when sea level was lower, it would have

flowed out through the Kamchatka Strait or a secondary outlet near the Commander–Near Strait at 2000 m (Fig. F1).

The unidirectional northward transport of water mass (0.8 Sv) from the Bering Sea through the Bering Strait to the Arctic Ocean contributes to the salinity and biogeochemical contrast between the Pacific and the Atlantic. The Bering Strait region is one of the most biologically productive regions in the world (324 g C/m²/y over a wide area [2.12×10^4 km²]) (Sambrotto et al., 1984). Much of this biologically produced organic matter and its associated nutrients flows into the Arctic Ocean because of the northward current direction. This may profoundly influence the present dominance of carbonate production in the Atlantic versus opal production in the Pacific, as described by models of basin-to-basin fractionation (Berger, 1970) and “carbonate ocean versus silica ocean” (Honjo, 1990). Flow through the Bering Strait, which is ~50 m deep today (fig. 5 in Takahashi, 2005), was certainly different at times of lower sea level or enhanced perennial sea ice cover. The closing of this gateway and the accompanying changes in ocean and river flow through time could have caused changes in global patterns of circulation or in nutrient and salinity distributions.

Relationship to previous drilling in the Bering Sea, the subarctic North Pacific, and the Arctic Ocean

During DSDP Leg 19 in 1971, six sites were drilled in the Bering Sea and four were drilled just south of the Aleutian Islands in order to generally characterize the sedimentary units and tectonic and structural evolution of the Bering Sea (Scholl and Creager, 1973). Although much of the sedimentary section was washed away and not cored, Leg 19 provided basic information on the types and ages of sediments in two of the regions (Umnak Plateau and Bowers Ridge) targeted by Expedition 323. Expedition 323 marks the first deployment of advanced piston corer (APC) technology in the region and thus the first collection of continuous high-resolution records for the past 5 m.y. in the Bering Sea. Specifically, the drilling of DSDP Sites 184 and 185 on Umnak Plateau revealed a Pleistocene to upper Miocene clay-rich diatomaceous ooze (Unit A) above clayey siltstone with sparse fossils (Unit B). At Site 188 on Bowers Ridge, sedimentary units similar in lithology and age to those found at the Umnak Plateau sites were found. Although DSDP Sites 190 and 191 were drilled close to Shirshov Ridge and the Kamchatka Strait, they were located in the deep basins around Shirshov Ridge (water depth >3800 m), and the sedi-

ments recovered were mainly turbidite sequences with reworked microfossils, making paleoceanographic interpretations difficult. Expedition 323 did not include drilling in the deep basins; rather, it targeted topographic highs above the basin floors, where the deposition of reworked sediments was expected to be minimal.

In 1992, several important sites adjacent to the Bering Sea were explored during Ocean Drilling Program (ODP) Leg 145: Sites 881, 882, 883, and 884 (Rea et al., 1995; Rea, Basov, Janecek, Palmer-Julson, et al., 1993; Rea, Basov, Scholl, and Allen, 1995). Maslin et al. (1996) observed a dramatic increase in ice-rafted debris (IRD), a decrease of >7.5°C in sea-surface temperature, a five-fold decrease in opal mass accumulation rates (MARs), and a decrease in both total organic carbon (TOC) and calcium carbonate MARs at Site 882 (50°22′N, 167°36′E; 3244 m) at 2.75 Ma, coeval with the IRD change found in the Norwegian Sea, which suggests that the Arctic and northeast Asia were significantly glaciated from 2.75 Ma onward. Furthermore, they suggested that the onset of Eurasian Arctic and northeast Asia glaciation occurred ~100 k.y. before the Alaskan glaciation and 200 k.y. before the glaciation of Greenland and the northeast American continent. McKelvey et al. (1995) and Kriesek (1995) suggested that the provenance of IRD in the northwest Pacific Ocean and the Gulf of Alaska is the Bering Sea off the Kamchatka Peninsula and southeastern Alaska, respectively. By studying the Bering Sea in relation to other regions, we can uncover details of the inception of glaciation in the Arctic and North Pacific regions at ~2.75 Ma. Furthermore, the reasons for differences in the timing of glaciation can be investigated in detail using sections from the Bering Sea, which can provide a much higher resolution record than those available in the open-ocean pelagic realm.

IODP Expedition 302 (Arctic Coring Expedition [ACEX]) to Lomonosov Ridge in the central Arctic Ocean took place in 2004, and the scientific community anticipated the acquisition of new information regarding the age and effects of the Bering Strait gateway to the Bering–Arctic. However, despite the expedition’s success in acquiring sediments spanning the Holocene to the Cretaceous (Backman, Moran, McInroy, Mayer, and the Expedition 302 Scientists, 2006; Moran et al., 2006), it has been difficult to advance our understanding of the significance of changes in flow through the Bering Strait gateway on global or regional climate change without being able to compare Arctic records to those from the Pacific side of the Bering Strait. Thus, the cores recovered during Expedition 323 are essential to deciphering the history of the Bering Strait gateway and its

potential impact on global and regional climatic and oceanic processes. The role of the exchange of heat and chemical constituents through the Bering Strait on Arctic and North Pacific environments, as well as the influence of changes in this exchange on Northern Hemisphere glaciation (NHG) and higher frequency climate oscillations, can only be assessed by comparing the results of Bering Sea drilling with those of Expedition 302.

Millennial-scale climate changes

The Bering Sea contains sediments with high accumulation rates appropriate for the reconstruction of surface water and deepwater conditions and for the validation of climate/ocean hypotheses that call on these regions as a variable source of open Pacific intermediate and deep water. In addition, climate change in the Bering Basin tends to be extremely sensitive to high-frequency changes due to the semi-isolated nature of the marginal sea. Sea level drop, for example, may produce a profound effect on watermass circulation, sea ice formation, salinity, and biological productivity in the basin (e.g., Takahashi, 1999). The pelagic signals of the open Pacific do not adequately provide a high-frequency climatic history of the northwest Pacific Rim.

Changes in the ventilation of subsurface water in the North Pacific may also influence climate downstream and may be tied to North Atlantic climate changes on millennial timescales. Interestingly, millennial cycles in climate proxy records are apparently correlative across the North Pacific, for example in the Bering Sea (Cook et al., 2005), the Sea of Okhotsk (Ono et al., 2005; Sakamoto et al., 2005), the California margin (e.g., Behl and Kennett, 1996), and the Sea of Japan (e.g., Tada et al., 1999). Although the mechanisms for the strong teleconnections between different sides of the North Pacific are not known, it has been proposed that changes in the source(s) of NPIW in the Okhotsk (Ono et al., 2005) or Bering seas could reach the California margin and influence the depth or strength of the OMZ (Cannariato and Kennett, 1999; Zheng et al., 2000), thereby connecting climate/ocean changes across the Pacific Ocean. The fact that millennial-scale records from the Pacific margins also appear to correlate to changes in North Atlantic climate (e.g., Behl and Kennett, 1996; Tada et al., 1999) indicates that the processes linking Atlantic and Pacific climate could play an important role in global climate change.

A number of theories explain paleoceanographic data from North Pacific marginal seas by implicating changes in NPIW formation caused by changes in flow through the Bering Strait (Hasumi, 2002; De Boer and Nof, 2004; Shaffer and Bendtsen, 1994) and

teleconnections from the tropics (Niebauer and Day, 1989; Alexander et al., 2002; Niebauer, 1998; Zhao et al., 2004; Gloersen, 1995). Our capacity to test these theories will benefit from the documentation of surface water and deepwater conditions in the Bering Sea. Drilling has allowed us to obtain long sequences of sediments for reconstructing climate cycles and evaluating whether the patterns observed in the last glacial cycle are characteristic of all glacial–interglacial cycles. Long records will also be used to compare millennial climate oscillations in the Bering Sea in the Pleistocene, when there were large Northern Hemisphere ice sheets, to those in the Pliocene warm period, when there were only small Northern Hemisphere ice sheets, thereby shedding light onto whether the generation of these oscillations is related to NPIW ventilation, ice sheet size and dynamics, ocean circulation, and/or rapid reorganization of atmospheric circulation.

Glacial–interglacial climate change

In the last glacial cycle, enhanced dense water formed, probably from the Okhotsk and Bering seas (e.g., Zahn et al., 1991; Gorbarenko, 1996). In fact, the degree of ventilation of deep and intermediate Pacific waters appears to have fluctuated during the cold and warm periods, implying changes in the configuration of Pacific Ocean circulation (Keigwin, 1995; Matsumoto et al., 2002). However, the use of different nutrient proxies ($\delta^{13}\text{C}$ versus Cd/Ca in benthic foraminifers) provides some contradictory results. Furthermore, the limited spatial coverage of sites in the open Pacific prevents the detailed identification of the exact source of intermediate and deep water, as well as the exact circulation path of subsurface watermasses. Observations of glacial records from the Bering Sea and just outside the Bering Sea on the Detroit Seamount in the North Pacific suggest a source of ventilated intermediate water coming from the Bering Sea and/or the Detroit Seamount region (Gorbarenko, 1996).

Two examples of the prospective reconstructions of Bering Sea paleoceanography by Bering Sea drilling were reported in recent studies performed on the piston cores collected during the 1999 R/V *Hakuho-Maru* site survey cruise (Takahashi et al., 2005). Sea ice distribution during the glacial period was modulated by surface water circulation, which was partially governed by the topography that resulted from the drop in sea level. The distribution of sea ice and watermasses was significantly different in the two basins west and east of Bowers Ridge because of the pattern of surface-ocean circulation (Katsuki and Takahashi, 2005). Past sources of NPIW formation were inferred from the intermediate water–dwelling

radiolarian species *Cycladophora davisiana* (Tanaka and Takahashi, 2005). The degree of ventilation of intermediate and deep water will be fully scrutinized with more detailed information from Expedition 323.

Despite evidence that Pacific circulation was different in the last glacial cycle, little is known about what caused circulation to change or what role the Pacific played in determining extreme climate conditions. Extensive studies of the North Atlantic clearly show that ice-sheet dynamics and changes in meridional overturning circulation in the Atlantic can readily influence climate, yet no widely accepted paradigm explains how the North Pacific participates in and possibly impacts global climate change. The construction of long records of glacial–interglacial changes by drilling, especially under a range of boundary conditions over the Pliocene–Pleistocene, will contribute critical information needed to formulate a new North Pacific climate change paradigm.

Pliocene–Pleistocene trends

Compelling evidence shows that North Pacific mid-depth water (~2500 m) had much lower nutrient concentrations in the warm Pliocene (~4.5–3.0 Ma) than today, indicating that it was more strongly ventilated (Kwiek and Ravelo, 1999; Ravelo and Andreasen, 2000). Although increased subsurface ventilation in the cold Last Glacial Maximum (LGM) and the warm Pliocene could be interpreted in a number of different ways and is likely not explained by the same processes, only data that directly reflect conditions in the Bering Sea (and the Sea of Okhotsk) can help constrain interpretations.

The end of the early Pliocene warm period is characterized by the development of modern density stratification in surface and deep North Pacific water. IRD recovered at DSDP and ODP sites indicates that increased watermass stratification coincides with more extensive glaciation (Haug et al., 1999; Kwiek and Ravelo, 1999; Ravelo and Andreasen, 2000; Rea and Schrader, 1985). Furthermore, more IRD is found along the Aleutian Islands (DSDP Site 192) than farther north in the Bering Sea (DSDP Sites 186 and 191) because there is more extensive ice cover in the north compared to the more seasonal ice cover at the Aleutian site (McKelvey et al., 1995; Kriisek, 1995). The fact that this North Pacific climate reorganization occurred synchronously with the onset of significant NHG, as recorded in the Atlantic Ocean, highlights the importance of studying North Pacific climate evolution as part of a comprehensive investigation of the regional expression of global climate trends.

The emergence of the Bering Land Bridge (Beringia) prior to the Neogene is not well understood. However, Pliocene climate change—and perhaps the onset of NHG, specifically—could have been affected by changes in the marine gateway connection through the Bering Strait region. The connection may have developed in the late Miocene or the early Pliocene based on the occurrences of Atlantic-type mollusks in Hokkaido, Kamchatka, and the Alaska Peninsula in the late Miocene and early Pliocene. The oldest ages for these occurrences range from 6.3–5.1 to 2.2 Ma (e.g., Uozumi et al., 1986), but a recent study documented the age of first occurrence as 5.5–5.4 Ma (Gladenkov, 2006). One of the aims of drilling was to recover better records of oceanographic evolution related to the Miocene/Pliocene gateway history. The oldest sediments recovered are ~5 Ma, and long-term trends in Pliocene circulation will be documented to assess the possible influence of the tectonic opening of the Bering Sea, if it happened as late as the Pliocene.

Flow through the Bering Strait is likely controlled mainly by sea level change and changes in the amount of perennial sea ice. Pacific to Arctic flow through the Bering Strait (~0.8 Sv) (Coachman and Aagaard, 1981) significantly influences the Pacific–Atlantic partitioning of physical and nutrient properties in the modern ocean and was possibly quite sensitive to past changes in sea level change because of its shallow sill of ~50 m (see Takahashi, 2005, for an illustration of the cross section). During glacial intervals, Atlantic Ocean biogenic sedimentation and preservation became more Pacific-like and vice versa, and there were major changes in nutrient distributions. Drilling near the Bering Strait will help resolve whether major changes in Pacific–Atlantic partitioning of oceanographic properties were related to changes in flow through the Bering Sea. *Neodenticula seminae*, a dominant extant subarctic Pacific diatom, was found recently in Atlantic waters, possibly because recent warming and melting sea ice in the Arctic Ocean provided a passage from the Pacific to the Atlantic (Berard-Therriault et al., 2002; Corbyn, 2007; Reid et al., 2007). This species has been extinct in the Atlantic since 0.8 Ma (Baldauf, 1987), and thus its recent reemergence in the Atlantic appears to be a significant indication that climate change in the Arctic influenced the distribution of this species.

Scientific objectives

The objectives of Expedition 323 are as follows:

1. To elucidate a detailed evolutionary history of climate and surface-ocean conditions since the

earliest Pliocene in the Bering Sea, where amplified high-resolution changes of climatic signals are recorded;

2. To shed light on temporal changes in the origin and intensity of NPIW and possibly deeper water-mass formation in the Bering Sea;
3. To characterize the history of continental glaciation, river discharges, and sea ice formation in order to investigate the link between continental and oceanic conditions of the Bering Sea and adjacent land areas;
4. To investigate linkages, through comparison to pelagic records, between the ocean/climate processes that occur in the more sensitive marginal sea environment of the Bering Sea and those that occur in the North Pacific and/or globally. This objective includes evaluating how the ocean/climate history of the Bering Strait gateway region may have affected North Pacific and global conditions; and
5. To constrain global models of seafloor biomass and microbial respiration by quantifying seafloor cell abundance and pore water chemistry in an extremely high productivity region of the ocean. We also aim to determine how seafloor community composition is influenced by high productivity in the overlying water column.

Summary of expedition results

Overview of ages and sedimentation rates

Expedition 323 focused on analyzing long-term ocean and climate trends and the evolution of higher frequency glacial–interglacial to millennial-scale oscillations through the Pliocene and Pleistocene. As such, our primary drilling objective was to obtain sediments whose components could be used to elucidate a detailed evolutionary history of climate, surface-ocean, and intermediate-water conditions since the earliest Pliocene in the Bering Sea, where amplified high-resolution changes of climatic signals are recorded. In addition, we sought to explore seafloor microbial activity in the Bering Sea because of its extremely high surface productivity.

Our objectives, in terms of acquiring sediment core samples as well as conducting shipboard research, have been adequately met because our targeted drill sites had extremely high sedimentation rates (Fig. F5) and contained abundant microfossils and other paleoceanographic proxies.

Among the three drill sites explored in the Bowers Ridge region (Fig. F6), both of the deepest holes drilled, Holes U1340A (605 meters below seafloor [mbsf]) and U1341B (600 mbsf), represent time spans

between the Holocene and ~5 Ma in the Pliocene (Fig. F5). The expedition's initial goal of penetrating to ~5 Ma was adequately accomplished at both sites, despite the failure of the extended core barrel (XCB) cutting shoe spacing sub in Hole U1340A, which had a target depth of penetration of 700 m. At the gateway region sites (at the Bering slope), two deep holes were drilled: Holes U1343E (744 mbsf) and U1344A (745 mbsf) (Fig. F7). Hole U1343E reached ~2.1 Ma, whereas Hole U1344A reached ~1.9 Ma (Fig. F5). At other drill sites, the bottom ages of the sedimentary sequences based on biomagnetostratigraphy are as follows: Site U1339 (Umnak Plateau; 0.74 Ma) (Fig. F8), Site U1342 (Bowers Ridge; 1.2 Ma [with the exception of middle Miocene sediments found just above basement]) (Fig. F6), and Site U1345 (gateway; 0.5 Ma) (Fig. F7).

The sediments recovered from Bowers Ridge display high sedimentation rates (average = ~14.5 cm/k.y. at Sites U1340 and U1341) (Figs. F9, F10; Tables T3, T4) without apparent hiatuses and are generally appropriate for high-resolution Pliocene–Pleistocene paleoceanography, with adequate calcareous benthic foraminiferal preservation in the Pleistocene but much lower preservation in the Pliocene. The sediments at these sites are generally barren of planktonic foraminifers and calcareous nannofossils, except for some intervals younger than ~2.5 and ~3 Ma. The abundance of all siliceous microfossils is generally high, enabling good biostratigraphy and paleoceanographic reconstruction. Furthermore, the upper part of Site U1340 (~20–150 m core composite depth below seafloor [CCSF-A]) had obvious soft-sediment deformation due to mass movement possibly caused by local seismic activity. Although such deformation hinders the continuous reconstruction of late Pleistocene high-resolution paleoceanography at this site, information from other drill sites can fill the gap. At Bowers Ridge Site U1342 (Fig. F6), sedimentation rates are relatively low, averaging ~4.5 cm/k.y. (Fig. F11; Table T5).

At Site U1339, to the south on the Bering slope, sedimentation rates are comparably high relative to other Bering slope sites, averaging ~29 cm/k.y. (Fig. F12; Table T6). In the region of the Arctic gateway sites proximal to the Bering slope, the observed sedimentation rates are overwhelmingly high: Hole U1343E has a sedimentation rate of 21–58 cm/k.y. (Fig. F13; Table T7) and Hole U1344A has a rate of 29–50 cm/k.y. (Fig. F14; Table T8). Sedimentation rates are so high, in fact, that drilling reached ages of only 2.1 and 1.9 Ma, respectively, despite penetration to 745 mbsf at each site (Fig. F5). At Site U1345, to the north on the Bering slope, sedimentation rates are also relatively high, averaging ~28 cm/k.y. (Fig.

F15; Table **T9**). Such high sedimentation rates stem from the deposition of silt and clays transported by the Yukon and other rivers as well as the terrigenous sediments once deposited on the shelf. In spite of the high percentage of terrigenous materials, pertinent biotic proxies, including benthic foraminifers and siliceous microfossils, are adequately preserved. Therefore, the overall coverage of excellent cores to ~5 Ma in the Bowers Ridge region and ~2 Ma in the gateway region allows for detailed, continuous high-resolution paleoceanographic studies relevant to global climate change.

Lithostratigraphic summary

The seven sites drilled during Expedition 323 provide a continuous high-resolution record of the evolution of marine sedimentation in the marginal Bering Sea (Fig. **F16**). Onboard lithologic and sedimentologic analyses of the core sediments were carried out with a combination of visual core description, smear slide analysis, and, for selected samples, X-ray diffractometry. Overall, the sediments recovered in the Bering Sea are a mixture of three components: biogenic (mainly diatom frustules with varying proportions of calcareous nannofossils, foraminifers, silicoflagellates, and radiolarians), siliciclastic (mainly silt and, secondarily, sand and isolated pebble- to cobble-sized IRD clasts), and volcanoclastic (mainly fine ash). Other accessory lithologies identified include authigenic carbonates (dolomite and aragonite) and sulfides. The most prominent sedimentary features observed are decimeter- to meter-scale bedded alternations of sediment color and texture reflecting alternations in lithology. The sediments are generally highly bioturbated. However, fine-scale lamination preserving alternations between millimeter-scale laminae of biogenic and terrigenous material are also present at several of the drilled sites (Fig. **F16**).

The distributions of the sedimentary components and sedimentary structures as well as their variability both within and between the Expedition 323 sites account for the changes in biogenic, glaciomarine, terrigenous, and volcanogenic sediment sources and the environmental conditions present during sediment deposition. The scales of these lithologic variations indicate that sedimentation in the Bering Sea has recorded long-term trends that include the critical period of reorganization of Earth's climate from the warm early Pliocene and the transition into the ice ages. Milankovitch-scale (bedding) to high-frequency, potentially annual (lamination) variability is also recorded. The physiographic setting of the different sites, their depths, and their locations relative

to sediment source areas (continents, ice sheets, volcanoes, and upwelling centers) account for the marked regional differences in sediment composition, especially between the Pleistocene sections of the Bowers Ridge and Bering slope sites.

The preliminary results from Expedition 323 suggest that the history of sedimentation in the Bering Sea is broadly characterized by three main sedimentary phases that occurred between ~5 and ~2.7 Ma, ~2.7 and ~1.74 Ma, and ~1.74 Ma to recent (Fig. **F16**).

Sediments of middle and early Pliocene age (between ~5 and ~2.7 Ma) were recovered only at Bowers Ridge Sites U1340 and U1341 (Figs. **F17**, **F18**). Sedimentation is relatively high during this period (Fig. **F5**) and is characterized by biogenic diatom ooze with minor amounts of diatom silt, sponge spicules, and vitric ash. Although the Pliocene sediments are commonly bioturbated, distinct intervals characterized by extensive lamination also occur. The oldest laminated intervals (<3.8 Ma) were observed at Site U1341. Stratigraphic intervals where laminations are concentrated are possibly indicative of the depth of the OMZ. Isolated IRD pebbles were observed in sediments older than 3.8 Ma only at Site U1340. Limited dropstone occurrence prior to 2.7 Ma was also reported at two sites drilled in the northern Pacific during Leg 145 (Sites 881 and 883) and in the Yakataga Formation in Alaska (Lagoe et al., 1993), which suggests the development of ice sheets prior to the onset of NHG (Krissek, 1995).

The middle sections of Sites U1340 and U1341 (between ~2.7 and 1.74 Ma) are characterized by beds of diatom ooze with minor amounts of calcareous nannofossils and foraminifer ooze, alternating with diatom silt beds. The latter are composed of subequal proportions of siliciclastic (silt-sized quartz, feldspar, and rock fragments and/or clay) and biogenic (mainly diatom and, secondarily, calcareous nannofossils, foraminifers, silicoflagellates, and sponge spicules) components and minor volcanoclastic components. Dropstone occurrence is common—indicating a peak in siliciclastic deposition that was also observed at Leg 145 sites—and coincides with the beginning of NHG. However, the dramatic drop in opal content recorded at Site 882 (Haug et al., 1999) is not present at the Bowers Ridge sites, where, conversely, the biogenic component and inferred paleo-productivity is high throughout the late Pliocene and Pleistocene.

All sites drilled during Expedition 323 preserve a record of sedimentation ranging from the late Pliocene through the Holocene (between 1.74 Ma and recent). Lithologies and sedimentation rates vary between the different sites, as indicated by a basin-wide com-

parison of the evolution of sedimentation in the Bering Sea during this period (Fig. F16). The lowest sedimentation rates (only 4.5 cm/k.y.) were observed at Site U1342, where laminated foraminifer-rich diatom ooze beds alternate with silty clay beds at scales ranging in the Milankovitch band (Fig. F19). The same temporal interval corresponds to a much thicker section at Sites U1340 and U1341 (Figs. F17, F18), where the bedding alternations are less distinct and the abundance of IRD is higher. Although lamination is common at Sites U1342 and U1340, laminae are very rare at the deeper Site U1341, suggesting a shallow depth of the OMZ during most of the Pleistocene. At the Bering Sea slope site, sedimentation rates are about three times higher than at the Bowers Ridge sites. At Sites U1339 (Fig. F20), U1343 (Fig. F21), U1344 (Fig. F22), and U1345 (Fig. F23), siliciclastic-rich beds (mostly diatom-rich silty clay) and mixed siliciclastic-biogenic beds (clay, silt, and diatom ooze with varying abundances of foraminifers, nannofossils, and sponge spicules) alternate rhythmically. The sections are pervasively bioturbated, and laminated intervals are rare. Overall, sedimentation on the Bering slope is characterized by a higher influence of both siliciclastic material delivered by ice sheets and terrigenous sedimentation derived from the continental shelf and slope, which are indented by some of the largest submarine canyons in the world. However, because of their proximity to the continents, it is not clear whether the sediments characterized by high siliciclastic content are recording periods of ice sheet expansion (stadials) or increased runoff (interstadials). Dropstones are common at all sites during this time period and increase significantly at ~1 Ma, as was also observed in coeval sediments from the North Pacific based on the results of Leg 145 (Krissek, 1995).

Cyclical siliciclastic deposition and its relationship to climate change

Expedition 323 is the first expedition to recover deep, continuous sections of sediment from the Bering Sea, providing an opportunity to study sediment distributions in time and space in this marginal sea. The plethora of climatic and sedimentary structure information in the cores will allow us to develop an understanding of the influence of climate changes on sedimentation. Clearly, siliciclastics are a dominant component of all Bering slope sites and are less dominant at the Bowers Ridge sites. Because the sediments at each site are primarily composed of mixtures of siliciclastics and diatom frustules, the physical magnetic properties and natural gamma ray (NGR) measurements made on the tracks and with the logging tools generally provide information

about the relative proportions of clays/silts versus diatoms (although ash is a significant component of the sediment at Site U1339). NGR records (Fig. F16) indicate clear cyclicity; amplitude and wavelength appear to change markedly with depth at the Bering slope sites but not at the Bowers Ridge sites. Specifically, in sediment younger than ~1 Ma at the Bering slope sites (U1339, U1343, U1344, and U1345), the NGR record appears to vary with lower amplitudes and across a wider range of frequencies >1/40 k.y. compared to NGR records in sediment older than 1 Ma (Fig. F16; see “Natural gamma radiation” in “Physical properties” in the “Site U1343” chapter and “Natural gamma radiation” in “Physical properties” in the “Site U1344” chapter). Because Sites U1339 and U1345 are short records younger than 1 Ma, long-term trends in the character of the variability can only be evaluated in the longer NGR records of Sites U1343 and U1344; however, the relatively high frequency variability of NGR data from the younger sediments is evident at all four slope sites.

This change in the character of variability is also apparent in the logging data from Sites U1343 and U1344 (Fig. F24). The downhole logging data provide our only opportunity to derive continuous records of lithologic variability in the deeper sections where only one hole was drilled and where continuous composites of data generated on the cores cannot be spliced together as they are in sections with multiple drill holes. Potassium concentrations (K%), as measured by the logging tool, are generally related to terrigenous clay concentrations, although variations in the mineralogy of the terrigenous fraction could have a secondary influence. In this sedimentary environment, it appears that NGR represents the amount of terrigenous material relative to biogenic material in the sediment. Although much more research is needed, shipboard data indicate that high siliciclastic relative to biogenic deposition probably occurred during colder periods or possibly during deglaciations.

Applying the shipboard age model to the K% record at Site U1343 and performing spectral analyses on the record (not shown) indicate that variability in K% dominantly occurs with 40 k.y. periodicity in periods older than ~1 Ma. In the portion of the record younger than 1 Ma, the variance is dispersed across many frequencies, and 40 k.y. periodicity does not dominate the spectrum. Benthic $\delta^{18}\text{O}$ records (Lisiecki and Raymo, 2005) indicate that the variability of ice volume, and therefore of eustatic sea level, occurs primarily with 40 k.y. periodicity prior to ~1 Ma (referred to as the “40 K world”). As such, it appears that sea level may control the timing of

pulses of sedimentation at the Bering slope sites. Sea level highstands in warm periods may have been times when sediment deposition on shelves occurred at the expense of deposition on the slope. As ice volume increased, sea level fell, the coastline moved seaward, and the flux of terrigenous material to the slope may have increased. This simple explanation may indicate how global climate change indirectly controlled the timing of sediment deposition at the slope sites during the 40 K world. After 1 Ma, the variability of the sediment composition changed, as reflected by logging K%. NGR core measurements do not appear to be simply related to sea level change, which occurred dominantly with ~100 k.y. variability; rather, variability in sedimentation appears to occur with much higher frequency. It is unclear why this happened, but the increase in sea ice diatom and sea ice dinoflagellate forms (discussed in the next section) at ~1 Ma may indicate that high-frequency variability in siliciclastic deposition related to sea ice processes is important—perhaps more important than global ice volume and concomitant sea level changes, which occur with lower frequency.

A close look at magnetic (Fig. F25) and density (not shown) data provides additional details about processes that may dictate terrigenous deposition. At first glance, the record of relative magnetic paleointensity of the sediment at Sites U1343 and U1344 agrees with the K% records and indicates a change in depositional style and cyclicity at ~1 Ma (Fig. F25), with lower frequency and higher amplitude changes prior to 1 Ma at the Bering slope sites. The ratio of natural remanent magnetization (NRM) to magnetic susceptibility is an index that attempts to normalize intensity by the concentration of magnetic grains. However, changes in grain-size distributions may also impact this ratio; low NRM/magnetic susceptibility values indicate that magnetic grains are coarser than those in sediment with higher NRM/magnetic susceptibility values. Grain-size differences can be related to a variety of climatically controlled factors as well as to diagenetic dissolution of the smallest clay-sized grains. The fact that NRM and magnetic susceptibility both show distinct variability on the same scale representing 40 k.y. cycles suggests that the primary factor controlling magnetic susceptibility and paleointensity records is related to the relative amount of terrigenous material. This also indicates that diagenetic overprints may alter but not obliterate the primary signal. The fact that the amplitude of changes in the paleointensity record (Fig. F25) downcore is even more extreme than that in the NGR and K% data suggests that, if anything, diagenetic overprints may amplify the contrast between

sediments with varying amounts of siliciclastics grains.

After 1 Ma, during the time period of large 100 k.y. ice volume cycles, gamma ray attenuation (GRA) bulk density records vary across a spectrum of frequencies. However, these records show long-period variance characteristic of the 100 k.y. ice age cycles more clearly than other physical parameter properties do. For example, after 1 Ma, paleointensity (Fig. F25) and NGR (Fig. F16) variability have power distributed across low (orbital) and suborbital frequencies. This indicates that terrigenous deposition at the Bering slope sites in the late Pleistocene was likely a combination of many processes, such as bottom water current deposition of fine-grained material (drift), IRD from sea ice and icebergs, and mass sediment transfer from the shelf to the lower slope and abyss. Superimposed on this are possibly independent or nonlinearly related changes in biogenic fluxes and postdepositional processes such as diagenesis and precipitation of authigenic minerals. The periodic and stochastic forces that drive each of these processes could be different, resulting in rich records of lithologic variability in the latest Pleistocene.

On Bowers Ridge at Sites U1340, U1341, and U1342, the trends and variability in siliciclastics appear to be notably different than those at the Bering slope sites, as indicated by NGR (Fig. F16), K% (Fig. F24), and NRM/magnetic susceptibility (Fig. F25) records. In contrast to the Bering slope sites, there are some marked long-term trends in the Bowers Ridge records. A notable change in Site U1341 logging K% data occurs at ~425 m depth (Fig. F24), along with an increase in observed silt content and dropstones in the sediment (Fig. F16). This depth in the section is equivalent in time to ~3 Ma and may signify that the Bering Sea regional expression of NHG includes an increase in clays and silts delivered via sea ice or icebergs to Bowers Ridge. The fact that K% decreases above this point in the section even while the ice ages persisted is difficult to explain. One possibility is that the warmer climate of the Pliocene facilitated the formation of K-rich clays on land, which were then shed into the Bering Sea once the ice ages began. K-rich clay formation could have then decreased when the climate cooled. NGR, magnetic susceptibility, and sedimentological smear slide and descriptive data indicate increasing amounts of terrigenous material upsection, with a pronounced increase at ~1 Ma, probably due to a greater supply of ice-rafted siliciclastics to Bowers Ridge once large 100 k.y. glaciations occurred.

As at the Bering slope sites, the variability of physical properties in sediments younger than 1 Ma at Bow-

ers Ridge appears to include higher frequency variability than the 100 k.y. ice volume cycles. Again, higher frequency climate variability, including changes in the distribution of sea ice and icebergs delivering sediment to Bowers Ridge, may dominate the mode of sediment deposition in the Bering Sea after 1 Ma. However, in contrast to the Bering slope sites, the variability of all studied lithologic parameters (NGR, magnetic susceptibility, and GRA bulk density) in sediment older than 1 Ma at Bowers Ridge is not dominantly paced by 40 k.y. ice volume cycles. One explanation is that, even in the 40 K world, sediment delivery to Bowers Ridge was paced at least in part by processes other than sea level change. Spectral analyses of K% data from Site U1341 at Bowers Ridge indicate that variability occurs across a spectrum of frequencies, with notable concentrations of variance at 40 k.y. and 23 k.y. periodicities. During the 40 K world, cycles and episodes of IRD deposition at Bowers Ridge were possibly impacted by regional climate changes responding to both obliquity (40 k.y.) and precession (23 k.y.) solar radiation changes. In contrast, at the Bering slope, sea level variations that occur dominantly with 40 k.y. periodicity were the main factor controlling sediment transport from the continent/shelf to the slope. The observation that high-latitude climate responded to precession forcing during the 40 K world has important implications, not only for theories that explain ice volume changes, but ultimately for our understanding of ice sheet dynamics and our ability to understand ice sheet response to radiative forcing.

History of sea ice development

The investigation of the evolutionary history of climate and surface-ocean conditions is primarily approached by studying microfossils, sedimentology, and the physical properties of sediments. This is particularly true for the influence of sea ice formation and the flow of the relatively warm oligotrophic Pacific surface waters into the Bering Sea.

One of the most striking findings of Expedition 323 is the general sea ice distribution history of the Bering Sea for the past 5 m.y. As described in “[Overview of ages and sedimentation rates](#),” the first sign of ice is the presence of a few pebbles, which are thought to have been transported as IRD starting at >3.8 Ma at Site U1340 (Fig. F16), indicating the formation of sea ice or iceberg transportation to the Bowers Ridge region. However, the bulk of the evolution of sea ice distribution has been interpreted from shipboard analyses of sea ice diatoms, sea ice-related dinoflagellate taxa, and, to a lesser extent, other dia-

tom taxa and intermediate water-dwelling radiolarians (see below for details).

The details of sea ice evolution are derived from changes in the relative abundance of sea ice diatom taxa, which are represented mainly by *Thalassiosira antarctica* spores (Abelmann, 1992a) and sea ice dinoflagellates (Fig. F26). The first signs of sea ice diatoms and dinoflagellates are subtle increases in their abundance at Bowers Ridge at Site U1340, starting at ~3.4 Ma for dinoflagellates and ~2.7 Ma for diatoms, coincident with NHG (Maslin et al., 1996). After ~2 Ma and into the present, sea ice assemblage signals become progressively stronger, reaching ~10%–20%. In contrast to the Bowers Ridge sites, sea ice cover at the Bering slope sites is markedly severe, indicated by sea ice assemblage percentages that are significantly higher than those observed at Bowers Ridge. Sea ice diatom values range from ~10% to 50% during the latest Pliocene and increase from ~30% to 70% during the Pleistocene. The abundance of sea ice dinoflagellates also increases but not to the same extent as sea ice diatoms. Notably, sea ice diatom and sea ice dinoflagellate assemblages clearly show a significant increase in both abundance and amplitude of variability around the mid-Pleistocene Transition (MPT) (Fig. F26). Analogous to sea ice-associated diatom and dinoflagellate taxa, a clear increasing trend in abundance of intermediate water-dwelling radiolarian taxa at the MPT was also observed at Sites U1343 and U1344. This is consistent with the interpretation that the surface water became gradually more affected by the formation of sea ice as climate progressively cooled; in the presence of sea ice, surface-dwelling radiolarians disappeared, and, as a consequence, the relative percentages of intermediate water dwellers such as *C. davisiana* were higher (Abelmann, 1992b; Okazaki et al., 2003).

At Sites U1343 and U1344, which are closer than the Bowers Ridge sites to the southern boundary of today's seasonal sea ice maximum extent, a dramatic change in the dominance of dinoflagellate cyst assemblages from autotrophic to heterotrophic taxa is evident at ~1.2–1.5 Ma. This suggests that sea ice formation occurred well before the time when the abundance of sea ice taxa significantly increased at ~1 Ma. Heterotrophic dinoflagellates feed mainly on diatoms (Jacobson and Anderson, 1986), and their abundance is most likely the result of food availability; hence, they can persist in ice-laden environments. On the other hand, the low production of their autotrophic counterparts, which dwell mainly in open waters without sea ice, could be related to these taxa being out-competed in the presence of blooming diatom populations in regions of seasonal

sea ice cover. Furthermore, heterotrophic dinoflagellate cysts dominate the assemblages in polar areas where sea ice occurs as long as 12 months per year (e.g., Rochon et al., 1999). The sea ice-associated dinoflagellate species *Islandinium minutum*, known to be very abundant or dominant in the Arctic Ocean and in subarctic regions with pronounced sea ice cover (Head et al., 2001; Hamel et al., 2002), appears to increase at ~1 Ma at Sites U1343 and U1344 (Fig. F26). Along with significant increases in both sea ice dinoflagellates and sea ice diatoms (e.g., *Thalassiosira antarctica* spores) at ~1 Ma at both sites, a rather significant drop in the abundance of *N. seminae*, a typical pelagic diatom, also occurs (Fig. F27). All of these biotic events are within the time interval of the MPT, which spans ~1.2–0.8 Ma and marks the transition from 41 k.y. obliquity ice volume cycles to larger ice age cycles that vary at ~100 k.y.

As noted above, the Bowers Ridge and Bering slope regions show distinct differences in the extent of sea ice cover throughout the last ~2.1 m.y., the time period covered by the sedimentary records of both regions. The extent of sea ice cover of the latter is substantially greater than that of the former because of the distal locations from the relatively warm Alaskan Stream subarctic Pacific water entry of the three Bering slope sites, which are most prone to perennial sea ice cover in the Bering Sea. The spatial differences in sea ice cover today are mainly attributed to the surface water circulation pattern (Fig. F2); this spatial difference appears to have persisted since at least 2.1 Ma, implying that surface water circulation patterns have also persisted (see below for details with *N. seminae* and other taxa). This is further supported by the fact that at Site U1339 on Umnak Plateau, the site closest to an entry point of Alaskan Stream subarctic Pacific water, sea ice taxa suggest lower levels of sea ice cover compared to the Bering slope sites farther north, which are not as heavily influenced by Alaskan Stream water. Furthermore, Katsuki and Takahashi (2005) illustrated that during the low sea level stand of the LGM, the relatively warm subarctic Alaskan Stream water entered the Bering Sea through the western Aleutian passes rather than through the eastern passes, whose shallow water depth would have inhibited flow during times of low sea level. After entry, the Alaskan Stream water turns eastward, flowing past Bowers Ridge and reaching the southeast corner of the Bering Sea close to Site U1339 on Umnak Plateau before turning northwest on its counter-clockwise path. Therefore, the spatial pattern of sea ice and surface water circulation observed in the last glacial period, including the stronger influence of warm Alaskan Stream water at Um-

nak Plateau, compared to its influence at the northern Bering slope, persists over long timescales.

Changes in biological productivity and the influence of the subarctic Pacific surface watermass flowing into the Bering Sea

Based on the spatial distributions of long-term temporal changes of three diatom taxa (*Coscinodiscus marginatus*, *Neodenticula* spp., and *Actinocyclus curvatus*), it is clear that the influence of subarctic Pacific (Alaskan Stream) waters flowing into the Bering Sea, which are relatively warm and less eutrophic than Bering Sea waters, has typically been strongest at the Bowers Ridge sites, followed by the Umnak Plateau site. The weakest influence of this relatively warm watermass occurred at the Bering slope sites (Fig. F27). This is the same pattern found by Katsuki and Takahashi's (2005) study of past watermass circulation patterns, in which they inferred sea ice distributions during the last glacial period. The longer records from Expedition 323 indicate that, as climate cooled through the Pleistocene, pelagic water influence at all sites progressively weakened. Furthermore, the sites closest to straits through which pelagic water flows into the Bering Sea have consistently higher abundances of subarctic pelagic diatom species than those downstream in the counter-clockwise circulation pattern of the surface watermasses.

From the bottom of the holes upward at the Bowers Ridge sites, a marked drop in *C. marginatus* was seen at ~3 Ma at Site U1341 and at ~2.6 Ma at Site U1340 (Fig. F27). This can be interpreted as resulting from a sharp reduction in nutrient supply due to the development of upper layer stratification. It is apparent that the diatom taxon *C. marginatus* requires a relatively high nutrient supply and tolerates low light intensity. This is substantiated by the fact that today this diatom taxon (1) dwells in the lower euphotic zone off of Spain (Nogueira et al., 2000; Nogueira and Figueiras, 2005) and (2) occurs during early winter (~November–January) in the subarctic Pacific and in the Bering Sea based on time-series sediment trapping (Takahashi, 1986; Takahashi et al., 1989; Onodera and Takahashi, 2009). Thus, a high nutrient supply demand and low light intensity demand is apparent for this taxon. In addition, heavily silicified species persist in glacial-like Pleistocene sediments at the Bering slope sites, supporting the contention that temperature is not the principal limiting factor. This timing of 3–2.6 Ma coincides approximately with the end of the so-called “opal dump” observed in the subarctic Pacific at ~2.7 Ma, which is coincident with the onset of NHG (Maslin et al., 1996). Al-

though the reduction in *C. marginatus* persisted around the time of NHG, an overwhelmingly continuous presence of diatom ooze and interbedded diatom ooze and silt sediments accumulated throughout the Pliocene–Pleistocene in the Bering Sea. This clearly suggests that a high amount of opal sedimentation continued after the onset of NHG well into the Pleistocene.

The 5 m.y. long-term trend of *Neodenticula* (*Neodenticula kamtschatica*, *Neodenticula koizumii*, *N. seminae*, and *Neodenticula* sp.) in the Bowers Ridge region shows the following two patterns. Slightly higher percentages were observed from the bottom of the hole until ~2.9–2.7 Ma compared to the sections above, particularly at Site U1340, but generally *Neodenticula* is an important component of the assemblage throughout. On the other hand, the abundance of *Actinocyclus* spp. (Fig. F27) clearly increases through the Pliocene, suggesting changes in stratification/watermass circulation as the colder climate developed. This is generally true for Sites U1340 and U1341 at Bowers Ridge and for Site U1343 off of the Bering slope. Data from Site U1344, however, provide a more complicated picture than this and do not show a clear trend, probably because of the overwhelmingly high abundance of sea ice-associated diatoms such as *T. antarctica* spores (Abelmann, 1992a) (~25% during 4–0.9 Ma; ~40% during 0.9–0 Ma) (Fig. F27). Both at Bowers Ridge and at the Bering slope, marked declines were seen for both taxa (*Actinocyclus* spp. and *N. seminae*) around the MPT (Fig. F27), although the exact timing of the decline is site and taxa specific. Nevertheless, the upheaval of both taxa at the MPT is notable. During intervals of high eutrophic levels, suggested by high *Actinocyclus* spp., cooler, low trophic subarctic Pacific waters, indicated by *N. seminae*, were introduced into the Bering Sea. This is based on the geographic and seasonal distributions of *A. curvatulus*, which appears to be ecologically similar to *Thalassiosira latimarginata* s.l. and, to a lesser extent, *N. seminae* (Sancetta, 1982; Takahashi, 1986; Takahashi et al., 1989). As surface waters became increasingly stratified, especially after ~0.9 Ma with Milankovitch-scale 100 k.y. climatic cyclic regimes, *N. seminae* declined with the emerging sea ice diatoms.

Changes in bottom water and intermediate-water conditions

Much of the Pacific water entering the Bering Sea is matched by outflow through the Aleutian Islands. The most significant outflow is through the Kamchatka Strait, which has a maximum water depth of 4420 m. If some component of North Pacific inter-

mediate or deep water formed in the Bering Sea in the past, particularly when sea level was lower, it would have flowed out through the Kamchatka Strait or a secondary outlet near the Commander–Near Strait at 2000 m (Fig. F1). One of the scientific objectives of Expedition 323 was to elucidate the history, temporal variability, and intensity of NPIW and deepwater formation in the Bering Sea and its links to surface water processes. This objective was partially fulfilled during the expedition but would have been more adequately addressed had we obtained permission to drill two important sites located in Russian territorial waters, Shirshov Ridge Site SHR-3B at 2232 m water depth and Site KST-1B inside the Kamchatka Strait at 3435 m water depth (Takahashi et al., 2009). The main objective at these sites was to monitor deepwater masses flowing out of the Bering Sea to the Pacific Ocean. Nevertheless, seven sites were successfully cored, and complete records of environmental variability of intermediate-water and deepwater sites spanning the Pleistocene to the Pliocene were recovered during Expedition 323. The sites range from 818 to 3174 m and allow for the characterization of past vertical watermass distribution and for the reconstruction of the history and distribution of the OMZ in the region (Fig. F4).

Previous observations made in glacial records from the Bering Sea and just outside the Bering Sea on the Detroit Seamount in the North Pacific suggest a source of ventilated intermediate water coming from the Bering Sea and/or the Detroit Seamount region (Gorbarenko, 1996). Furthermore, other paleoceanographic reconstructions of the Bering Sea, made possible by the *Hakuhou-Maru* piston coring survey cruise in 1999, show past NPIW formation during four different time slices, reconstructed based on the high-oxygen indicator and intermediate water-dwelling radiolarian species *C. davisiana*. According to these studies, the role of the Bering Sea in NPIW formation is apparently visible during the cold intervals (Tanaka and Takahashi, 2005).

Shipboard analyses of sediment samples recovered during Expedition 323 show a continuous recovery of Pliocene to Holocene deep-sea benthic foraminifers and midwater radiolarians at all sites (Figs. F28, F29), although calcareous benthic foraminifers appear to be rare in the middle and early Pliocene. The benthic foraminifer faunal composition displays large assemblage changes and shifts in species dominance. These changes are likely related to variability in local oxygen concentration in the bottom waters associated with surface water productivity and/or deepwater ventilation, possibly on Milankovitch and other timescales. For example, *Bulimina* aff. *exilis*, a

common species in the Bering Sea samples, is generally regarded as a low oxygen/deep infaunal species and has been found in samples associated with high productivity and low sea ice (e.g., Bubenshchikova et al., 2008; Kaiho, 1994).

Bering Sea benthic foraminifers show affinities to assemblages found within or near the OMZ in the Sea of Okhotsk and also to more common deep Pacific Ocean assemblages. The faunal similarity between the two marginal seas and the deep Pacific Ocean will allow for reconstruction of the physico-chemical characteristics of deep and intermediate watermasses as a result of changes in surface productivity, deep-water ventilation, sea ice coverage, and continental glaciation.

Previous piston core studies showed a significant intensification of the OMZ during the last deglacial at Umnak Plateau (Okazaki et al., 2005), suggesting a relationship between productivity and terrestrial nutrient supply from melting. However, there is no information regarding the longer timescale relationship through the Pleistocene. Analysis of faunas from the newly drilled Bering Sea sites will be particularly important in extending this record through the entire Pliocene (at Bowers Ridge) and Pleistocene (at Bowers Ridge and the Bering slope) and will allow us to decipher the onset and evolution of the OMZ and provide further insight into NPIW production at this marginal sea. Furthermore, Site U1344 (~3200 m) is presently located below the OMZ and also has the potential to monitor past deepwater changes.

A striking finding of the expedition was the relatively low oxygen content of intermediate watermass conditions at most sites during the last 5 m.y., as indicated by the presence of episodic laminated sediment intervals throughout the entire sections, particularly in the late Pliocene and Pleistocene. The benthic foraminifer faunas recovered from deep cored Sites U1340 and U1341 generally support this, indicating that Bering Sea intermediate and deep waters were better oxygenated in the early Pliocene, as suggested by the presence of the agglutinated foraminifer *Martinottiella communis* (Fig. F29), and less oxygenated during the last ~2 m.y., as suggested by the increase in deep infaunal benthic foraminifers (Fig. F28). This assemblage is composed of abundant calcareous benthic genera that are typically indicative of reduced-oxygen conditions (Bubenshchikova et al., 2008).

High sedimentation-rate Sites U1339 and U1345, located within the OMZ today (Fig. F4), reveal high-amplitude variability in the relative abundance of the deep infaunal assemblage since 0.8 Ma. This ap-

pears to be associated with interglacial–deglacial cyclicity, showing a higher abundance of deep infaunal species (reflecting the lowest bottom water oxygen conditions) during interglacials, in particular strong interglacial marine isotope Stages (MIS) 1, 5, and 11. Higher bottom water oxygen conditions appear to correlate with glacials. Furthermore, Sites U1340, U1343, and U1344 contain well-preserved foraminifers over the last 2 m.y., with increasing absolute abundances of benthic and planktonic taxa across the MPT (~0.8–1.1 Ma), in association with an increase in abundance of the polar planktonic foraminifer *Neogloboquadrina pachyderma* (sinistral). This cooling trend was also observed as an increase in the abundance of sea ice dinoflagellates and diatoms and intermediate water–dwelling radiolarians (e.g., *C. davisiana*). Cooling of the surface waters would have enhanced ventilation of the intermediate waters during glacials and increased density stratification during interglacials, contributing to the drop in dissolved-oxygen content in the intermediate and bottom waters at these times, which is suggested by the increase in deep infaunal benthic foraminifer taxa.

Microbiology in high–surface-productivity environments

The microbiological objectives of Expedition 323 were to constrain global models of subseafloor biomass and microbial respiration by quantifying subseafloor cell abundance and interstitial water chemistry in an extremely high productivity region of the ocean. We also sought to determine how subseafloor community composition is influenced by high productivity in the overlying water column.

To meet these objectives, high-resolution sampling for microbiological analyses and interstitial water chemistry took place at five sites in the Bering Sea. Each site was selected based upon its distance from land and its marine productivity, as determined by annual chlorophyll-a concentrations in the water column.

Four cores were drilled using the APC system to ~40 mbsf at each microbiology-dedicated hole. Contamination tests using perfluorocarbon tracer (PFT) and fluorescent beads (Smith et al., 2000) were performed in each hole, showing that contamination from drilling fluid was insignificant.

Sediment samples were taken for determining the cell abundance (a proxy for microbial biomass) and diversity of the microbial community. In general, these samples were taken every 25 cm for Sections 1H-1 through 2H-3 (or 2H-6) and every 75 cm for

Core 3H. Below Core 3H, the sampling resolution was once per core. Interstitial water whole-rounds adjacent to microbiology whole-rounds were taken at the same resolution. In addition, 10 cm whole-rounds were taken for interstitial water and microbiological analyses once per core until APC refusal. Interstitial water sampling continued at this resolution in XCB cores, and microbiology samples for prokaryotic cell abundance, diversity, and community structure were collected at ~400 and ~700 mbsf. PFT analyses showed no drilling fluid contamination at these depths.

Interstitial water samples were extracted on board, and aliquots were fixed for shore-based and shipboard analyses. Shipboard aliquots were used to determine concentrations of dissolved inorganic carbon (DIC), alkalinity, sulfate, sulfide, ammonium, phosphate, major ions (e.g., Ca, Na, and K), and minor ions (e.g., Fe and Mn). These data, along with formation factor, allow for a quantitative determination of microbial respiration rates (D'Hondt et al., 2002).

Geochemical data obtained during the expedition show that microbial activity along the slope sites (i.e., Sites U1339, U1343, U1344, and U1345) is substantially higher than at Site U1342 on Bowers Ridge. At the slope sites, the concentrations of microbial respiration products such as DIC, ammonium, and phosphate are approximately an order of magnitude higher than at Bowers Ridge (Fig. F30). A shallow sulfate–methane transition zone (SMTZ) (~6–11 mbsf) is present (Fig. F30) at these sites, highlighting the importance of methanogenesis and sulfate reduction coupled to the anaerobic oxidation of methane (AOM) for sediment geochemistry. Interstitial water data suggest the presence of microbially mediated Fe- and Mn-oxide reduction. Interestingly, the geochemical profiles suggest significant microbial activity as deep as 700 mbsf. In contrast, at Bowers Ridge, sulfate concentrations decrease subtly and penetrate to the basement at Site U1342, suggesting very low rates of microbially mediated sulfate reduction and the absence of AOM at present. The difference in microbial activity at these sites might be caused by different rates of water column productivity and sedimentation.

We expect that the differences in geochemistry between the slope and ridge sites will be reflected in microbial cell abundance and diversity. Specifically, we expect elevated cell abundance and a consortium

of sulfate-reducing bacteria and methane-oxidizing archaea in the SMTZ.

References

- Abelmann, A., 1992a. Diatom assemblages in Arctic sea ice—indicator for ice drift pathways. *Deep-Sea Res., Part A*, 39(2–1):S525–S538. doi:10.1016/S0198-0149(06)80019-1
- Abelmann, A., 1992b. Radiolarian flux in Antarctic waters (Drake Passage, Powell Basin, Bransfield Strait). *Polar Biol.*, 12(3–4):357–372. doi:10.1007/BF00243107
- Alexander, M.A., Bladé, I., Newman, M., Lanzante, J.R., Lau, N.-C., and Scott, J.D., 2002. The atmospheric bridge: the influence of ENSO teleconnections on air–sea interaction over the global oceans. *J. Clim.*, 15(16):2205–2231. doi:10.1175/1520-0442(2002)015<2205:TABTIO>2.0.CO;2
- Backman, J., Moran, K., McNroy, D.B., Mayer, L.A., and the Expedition 302 Scientists, 2006. *Proc. IODP, 302: Edinburgh (Integrated Ocean Drilling Program Management International, Inc.)*. doi:10.2204/iodp.proc.302.2006
- Baldauf, J.G., 1987. Diatom biostratigraphy of the middle- and high-latitude North Atlantic Ocean, Deep Sea Drilling Project Leg 94. In Ruddiman, W.F., Kidd, R.B., Thomas, E., et al., *Init. Repts. DSDP, 94*: Washington, DC (U.S. Govt. Printing Office), 729–762. doi:10.2973/dsdp.proc.94.115.1987
- Behl, R.J., and Kennett, J.P., 1996. Brief interstadial events in the Santa Barbara Basin, NE Pacific, during the last 60 kyr. *Nature (London, U. K.)*, 379(6562):243–246. doi:10.1038/379243a0
- Berard-Therriault, L., Starr, M., Poulin, M., and Roy, S., 2002. A very unusual spring bloom in the Gulf of St. Lawrence, eastern Canada: the rebirth of diatom *Neodenticula seminae*. *Proc. 17th Int. Diatom Symp.*, 17:9.
- Berger, W.H., 1970. Biogenous deep-sea sediments: fractionation by deep-sea circulation. *Geol. Soc. Am. Bull.*, 81(5):1385–1402. doi:10.1130/0016-7606(1970)81[1385:BDSFBD]2.0.CO;2
- Bubenshchikova, N., Nürnberg, D., Lembke-Jene, L., and Pavlova, G., 2008. Living benthic foraminifera of the Okhotsk Sea: faunal composition, standing stocks and microhabitats. *Mar. Micropaleontol.*, 69(3–4):314–333. doi:10.1016/j.marmicro.2008.09.002
- Cannariato, K.G., and Kennett, J.P., 1999. Climatically related millennial-scale fluctuations in strength of California margin oxygen-minimum zone during the past 60 k.y. *Geology*, 27(11):975–978. doi:10.1130/0091-7613(1999)027<0975:CRMSFI>2.3.CO;2
- Coachman, L.K., and Aagaard, K., 1981. Re-evaluation of water transports in the vicinity of the Bering Strait. In Hood, D.W., and Calder, J.A. (Eds.), *The Eastern Bering Sea Shelf: Oceanography and Resources*: Seattle (Univ. Washington Press), 95–110.
- Cook, M.S., Keigwin, L.D., and Sancetta, C.A., 2005. The deglacial history of surface and intermediate water of

- the Bering Sea. *Deep-Sea Res., Part II*, 52(16–18):2163–2173. doi:10.1016/j.dsr2.2005.07.004
- Corbyn, Z., 2007. Atlantic invaders. *Nature Rep. Clim. Change*, 6(711):82. doi:10.1038/climate.2007.61
- D'Hondt, S., Rutherford, S., and Spivack, A.J., 2002. Metabolic activity of the subsurface life in deep-sea sediments. *Science*, 295(5562):2067–2070. doi:10.1126/science.1064878
- De Boer, A.M., and Nof, D., 2004. The Bering Strait's grip on the Northern Hemisphere climate. *Deep-Sea Res., Part I*, 51(10):1347–1366. doi:10.1016/j.dsr.2004.05.003
- Gladenkov, A.Y., 2006. Neogene diatoms from the Sandy Ridge section, Alaska Peninsula: significance for stratigraphic and paleogeographic reconstructions. *Stratigr. Geol. Correl.*, 14(1):73–90. doi:10.1134/S0869593806010059
- Gloersen, P., 1995. Modulation of hemispheric sea-ice cover by ENSO events. *Nature (London, U. K.)*, 373(6514):503–506. doi:10.1038/373503a0
- Gorbarenko, S.A., 1996. Stable isotope and lithological evidence of late glacial and Holocene oceanography of the northwestern Pacific and its marginal seas. *Quat. Res.*, 46(3):230–250. doi:10.1006/qres.1996.0063
- Hamel, D., de Vernal, A., Gosselin, M., and Hillaire-Marcel, C., 2002. Organic-walled microfossils and geochemical tracers: sedimentary indicators of productivity changes in the North Water and northern Baffin Bay during the last centuries. *Deep-Sea Res., Part II*, 49(22–23):5277–5295. doi:10.1016/S0967-0645(02)00190-X
- Hasumi, H., 2002. Sensitivity of the global thermohaline circulation to interbasin freshwater transport by the atmosphere and the Bering Sea throughflow. *J. Clim.*, 15(17):2516–2526. doi:10.1175/1520-0442(2002)015<2516:SOTGTC>2.0.CO;2
- Haug, G.H., Sigman, D.M., Tiedemann, R., Pedersen, T.F., and Sarnthein, M., 1999. Onset of permanent stratification in the subarctic Pacific Ocean. *Nature (London, U. K.)*, 401(6755):779–782. doi:10.1038/44550
- Head, M.J., Harland, R., and Matthiessen, J., 2001. Cold marine indicators of the late Quaternary: the new dinoflagellate cyst genus *Islandinium* and related morphotypes. *J. Quat. Sci.*, 16(7):621–636. doi:10.1002/jqs.657
- Hendy, I.L., and Kennett, J.P., 2003. Tropical forcing of North Pacific intermediate water distribution during late Quaternary rapid climate change? *Quat. Sci. Rev.*, 22(5–7):673–689. doi:10.1016/S0277-3791(02)00186-5
- Honjo, S., 1990. Particle fluxes and modern sedimentation in the polar oceans. In Smith, W.O., Jr. (Ed.), *Polar Oceanography (Pt. B): Chemistry, Biology, and Geology*: New York (Academic), 687–739.
- Hood, D.W., 1983. The Bering Sea. In Ketchum, B.H. (Ed.), *Estuaries and Enclosed Seas: The Netherlands* (Elsevier), 337–373
- Jacobson, D.M., and Anderson, D.M., 1986. Thecate heterotrophic dinoflagellates: feeding behavior and mechanisms. *J. Phycol.*, 22(3):249–258. doi:10.1111/j.1529-8817.1986.tb00021.x
- Kaiho, K., 1994. Benthic foraminiferal dissolved-oxygen index and dissolved-oxygen levels in the modern ocean. *Geology*, 22(8):719–722. doi:10.1130/0091-7613(1994)022<0719:BFDIOIA>2.3.CO;2
- Katsuki, K., and Takahashi, K., 2005. Diatoms as paleoenvironmental proxies for seasonal productivity, sea-ice and surface circulation in the Bering Sea during the late Quaternary. *Deep-Sea Res., Part II*, 52(16–18):2110–2130. doi:10.1016/j.dsr2.2005.07.001
- Keigwin, L.D., 1995. Northwest Pacific paleohydrography. In Tsunogai, S., Iseki, K., Koike, I., and Oba, T. (Eds.), *Global Fluxes of Carbon and Its Related Substances in the Coastal Sea-Ocean-Atmosphere System: Proceedings of the 1994 Sapporo IGBP Symposium: Yokohama (M and J Int.)*, 473–478.
- Krissek, L.A., 1995. Late Cenozoic ice-rafting records from Leg 145 sites in the North Pacific: late Miocene onset, late Pliocene intensification, and Pliocene–Pleistocene events. In Rea, D.K., Basov, I.A., Scholl, D.W., and Allan, J.F. (Eds.), *Proc. ODP, Sci. Results*, 145: College Station, TX (Ocean Drilling Program), 179–194. doi:10.2973/odp.proc.sr.145.118.1995
- Kwiek, P.B., and Ravelo, A.C., 1999. Pacific Ocean intermediate and deep water circulation during the Pliocene. *Palaeogeogr., Palaeoclimatol., Palaeoecol.*, 154(3):191–217. doi:10.1016/S0031-0182(99)00111-X
- Lagoe, M.B., Eyles, C.H., Eyles, N., and Hale, C., 1993. Timing of late Cenozoic tidewater glaciation in the far North Pacific. *Geol. Soc. Am. Bull.*, 105(12):1542–1560. doi:10.1130/0016-7606(1993)105<1542:TOLCTG>2.3.CO;2
- Lehmann, M.F., Sigman, D.M., McCorkle, D.C., Brunelle, B.G., Hoffmann, S., Kienast, M., Cane, G., and Clement, J., 2005. Origin of the deep Bering Sea nitrate deficit: constraints from the nitrogen and oxygen isotopic composition of water column nitrate and benthic nitrate fluxes. *Global Biogeochem. Cycles*, 19(4):GB4005. doi:10.1029/2005GB002508
- Lisiecki, L.E., and Raymo, M.E., 2005. A Pliocene–Pleistocene stack of 57 globally distributed benthic $\delta^{18}\text{O}$ records. *Paleoceanography*, 20(1):PA1003. doi:10.1029/2004PA001071
- Maslin, M.A., Haug, G.H., Sarnthein, M., and Tiedemann, R., 1996. The progressive intensification of Northern Hemisphere glaciation as seen from the North Pacific. *Geol. Rundsch.* 85(3):452–465. doi:10.1007/BF02369002
- Matsumoto, K., Oba, T., Lynch-Stieglitz, J., and Yamamoto, H., 2002. Interior hydrography and circulation of the glacial Pacific Ocean. *Quat. Sci. Rev.*, 21(14–15):1693–1704. doi:10.1016/S0277-3791(01)00142-1
- McKelvey, B.C., Chen, W., and Arculus, R.J., 1995. Provenance of Pliocene–Pleistocene ice-rafted debris, Leg 145, northern Pacific Ocean. In Rea, D.K., Basov, I.A., Scholl, D.W., and Allan, J.F. (Eds.), *Proc. ODP, Sci. Results*, 145: College Station, TX (Ocean Drilling Program), 195–204. doi:10.2973/odp.proc.sr.145.120.1995
- Moran, K., Backman, J., Brinkhuis, H., Clemens, S.C., Cronin, T., Dickens, G.R., Eynaud, F., Gattacceca, J.,

- Jakobsson, M., Jordan, R.W., Kaminski, M., King, J., Koc, N., Krylov, A., Martinez, N., Matthiessen, J., McInroy, D., Moore, T.C., Onodera, J., O'Regan, M., Pälke, H., Rea, B., Rio, D., Sakamoto, T., Smith, D.C., Stein, R., St. John, K., Suto, I., Suzuki, N., Takahashi, K., Watanabe, M., Yamamoto, M., Farrell, J., Frank, M., Kubik, P., Jokat, W., and Kristoffersen, Y., 2006. The Cenozoic palaeoenvironment of the Arctic Ocean. *Nature (London, U. K.)*, 441(7093):601–605. doi:10.1038/nature04800
- Nedashkovskiy, A.P., and Sapozhnikov, V.V., 1999. Variability in the components of the carbonate system and dynamics of inorganic carbon in the western Bering Sea in summer. In Loughlin, T.R., and Ohtani, K. (Eds.), *Dynamics of the Bering Sea*: Fairbanks (Univ. Alaska Sea Grant), 311–322.
- Niebauer, H.J., 1998. Variability in Bering Sea ice cover as affected by a regime shift in the North Pacific in the period 1947–1996. *J. Geophys. Res.*, 103(C12):27717–27737. doi:10.1029/98JC02499
- Niebauer, H.J., and Day, R.H., 1989. Causes of interannual variability in the sea ice cover of the eastern Bering Sea. *Geojournal*, 18(1):45–59. doi:10.1007/BF00722385
- Nogueira, E., and Figueiras, F.G., 2005. The microplankton succession in the Ria de Vigo revisited: species assemblages and the role of weather-induced, hydrodynamic variability. *J. Mar. Syst.*, 54(1–4):139–155. doi:10.1016/j.jmarsys.2004.07.009
- Nogueira, E., Ibanez, F., and Figueiras, F.G., 2000. Effect of meteorological and hydrographic disturbances on the microplankton community structure in the Ría de Vigo (NW Spain). *Mar. Ecol.: Prog. Ser.*, 203:23–45. doi:10.3354/meps203023
- Ohtani, K., 1965. On the Alaskan Stream in summer. *Bull. Fac. Fish., Hokkaido Univ.*, 15:260–273. (In Japanese).
- Okazaki, Y., Takahashi, K., Asahi, H., Katsuki, K., Hori, J., Yasuda, H., Sagawa, Y., and Tokuyama, H., 2005. Productivity changes in the Bering Sea during the late Quaternary. *Deep-Sea Res., Part II*, 52(16–18):2150–2162. doi:10.1016/j.dsr2.2005.07.003
- Okazaki, Y., Takahashi, K., Yoshitani, H., Nakatsuka, T., Ikehara, M., and Wakatsuchi, M., 2003. Radiolarians under the seasonally sea-ice covered conditions in the Okhotsk Sea: flux and their implications for paleoceanography. *Mar. Micropaleontol.*, 49(3):195–230. doi:10.1016/S0377-8398(03)00037-9
- Ono, A., Takahashi, K., Katsuki, K., Okazaki, Y., and Sakamoto, T., 2005. The Dansgaard–Oeschger cycles discovered in the up stream source region of the North Pacific Intermediate Water formation. *Geophys. Res. Lett.*, 32(11):L11607. doi:10.1029/2004GL022260
- Onodera, J., and Takahashi, K., 2009. Long-term diatom fluxes in response to oceanographic conditions at Stations AB and SA in the central subarctic Pacific and the Bering Sea, 1990–1998. *Deep-Sea Res., Part I*, 56(2):189–211. doi:10.1016/j.dsr.2008.08.006
- Ravelo, A.C., and Andreasen, D.H., 2000. Enhanced circulation during a warm period. *Geophys. Res. Lett.*, 27(7):1001–1004. doi:10.1029/1999GL007000
- Rea, D.K., Basov, I.A., Janecek, T.R., Palmer-Julson, A., et al., 1993. *Proc. ODP, Init. Repts.*, 145: College Station, TX (Ocean Drilling Program). doi:10.2973/odp.proc.ir.145.1993
- Rea, D.K., Basov, I.A., Krissek, L.A., and the Leg 145 Scientific Party, 1995. Scientific results of drilling the North Pacific transect. In Rea, D.K., Basov, I.A., Scholl, D.W., and Allan, J.F. (Eds.), *Proc. ODP, Sci. Results*, 145: College Station, TX (Ocean Drilling Program), 577–596. doi:10.2973/odp.proc.sr.145.146.1995
- Rea, D.K., Basov, I.A., Scholl, D.W., and Allan, J.F. (Eds.), 1995. *Proc. ODP, Sci. Results*, 145: College Station, TX (Ocean Drilling Program). doi:10.2973/odp.proc.sr.145.1995
- Rea, D.K., and Schrader, H., 1985. Late Pliocene onset of glaciation: ice-rafting and diatom stratigraphy of North Pacific DSDP cores. *Palaeogeogr., Palaeoclimatol., Palaeoecol.*, 49(3–4):313–325. doi:10.1016/0031-0182(85)90059-8
- Reid, P.C., Johns, D.G., Edwards, M., Starr, M., Poulin, M., and Snoeijs, P., 2007. A biological consequence of reducing Arctic ice cover: arrival of the Pacific diatom *Neodenticula seminae* in the North Atlantic for the first time in 800,000 years. *Global Change Biol.*, 13(9):1910–1921. doi:10.1111/j.1365-2486.2007.01413.x
- Rochon, A., de Vernal, A., Turon, J.L., Mathiessen, J., and Head, M.J., 1999. Distribution of recent dinoflagellate cysts in surface sediments from the North Atlantic Ocean and adjacent seas in relation to sea-surface parameters. *Am. Assoc. Strat. Palynol. Found. Contrib. Ser.*, Vol. 35.
- Sakamoto, T., Ikehara, M., Aoki, K., Iijima, K., Kimura, N., Nakatsuka, T., and Wakatsuchi, M., 2005. Ice-rafted debris (IRD)-based sea-ice expansion events during the past 100 kyrs in the Okhotsk Sea. *Deep Sea Res., Part II*, 52(16–18):2275–2301. doi:10.1016/j.dsr2.2005.08.007
- Sambrotto, R.N., Goering, J.J., and McRoy, C.P., 1984. Large yearly production of phytoplankton in the western Bering Strait. *Science*, 225(4667):1147–1150. doi:10.1126/science.225.4667.1147
- Sancetta, C., 1982. Distribution of diatom species in surface sediments of the Bering and Okhotsk Seas. *Micropaleontology*, 28(3):221–257. doi:10.2307/1485181
- Scholl, D.W., and Creager, J.S., 1973. Geologic synthesis of Leg 19 (DSDP) results; far North Pacific, and Aleutian Ridge, and Bering Sea. In Creager, J.S., Scholl, D.W., et al., *Init. Repts. DSDP*, 19: Washington, DC (U.S. Govt. Printing Office), 897–913. doi:10.2973/dsdp.proc.19.137.1973
- Shaffer, G., and Bendtsen, J., 1994. Role of the Bering Strait in controlling North Atlantic ocean circulation and climate. *Nature (London, U. K.)*, 367(6461):354–357. doi:10.1038/367354a0
- Smith, D.C., Spivack, A.J., Fisk, M.R., Haveman, S.A., Staudigel, H., and the Leg 185 Shipboard Scientific Party, 2000. Methods for quantifying potential microbial contamination during deep ocean coring. *ODP Tech. Note*, 28. doi:10.2973/odp.tn.28.2000
- Solomon, S., Qin, D., Manning, M., Marquis, M., Averyt, K., Tignor, M.M.B., Miller, H.L., Jr., and Chen, Z. (Eds.), 2007. *Climate Change 2007: The Physical Science Basis*: Cambridge (Cambridge Univ. Press).

- Stabeno, P.J., Schumacher, J.D., and Ohtani, K., 1999. The physical oceanography of the Bering Sea. In Loughlin, T.R., and Ohtani, K. (Eds.), *Dynamics of the Bering Sea: A Summary of Physical, Chemical, and Biological Characteristics, and a Synopsis of Research on the Bering Sea*: Fairbanks (Univ. Alaska Sea Grant), 1–28.
- Tada, R., Irino, T., and Koizumi, I., 1999. Land-ocean linkages over orbital and millennial timescales recorded in late Quaternary sediments of the Japan Sea. *Paleoceanography*, 14(2):236–247. doi:10.1029/1998PA900016
- Takahashi, K., 1986. Seasonal fluxes of pelagic diatoms in the subarctic Pacific, 1982–1983. *Deep-Sea Res., Part A*, 33:1225–1251. doi:10.1016/0198-0149(86)90022-1
- Takahashi, K., 1999. Paleoceanographic changes and present environment of the Bering Sea. In Loughlin, T.R., and Ohtani, K. (Eds.), *Dynamics of the Bering Sea*: Fairbanks (Univ. Alaska Sea Grant), 365–385.
- Takahashi, K., 2005. The Bering Sea and paleoceanography. *Deep-Sea Res., Part II*, 52(16–18):2080–2091. doi:10.1016/j.dsr2.2005.08.003
- Takahashi, K., Honjo, S., and Tabata, S. 1989. Siliceous phytoplankton flux: interannual variability and response to hydrographic changes in the northeastern Pacific. In Peterson, D. (Ed.), *Aspects of Climate Variability in the Pacific and Western Americas*. Geophys. Monogr., 151–160.
- Takahashi, K., Jordan, R.W., and Boltovskoy, D. (Eds.), 2005. Preface. *Deep-Sea Res., Part II*, 52(16–18):2079. doi:10.1016/j.dsr2.2005.08.002
- Takahashi, K., Ravelo, A.C., and Alvarez Zarikian, C.A., 2009. Pliocene–Pleistocene paleoceanography and climate history of the Bering Sea. *IODP Sci. Prosp.*, 323. doi:10.2204/iodp.sp.323.2009
- Tanaka, S., and Takahashi, K., 2005. Late Quaternary paleoceanographic changes in the Bering Sea and the western subarctic Pacific based on radiolarian assemblages. *Deep-Sea Res., Part II*, 52(16–18):2131–2149. doi:10.1016/j.dsr2.2005.07.002
- Uozumi, S., Akamatsu, M., and Takagi, T., 1986. Takikawa-Honbetsu and Tatsunokuchi faunas (*Fortipecten takahashii*-bearing Pliocene faunas). *Spec. Pap.—Palaeontol. Soc. Japan*, 29:211–226.
- Warner, M.J., and Roden, G.I., 1995. Chlorofluorocarbon evidence for recent ventilation of the deep Bering Sea. *Nature (London, U. K.)*, 373(6513):409–412. doi:10.1038/373409a0
- Zahn, R., Rushdi, A., Pisias, N.G., Bornhold, B.D., Blaise, B., and Karlin, R., 1991. Carbonate deposition and benthic $\delta^{13}\text{C}$ in the subarctic Pacific: implications for changes of the oceanic carbonate system during the past 750,000 years. *Earth Planet. Sci. Lett.*, 103(1–4):116–132. doi:10.1016/0012-821X(91)90154-A
- Zhao, P., Zhang, X., Zhou, X., Ikeda, M., and Yin, Y., 2004. The sea ice extent anomaly in the North Pacific and its impact on the east Asian summer monsoon rainfall. *J. Clim.*, 17(17):3434–3447. doi:10.1175/1520-0442(2004)017<3434:TSIEAI>2.0.CO;2
- Zheng, Y., van Geen, A., Anderson, R.F., Gardner, J.V., and Dean, W.E., 2000. Intensification of the northeast Pacific oxygen minimum zone during the Bölling-Alleröd warm period. *Paleoceanography*, 15(5):528–536. doi:10.1029/1999PA000473

Publication: 15 March 2011
MS 323-101

Figure F1. Map illustrating the locations of the seven sites drilled and cored during IODP Expedition 323 in the Bering Sea, along with cross sections of the passes with volume transport (S_v) in the Aleutian Island arc and the Bering Strait. Note that the horizontal and vertical scales of the Bering Strait are twice that of the Aleutians (from Stabeno et al., 1999; Takahashi, 2005). DSDP = Deep Sea Drilling Project.

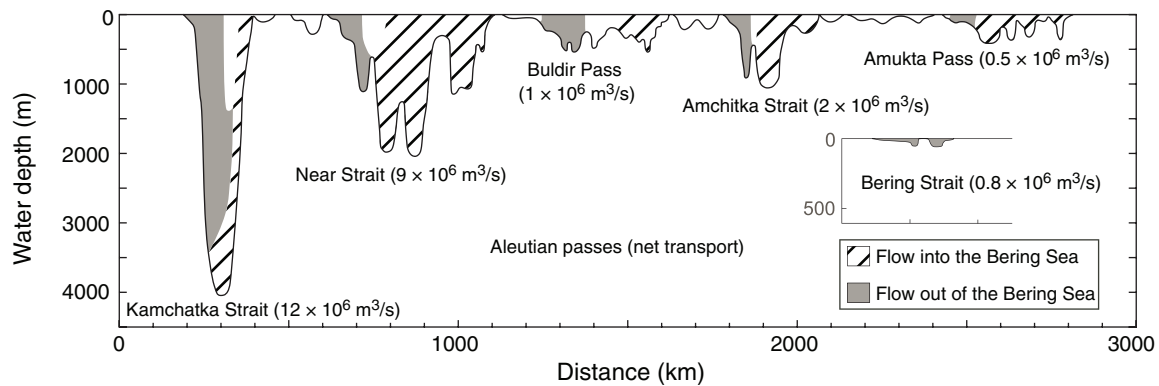
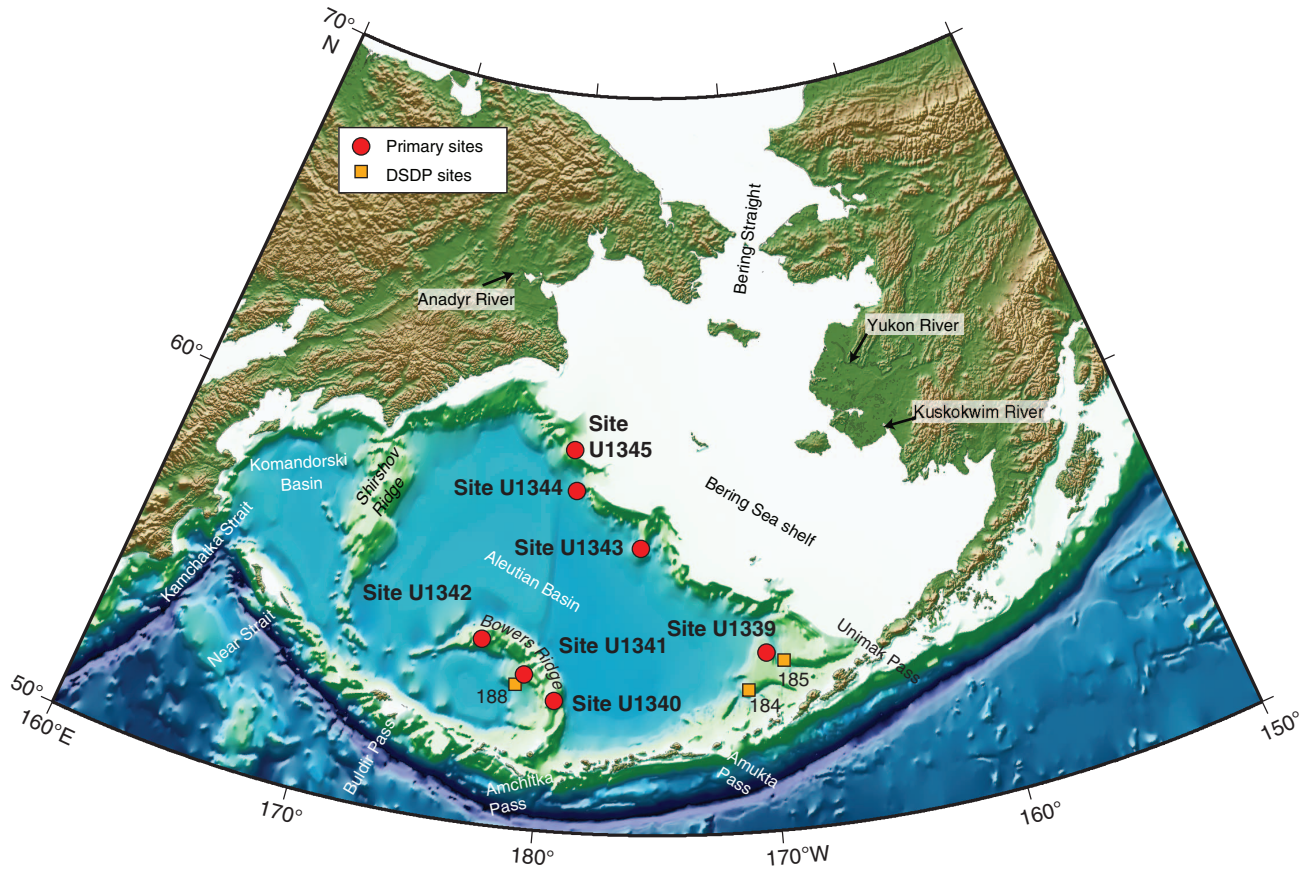


Figure F2. Map showing surface water circulation and topography in the Bering Sea (from Stabeno et al., 1999). The Alaskan Stream, Kamchatka Current, Bering Slope Current (BSC), and Aleutian North Slope Current (ANSC) are indicated.

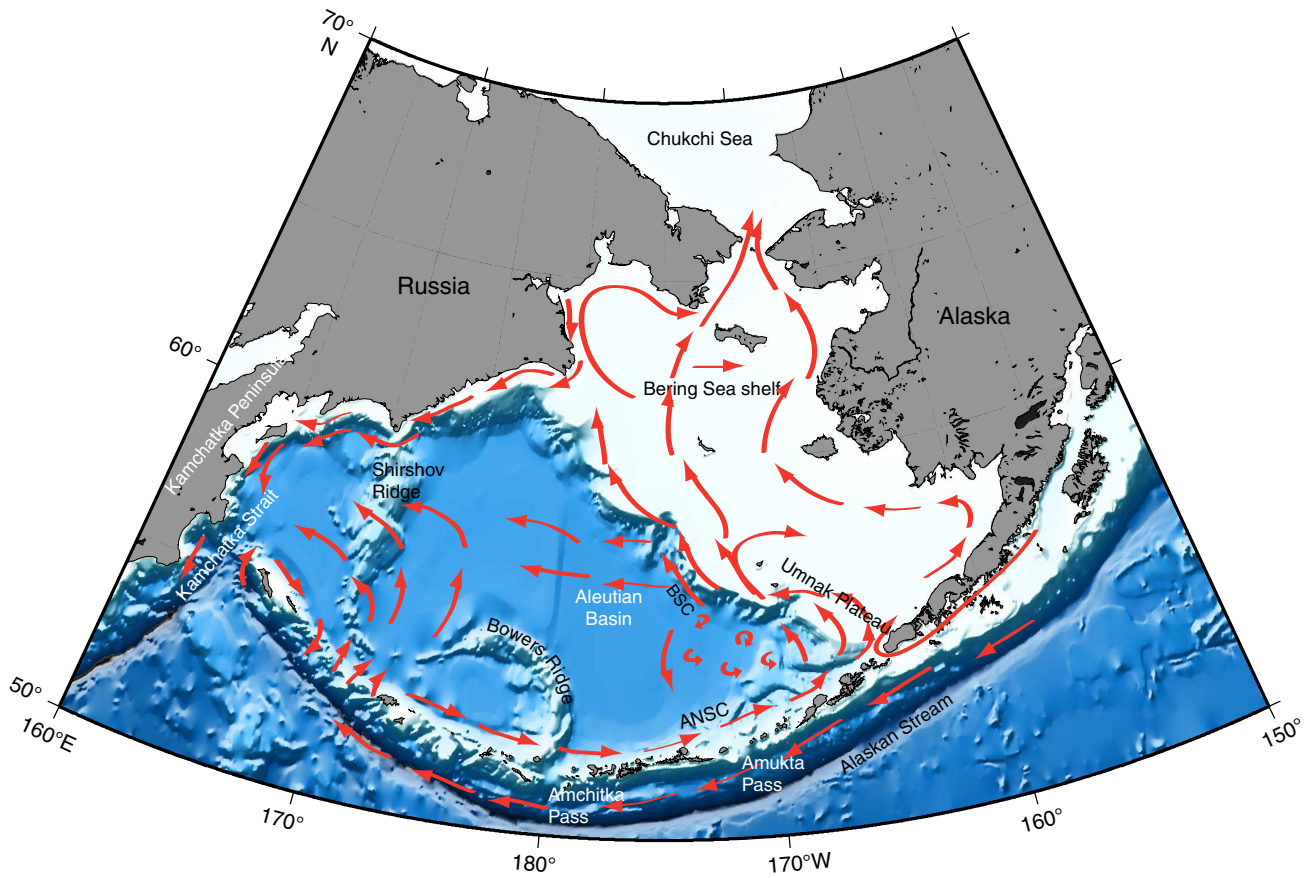


Figure F3. Map showing subsurface water circulation and topography in the Bering Sea (from Stabeno et al., 1999).

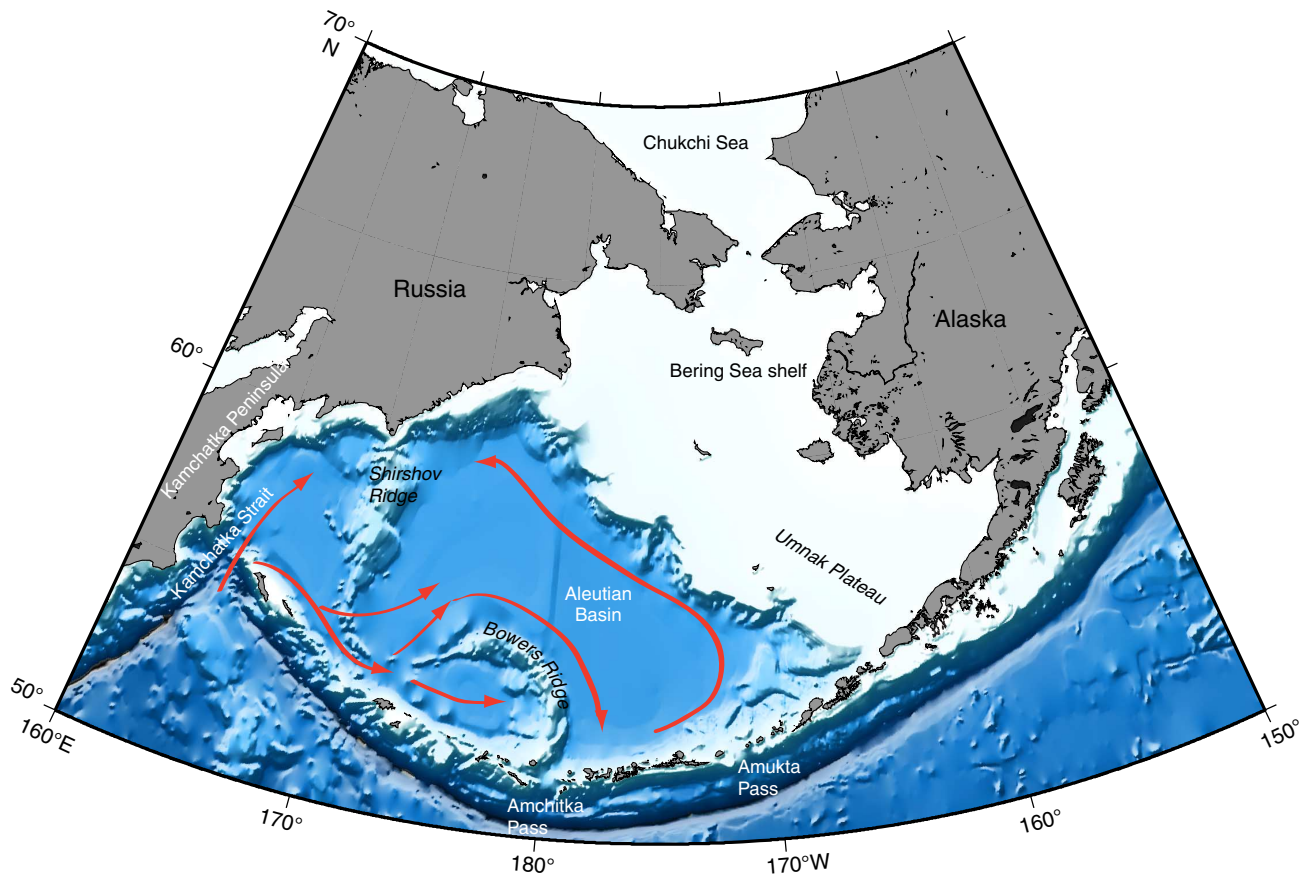




Figure F4. Vertical profiles of (A) temperature, (B) salinity, and (C) dissolved oxygen and (D) along the transect on 180° on the map of the Bering Sea (data from World Ocean Atlas [2005]; figures drawn by Ocean Data View).

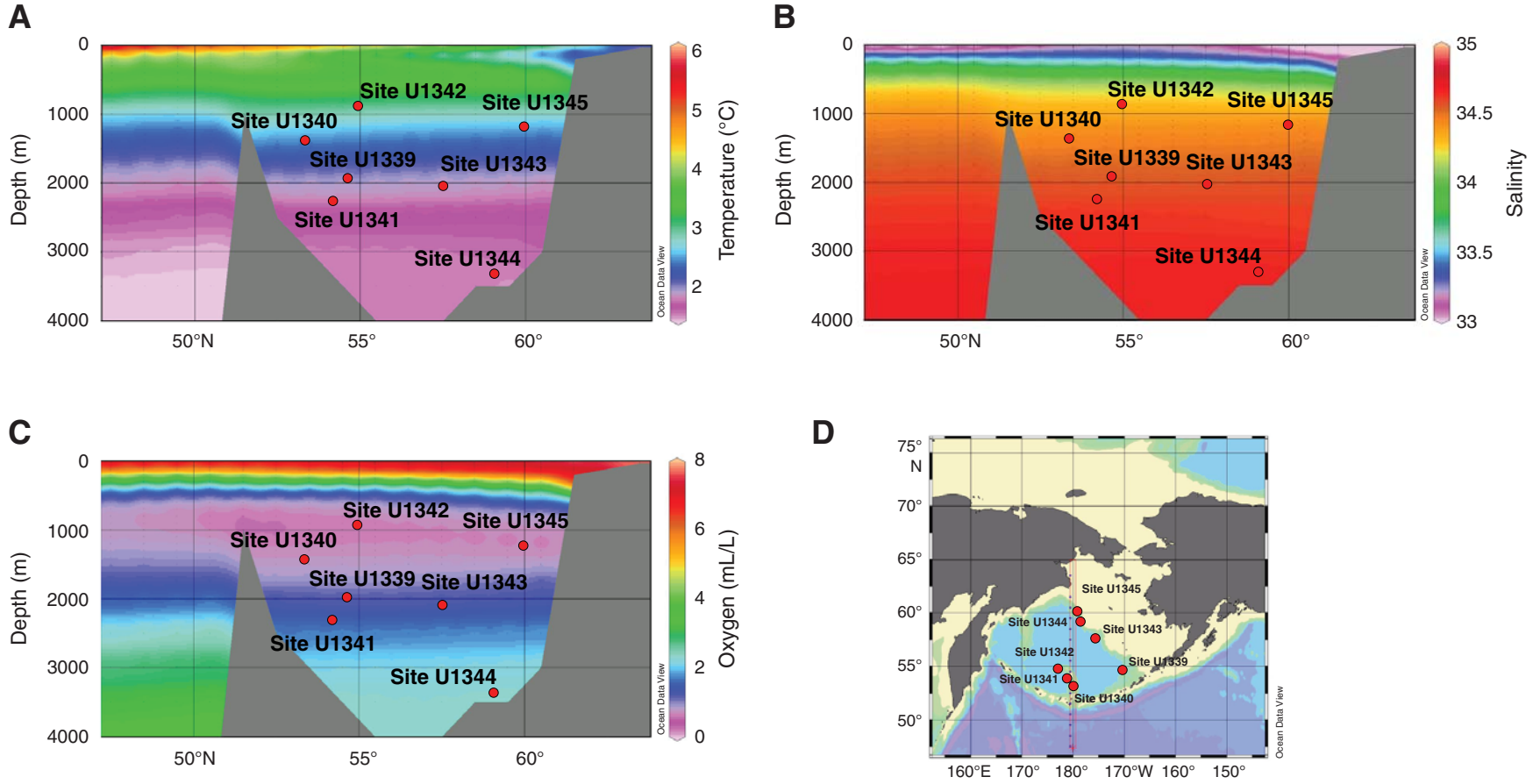


Figure F5. Sedimentation rates observed for Sites U1339–U1345.

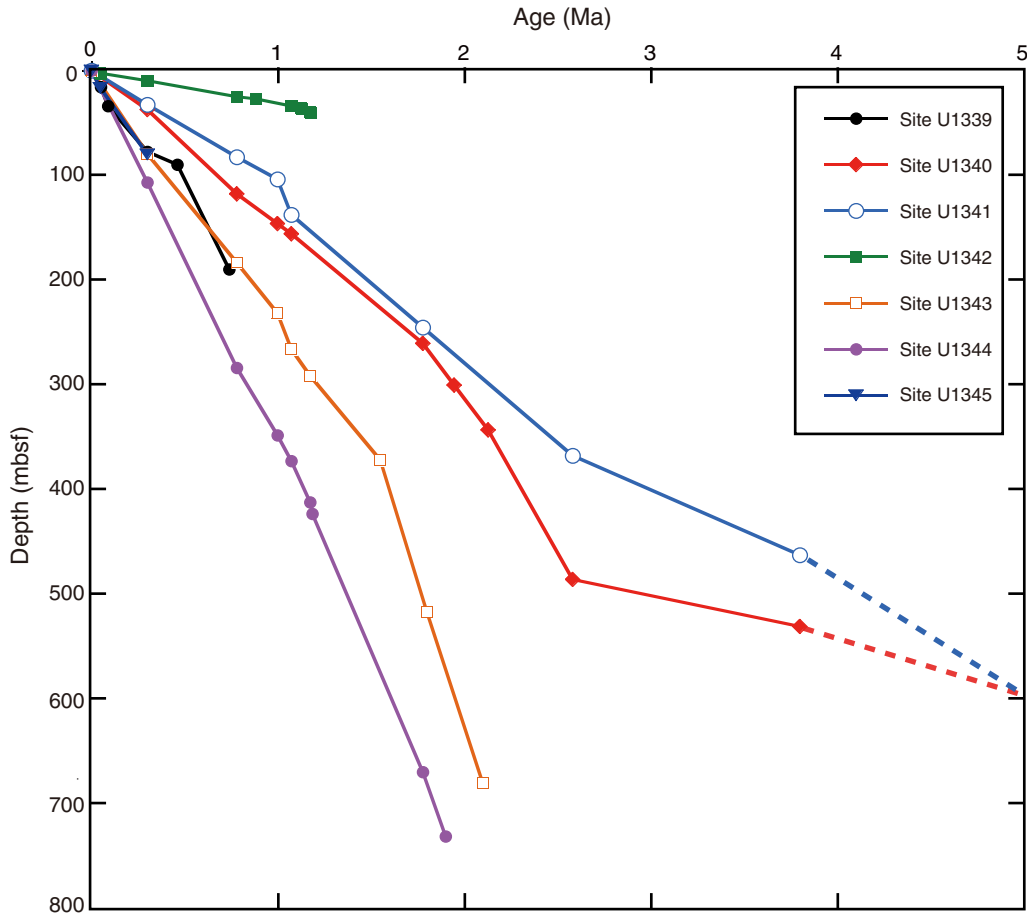


Figure F6. Location map showing Site U1340 on Bowers Ridge. Sites U1341 and U1342 are also shown.

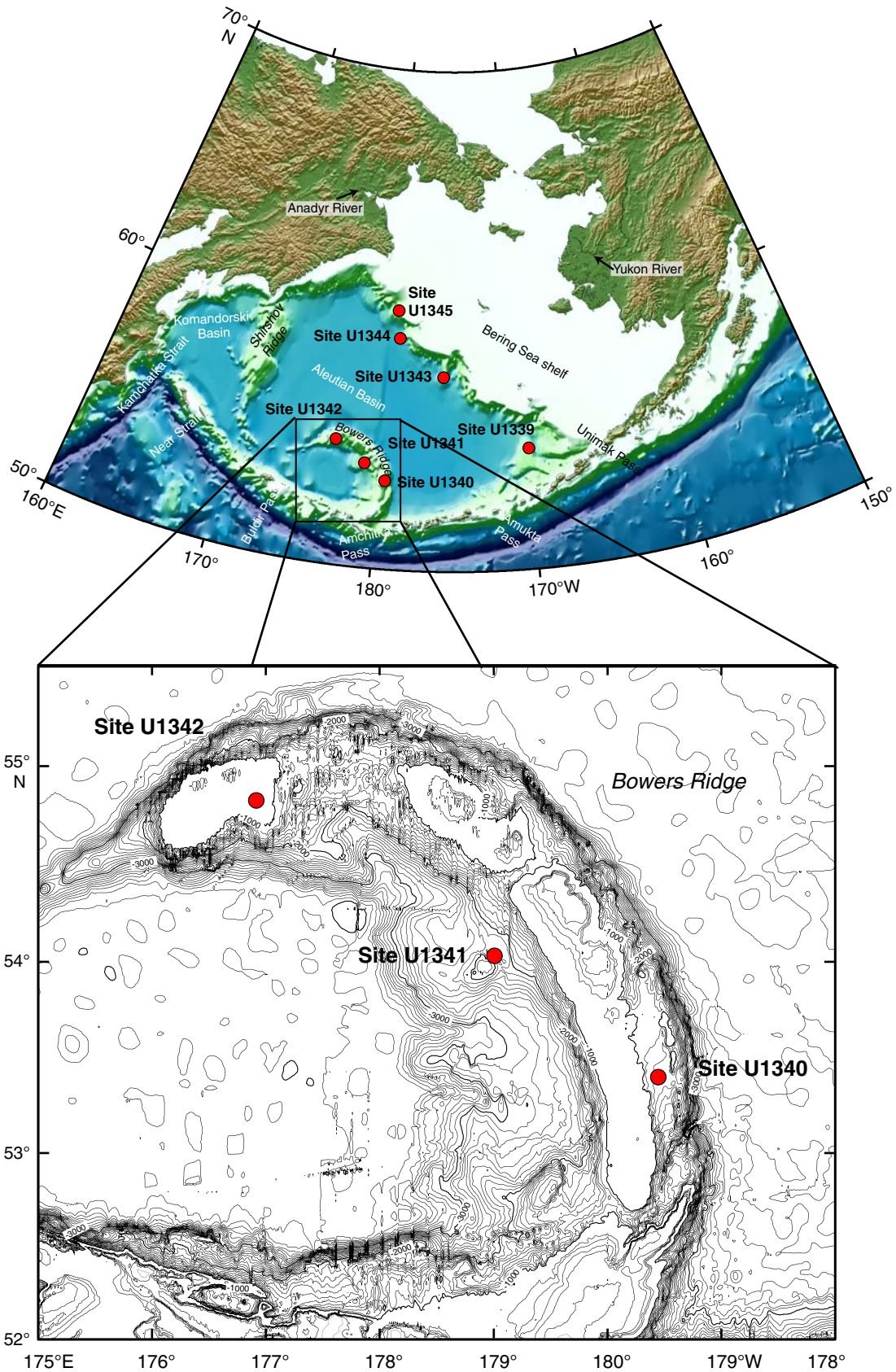


Figure F7. Location map showing Sites U1343, U1344, and U1345.

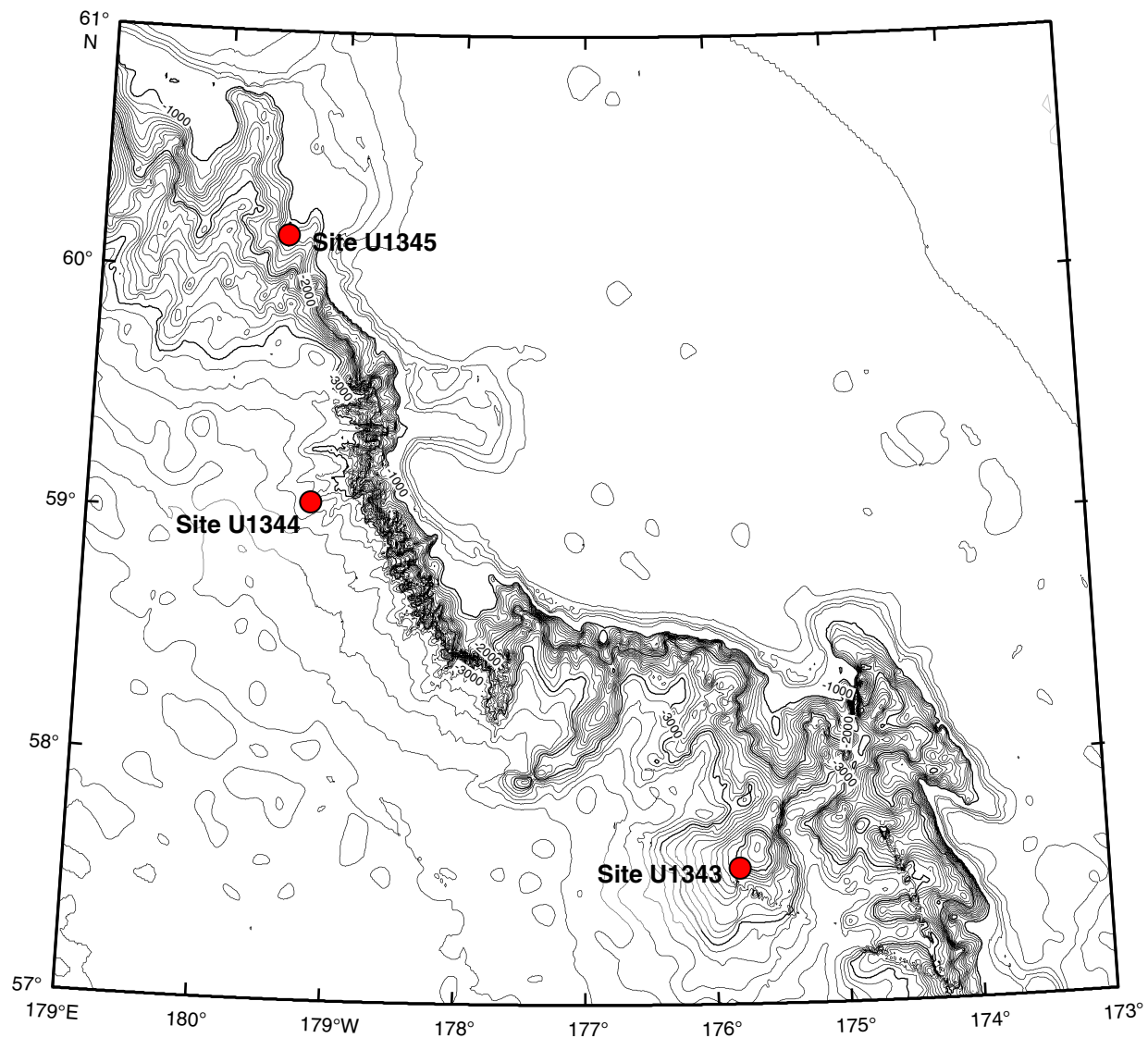




Figure F8. Map showing location of Site U1339 on Umnak Plateau and seismic navigation lines around Site U1339. See also “**Background and objectives**” in the “Site U1339” chapter.

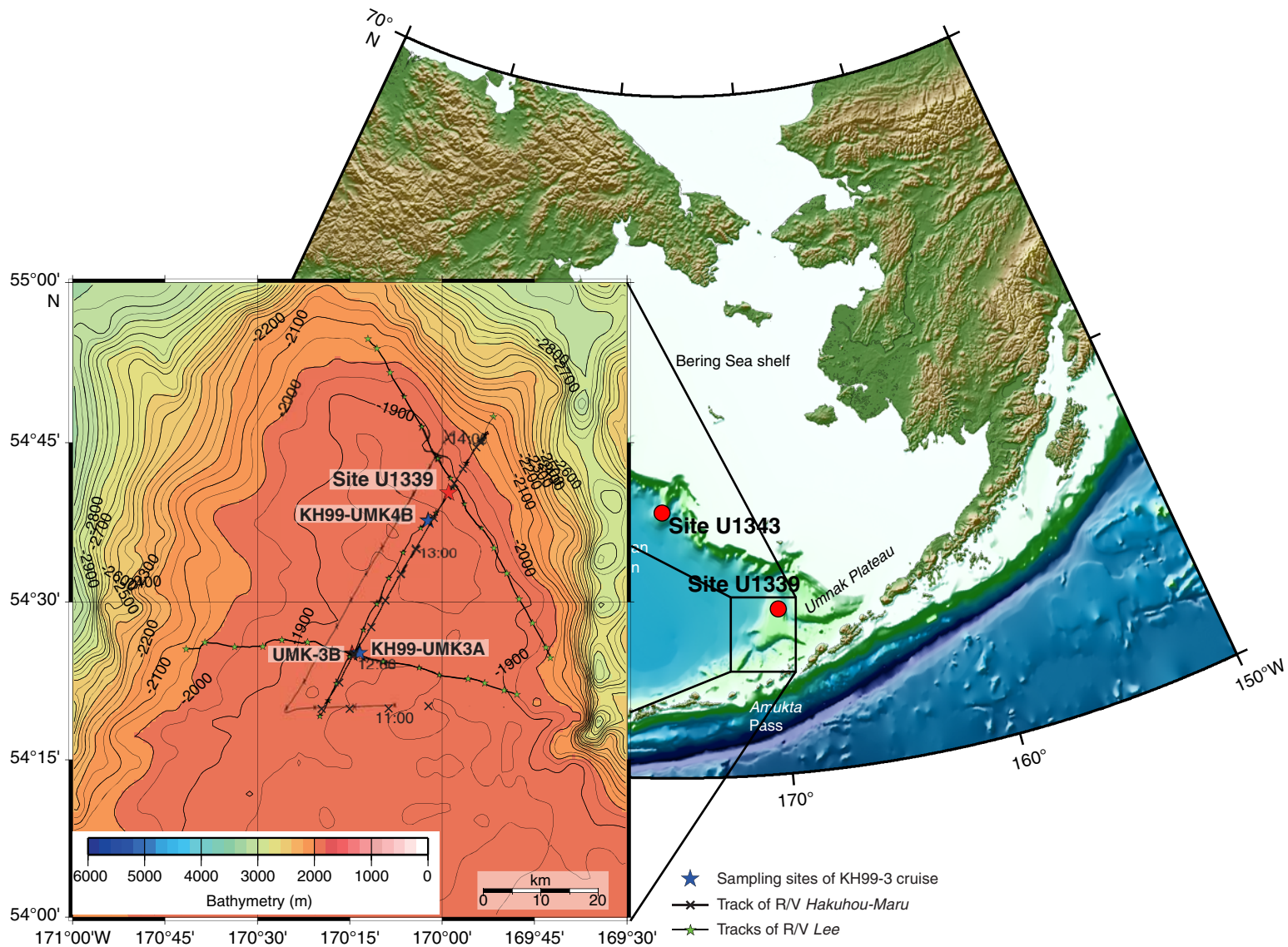


Figure F9. Age-depth plot for Hole U1340A showing biostratigraphic and paleomagnetic datums. Sedimentation rates are based only on paleomagnetic reversal data.

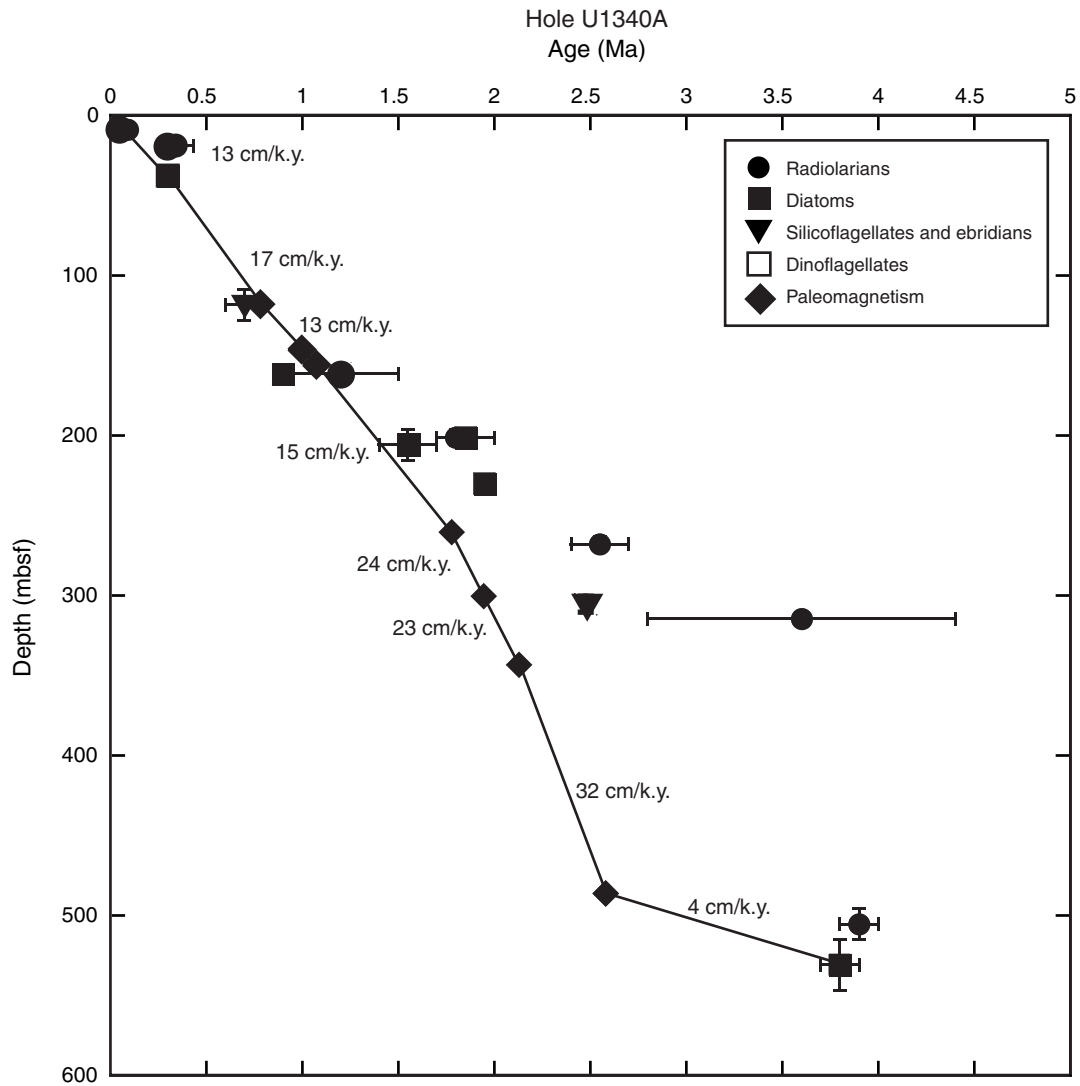


Figure F10. Age-depth plot for Site U1341 showing biostratigraphic and paleomagnetic datums. Sedimentation rates are based on paleomagnetic reversal data and a few biostratigraphic datums.

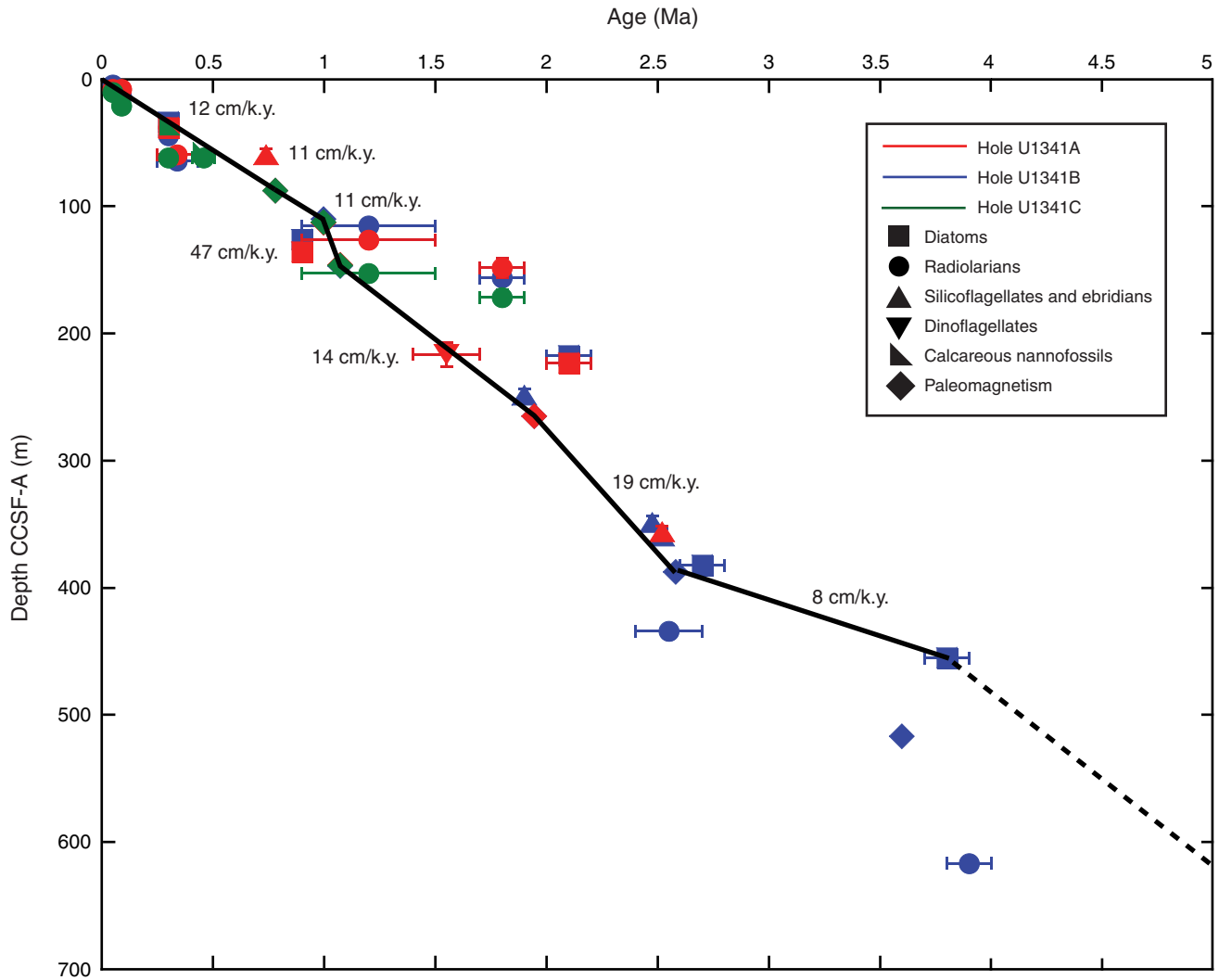


Figure F11. Age-depth plot for Site U1342 showing biostratigraphic and paleomagnetic datums. Sedimentation rates are based on paleomagnetic reversal data and a few biostratigraphic datums.

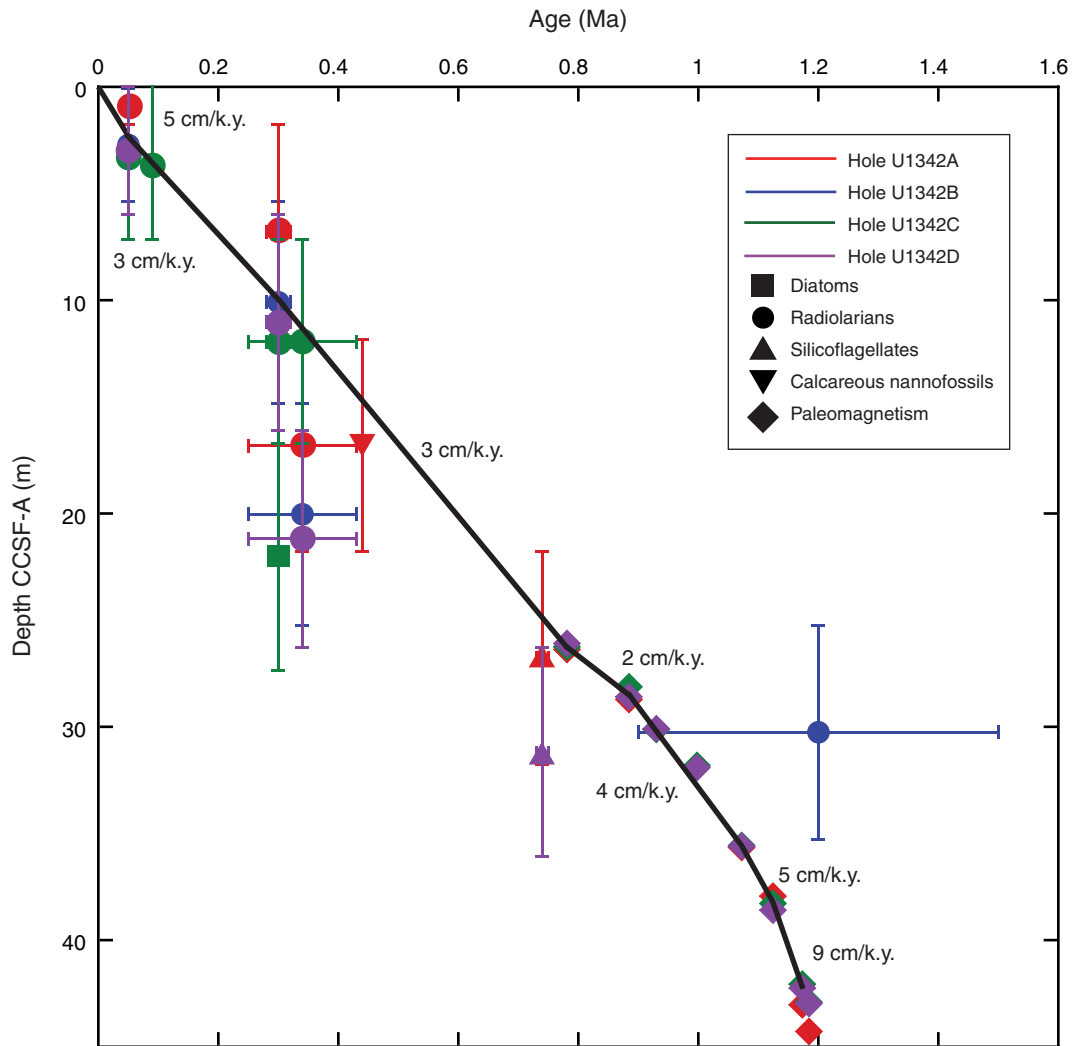


Figure F12. Age-depth plot for Site U1339. Note that four radiolarian datum levels appear below the line of the interpreted sedimentation rates because of unreliable datums caused by rare abundances of radiolarians *A. aquilonium* and *S. universus*, which occur extremely rarely in the samples.

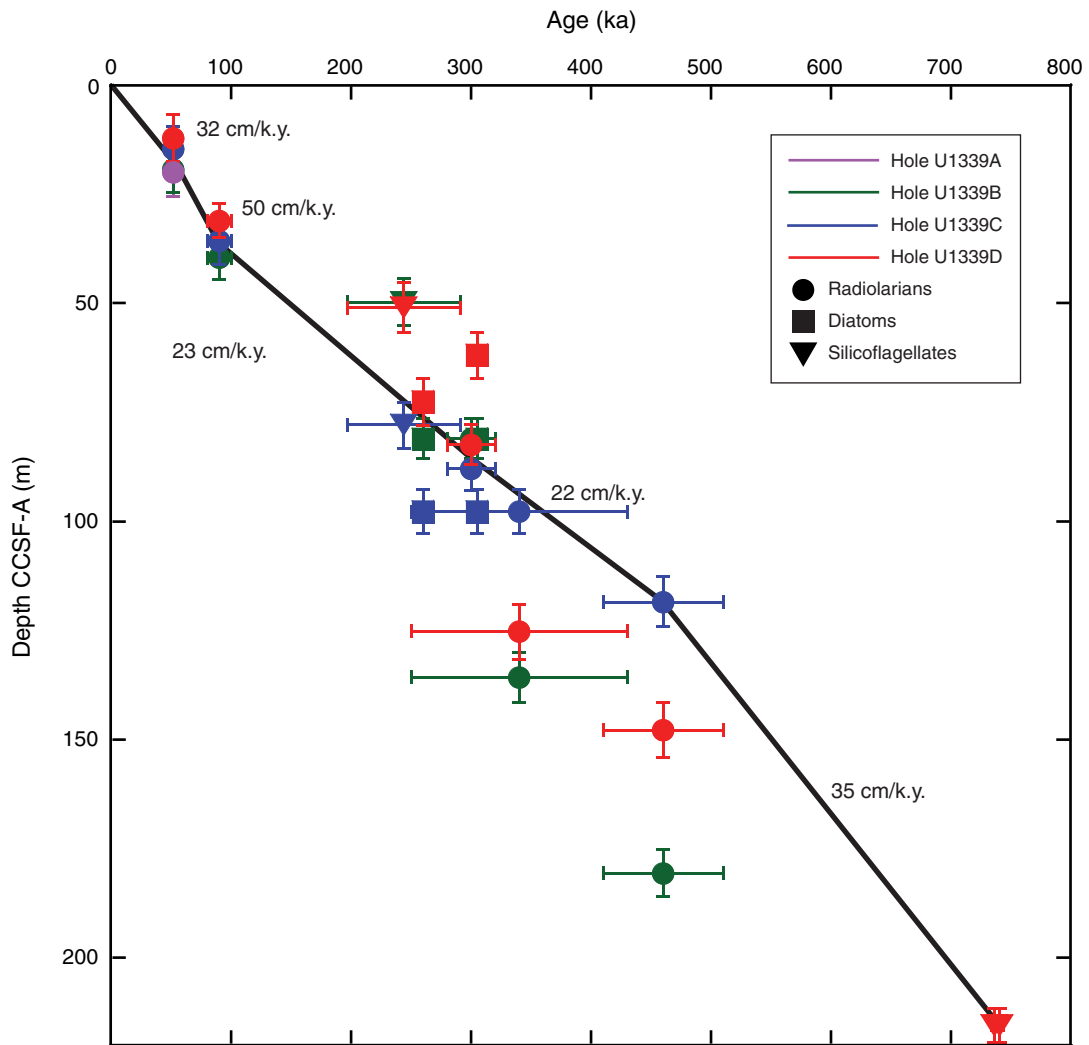


Figure F13. Age-depth plot for Site U1343 showing biostratigraphic and paleomagnetic datums.

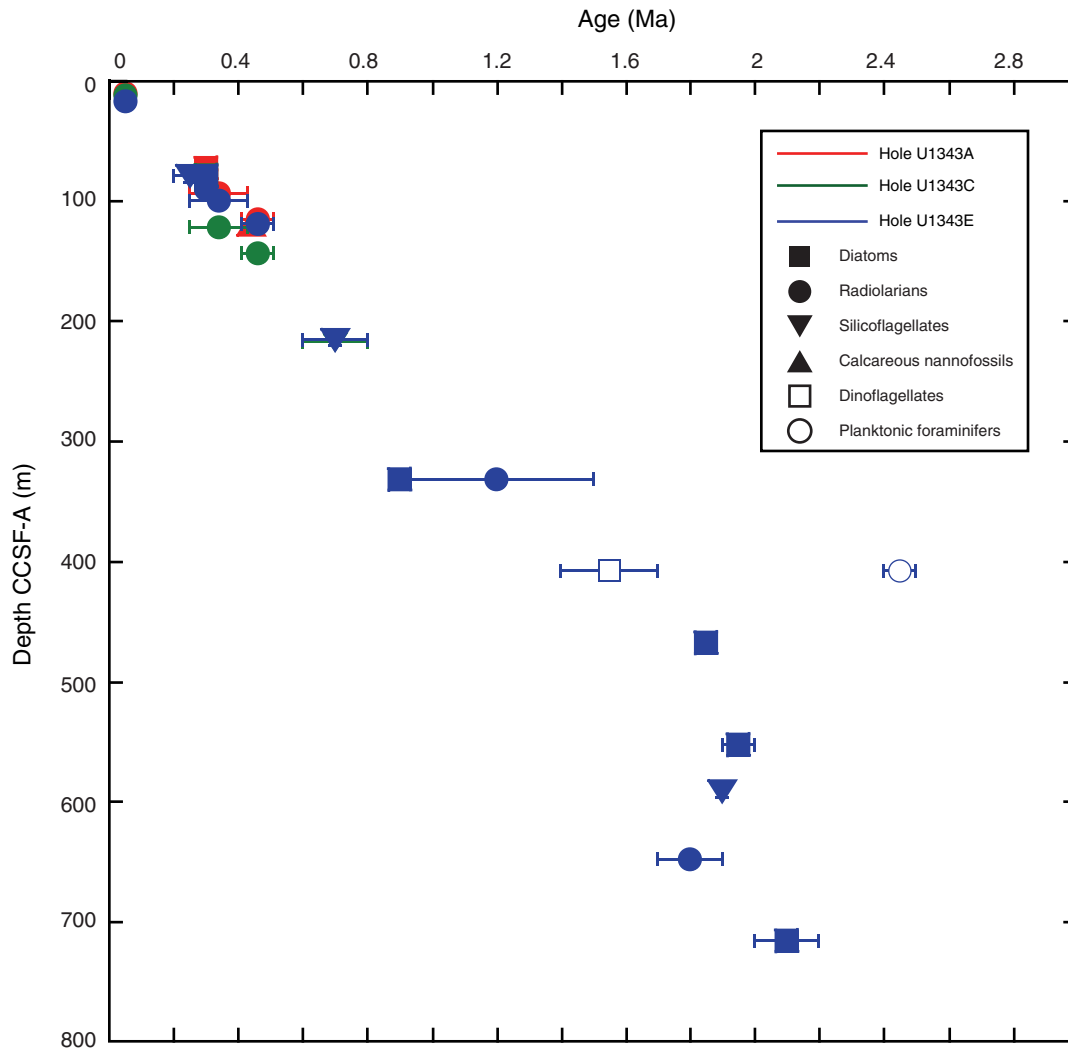


Figure F14. Age-depth plot for Site U1344 showing biostratigraphic and paleomagnetic datums. Sedimentation rates are based on paleomagnetic reversal data and a few biostratigraphic datums.

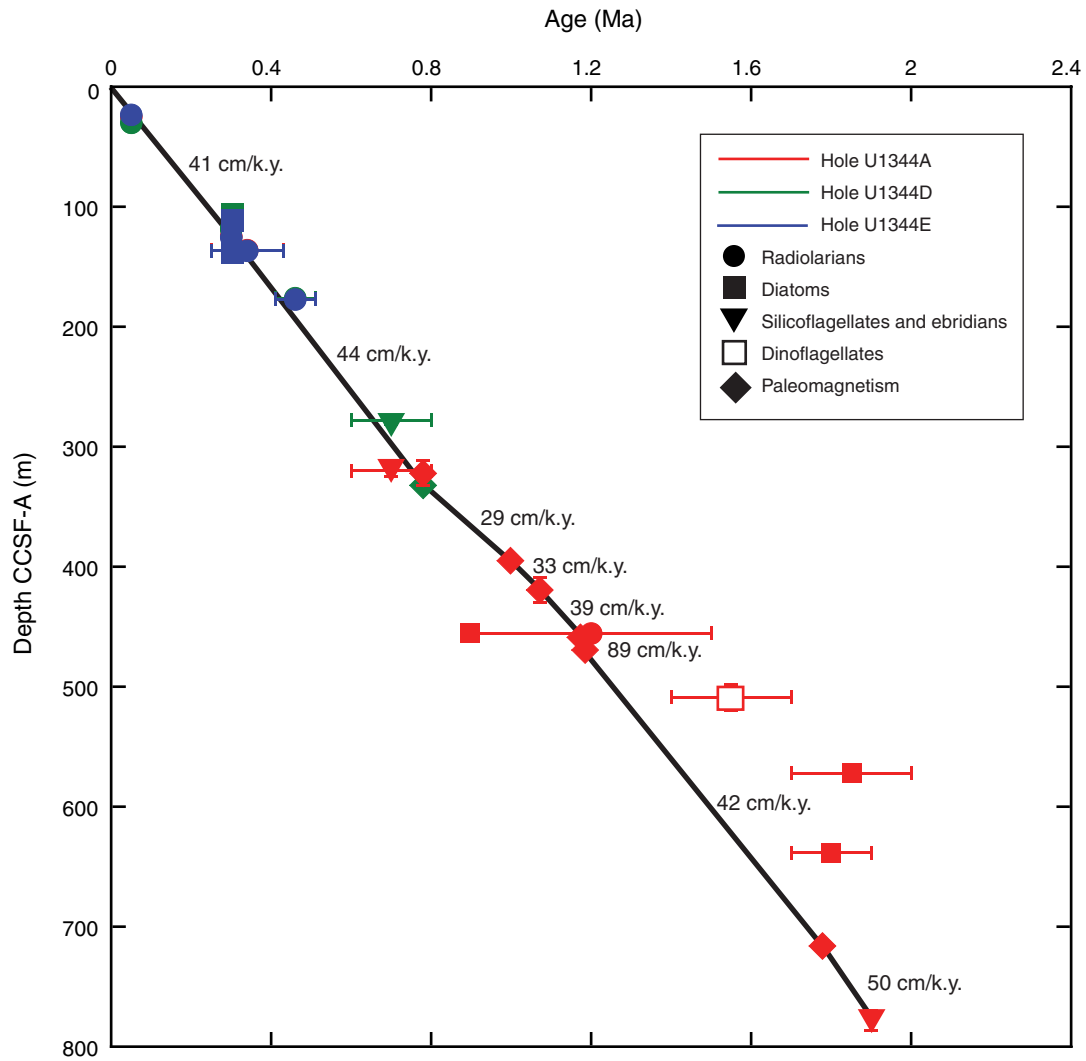


Figure F15. Age-depth plot for Site U1345 showing biostratigraphic and paleomagnetic datums. Sedimentation rates are based on paleomagnetic reversal data and a few biostratigraphic datums.

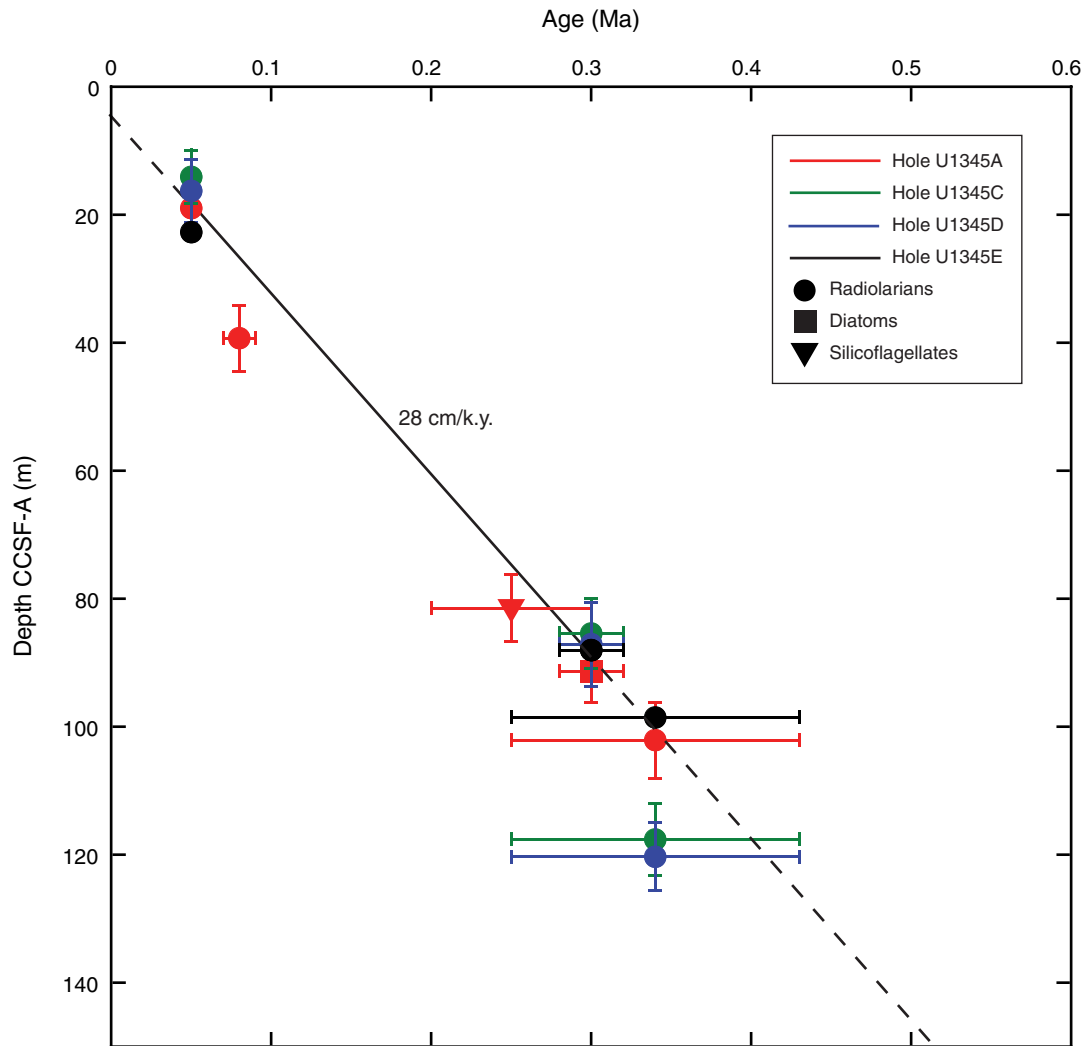


Figure F16. Lithostratigraphic summary of Expedition 323 drill sites. Natural gamma ray (NGR) data are plotted along with lithology.

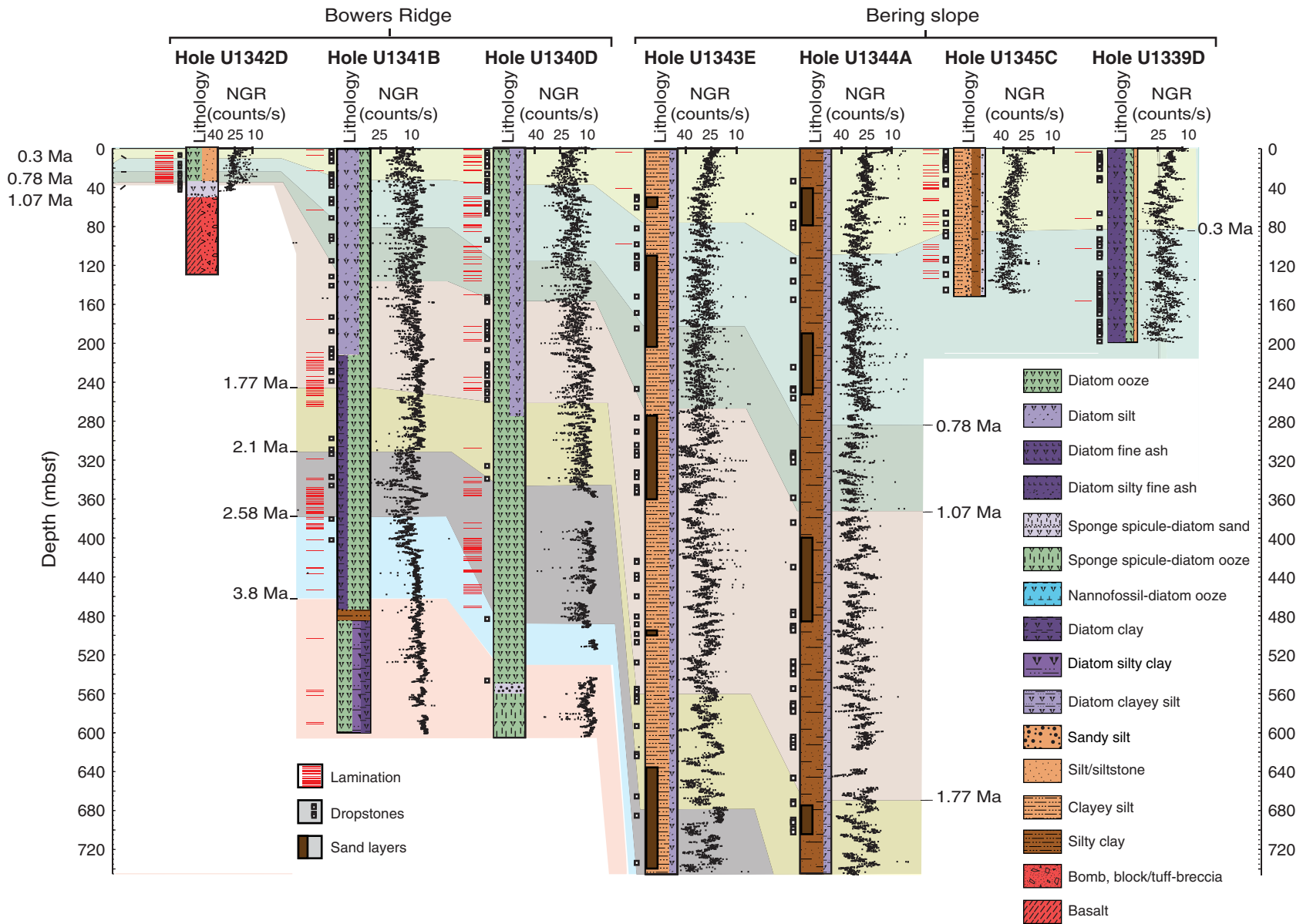




Figure F17. Summary of some shipboard analyses at Site U1340: core recovery, core images, lithology and lithologic units and subunits, age, paleomagnetic chronology, zone of biostratigraphically important radiolarians, diatoms, and silicoflagellates, and spliced records of natural gamma radiation (NGR), gamma ray attenuation (GRA) bulk density, magnetic susceptibility, and color reflectance parameter b^* .

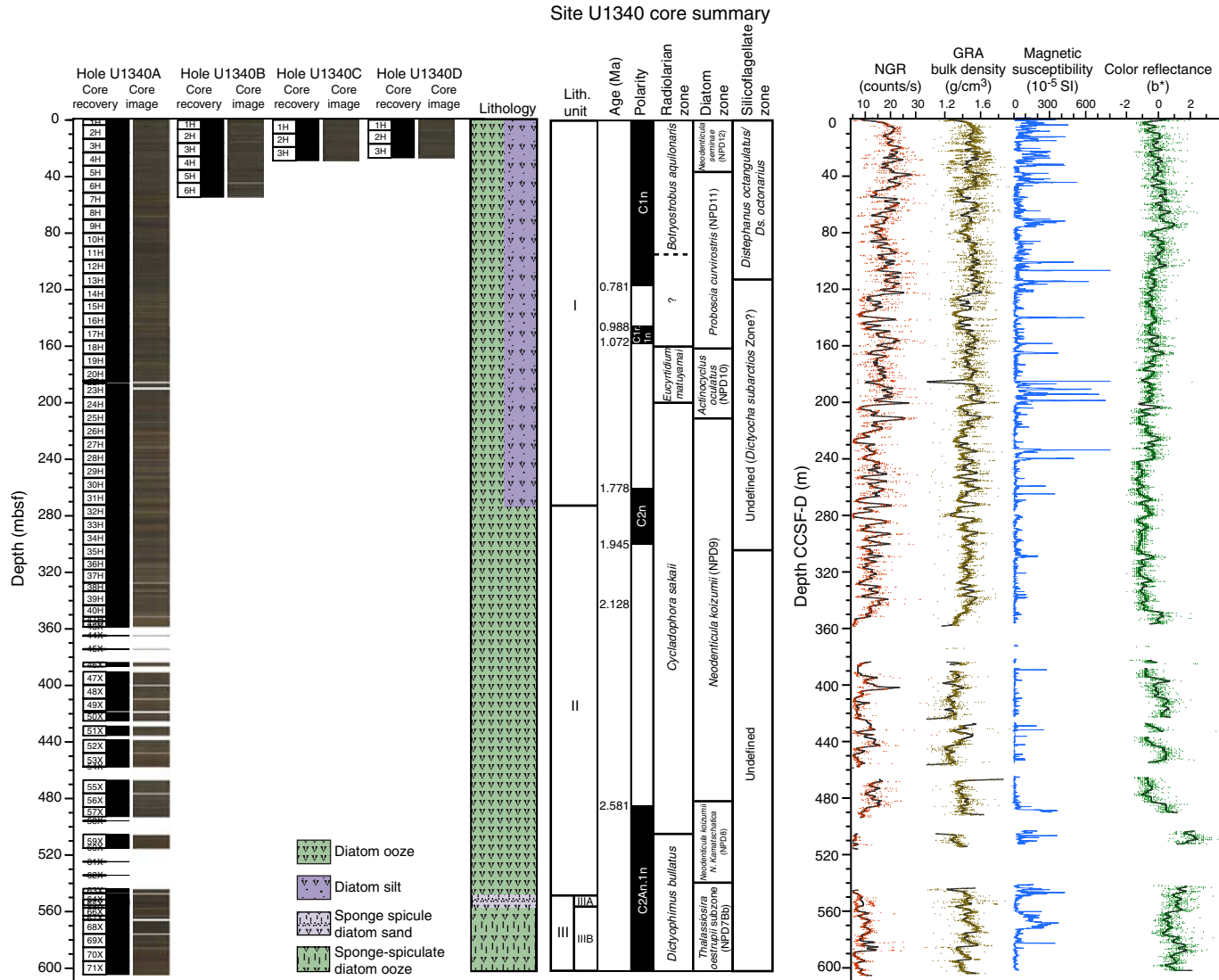




Figure F18. Summary of some shipboard analyses at Site U1341: core recovery, core images, lithology, lithologic units and subunits, age, paleomagnetic chronology, zone of biostratigraphically important radiolarians, diatoms, and silicoflagellates, and spliced records of natural gamma radiation (NGR), gamma ray attenuation (GRA) bulk density, magnetic susceptibility, and color reflectance parameter b^* .

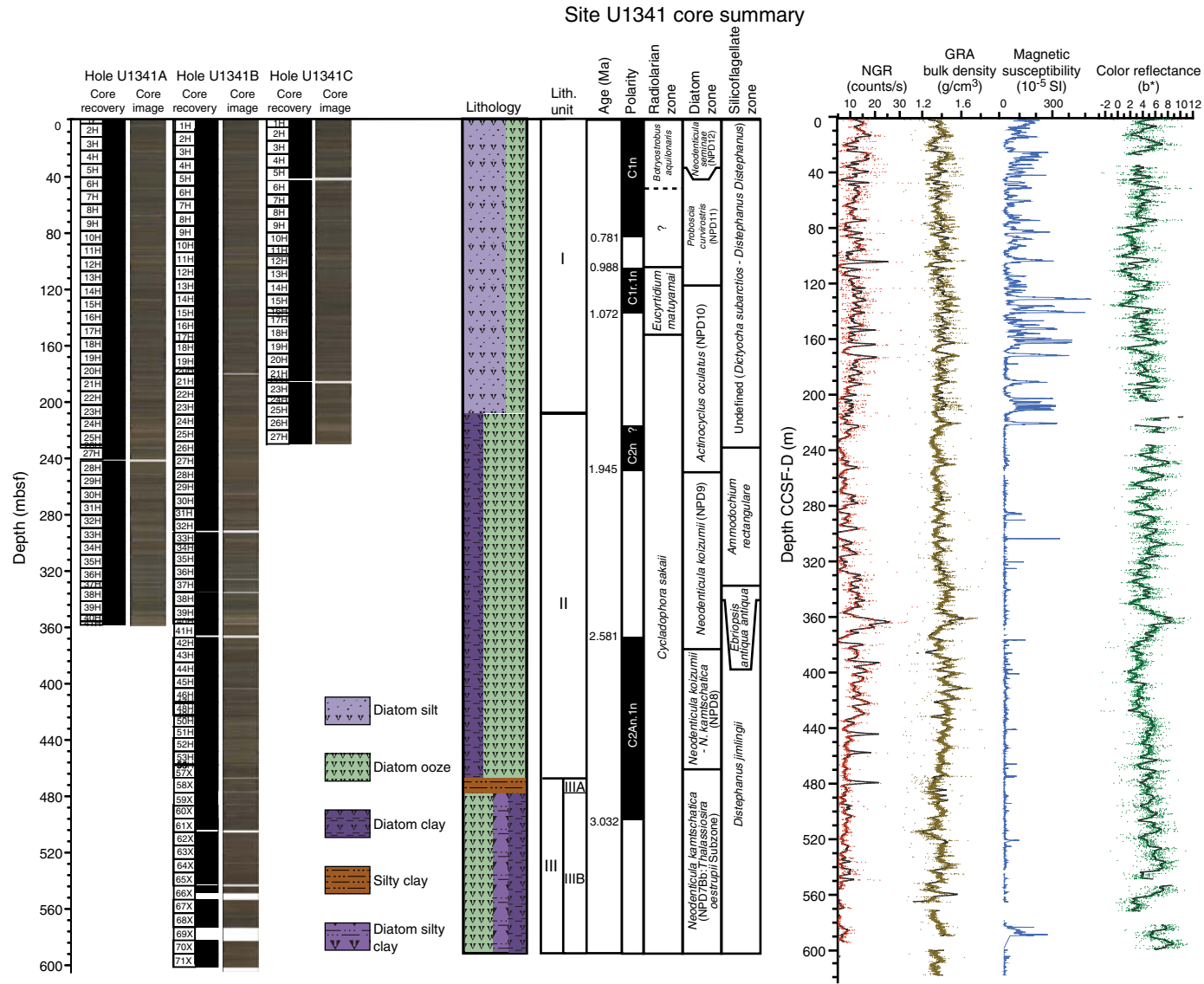




Figure F19. Summary of some shipboard analyses at Site U1342: core recovery, core images, lithology, lithologic units and subunits, age, paleomagnetic chronology, zone of biostratigraphically important radiolarians, diatoms, and silicoflagellates, and spliced records of natural gamma radiation (NGR), gamma ray attenuation (GRA) bulk density, magnetic susceptibility, and color reflectance parameter b^* .

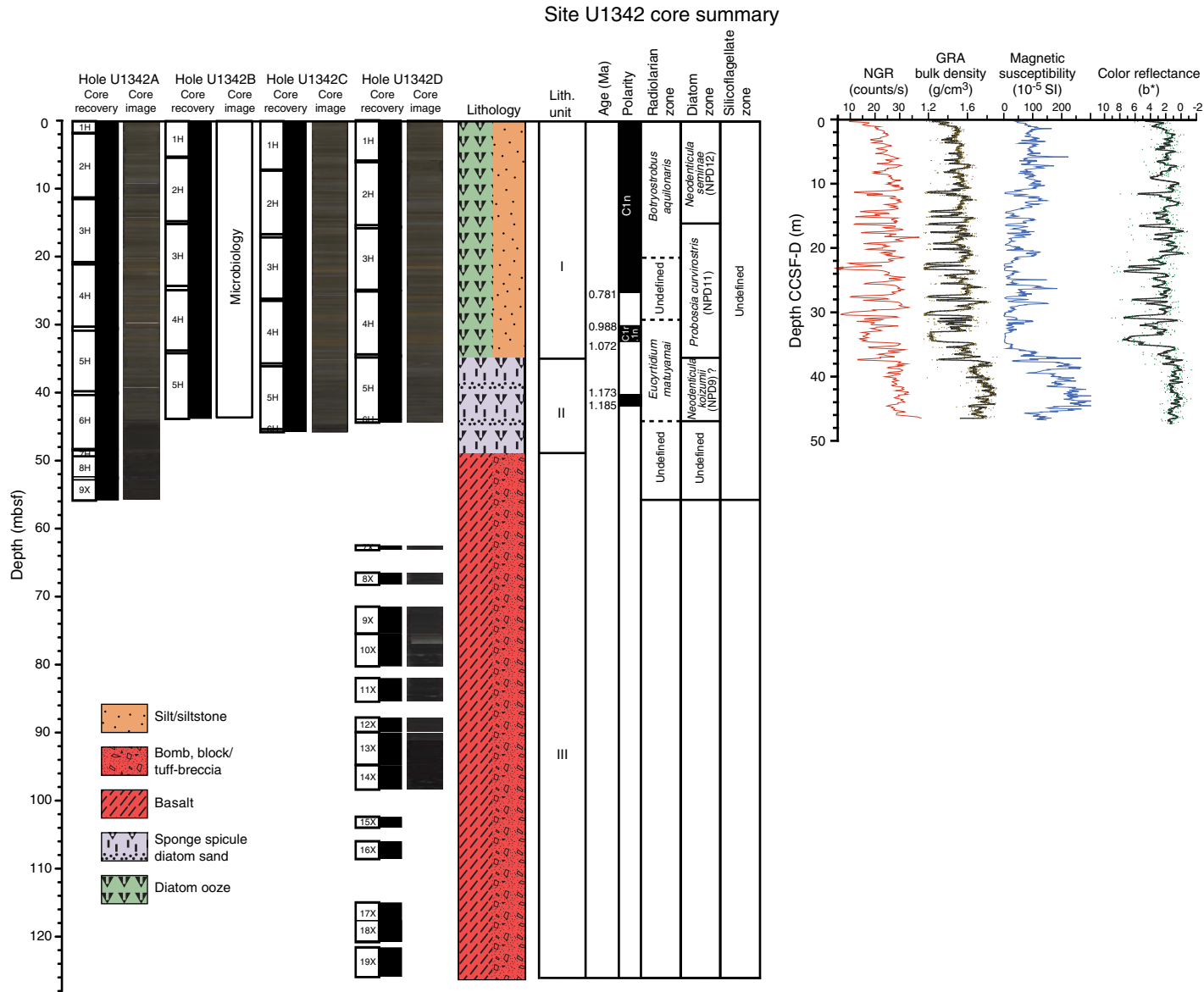




Figure F20. Summary of some shipboard analyses at Site U1339: core recovery, core images, lithology, lithologic units and subunits, age, paleomagnetic chronology, zone of biostratigraphically important radiolarians, diatoms, and silicoflagellates, and spliced records of natural gamma radiation (NGR), gamma ray attenuation (GRA) bulk density, magnetic susceptibility, and color reflectance parameter b^* .

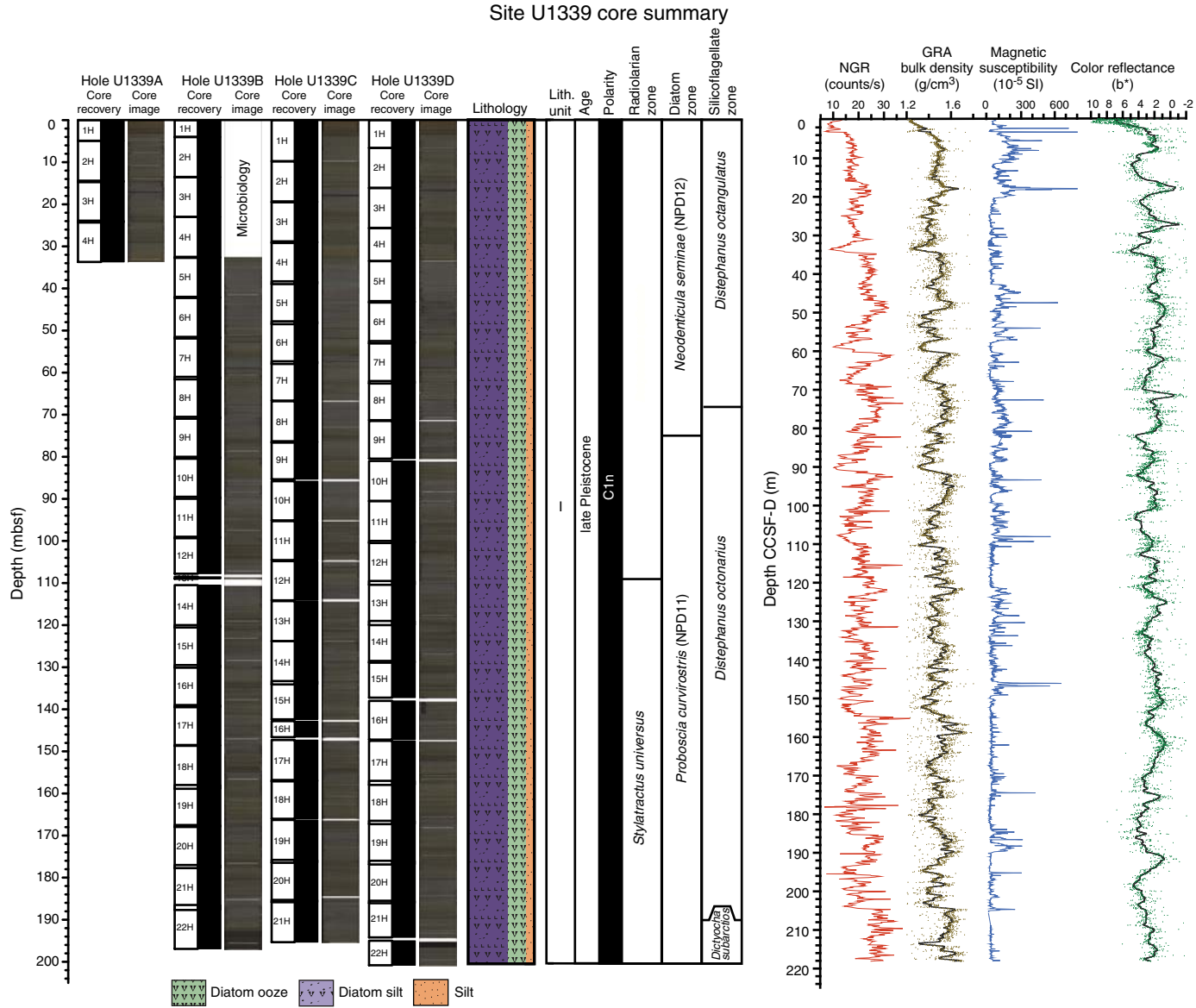




Figure F21. Summary of some shipboard analyses at Site U1343: core recovery, core images, lithology, lithologic units and subunits, age, paleomagnetic chronology, zone of biostratigraphically important radiolarians, diatoms, and silicoflagellates, and spliced records of natural gamma radiation (NGR), gamma ray attenuation (GRA) bulk density, magnetic susceptibility, and color reflectance parameter b^* .

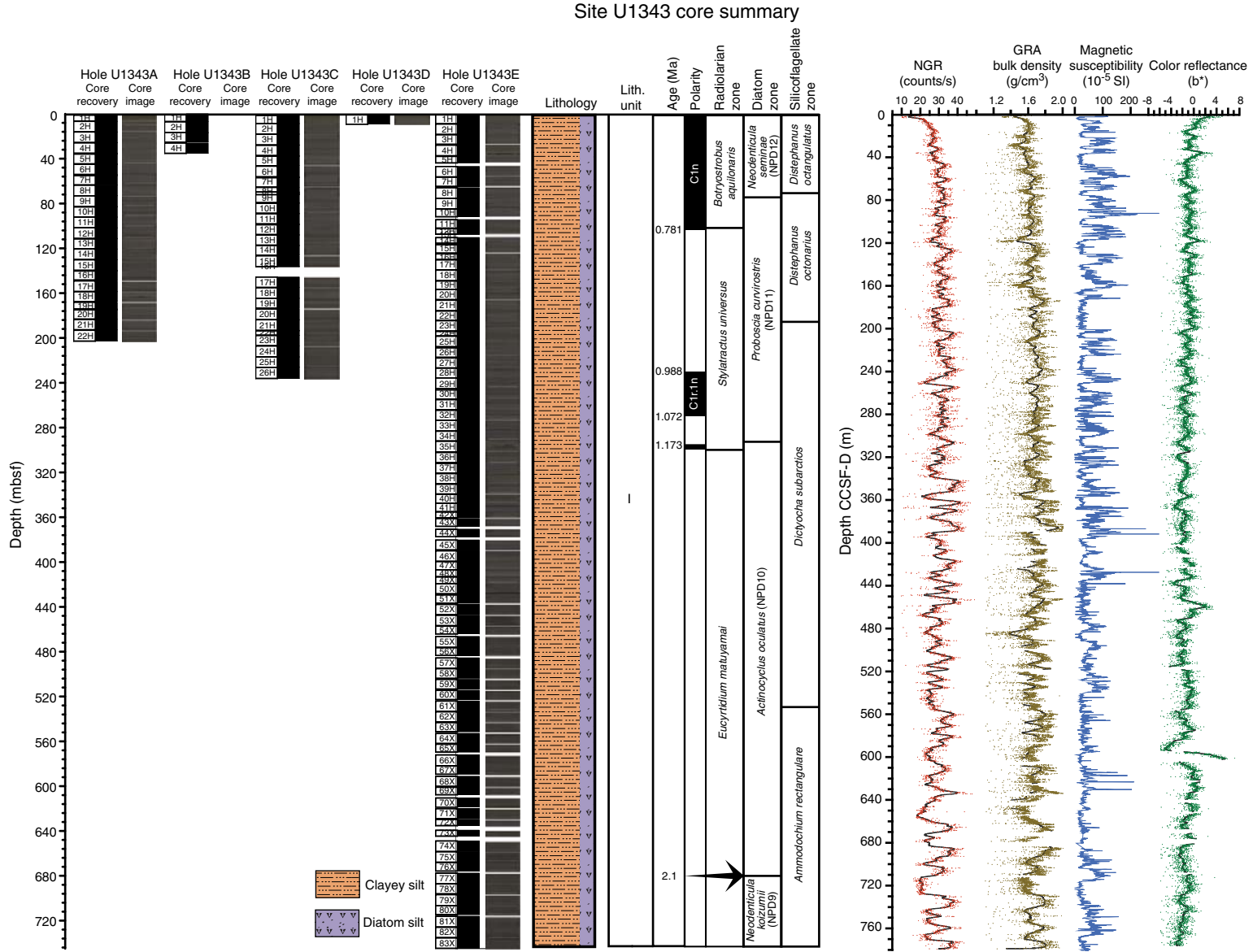




Figure F22. Summary of some shipboard analyses at Site U1344: core recovery, core images, lithology, lithologic units and subunits, age, paleomagnetic chronology, zone of biostratigraphically important radiolarians, diatoms, and silicoflagellates, and spliced records of natural gamma radiation (NGR), gamma ray attenuation (GRA) bulk density, magnetic susceptibility, and color reflectance parameter b*.

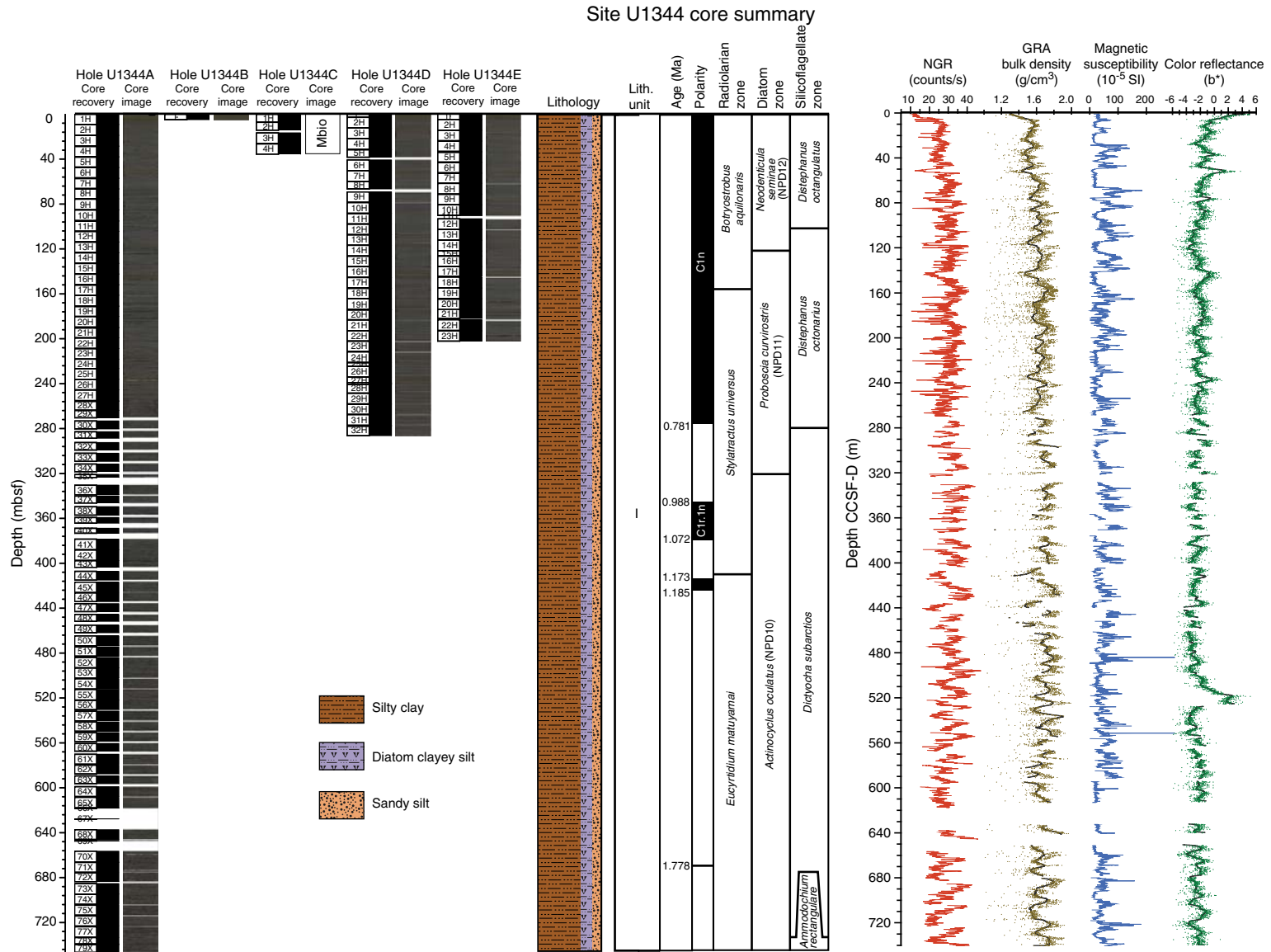




Figure F23. Summary of some shipboard analyses at Site U1345: core recovery, core images, lithology, lithologic units and subunits, age, paleomagnetic chronology, zone of biostratigraphically important radiolarians, diatoms, and silicoflagellates, and spliced records of natural gamma radiation (NGR), gamma ray attenuation (GRA) bulk density, magnetic susceptibility, and color reflectance parameter b^* .

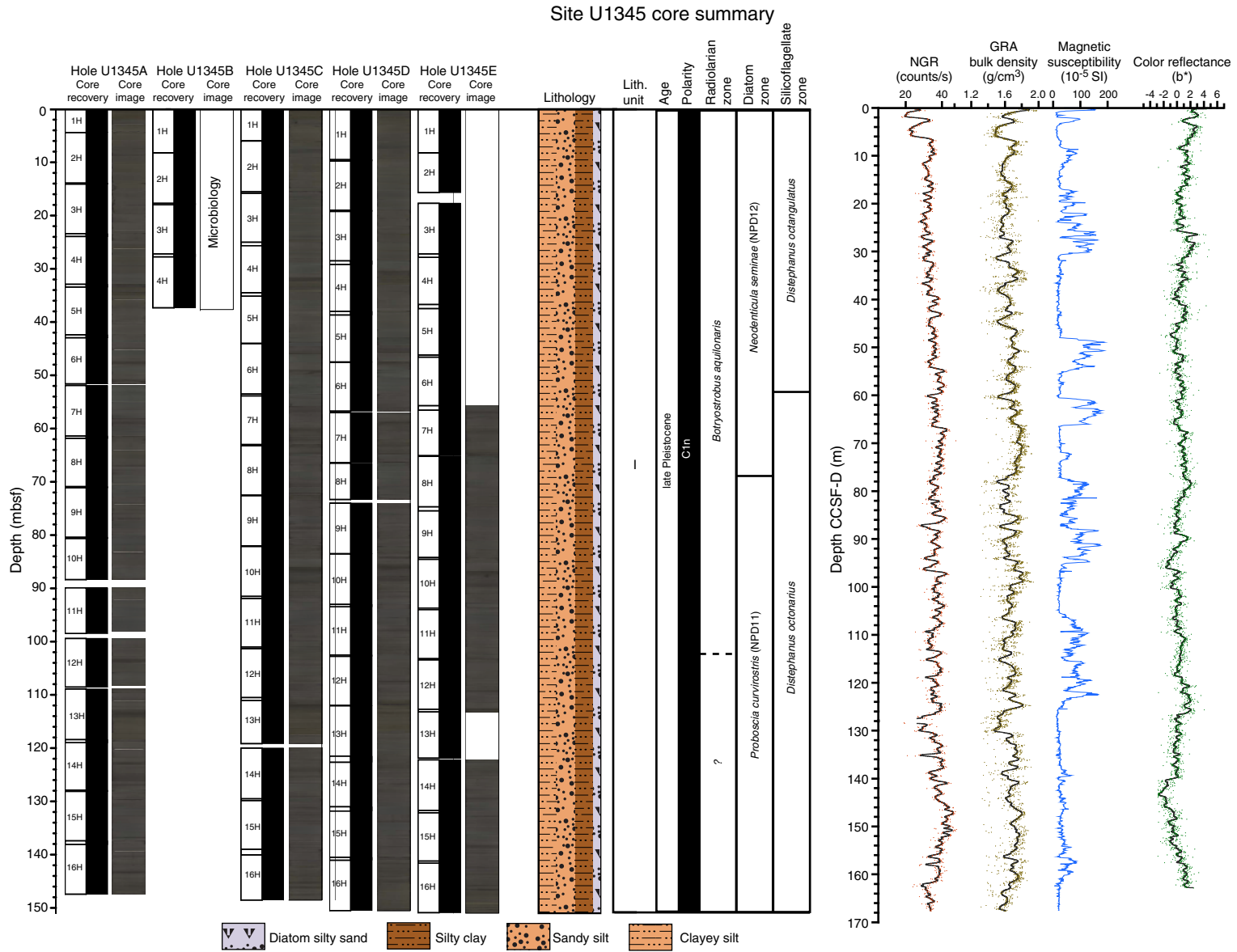


Figure F24. Variations in potassium content measured by downhole logging in Holes U1341B, U1343E, and U1344A, illustrating changes in frequency and amplitude. Biostratigraphic (black) and paleomagnetic (red) age estimates are also shown.

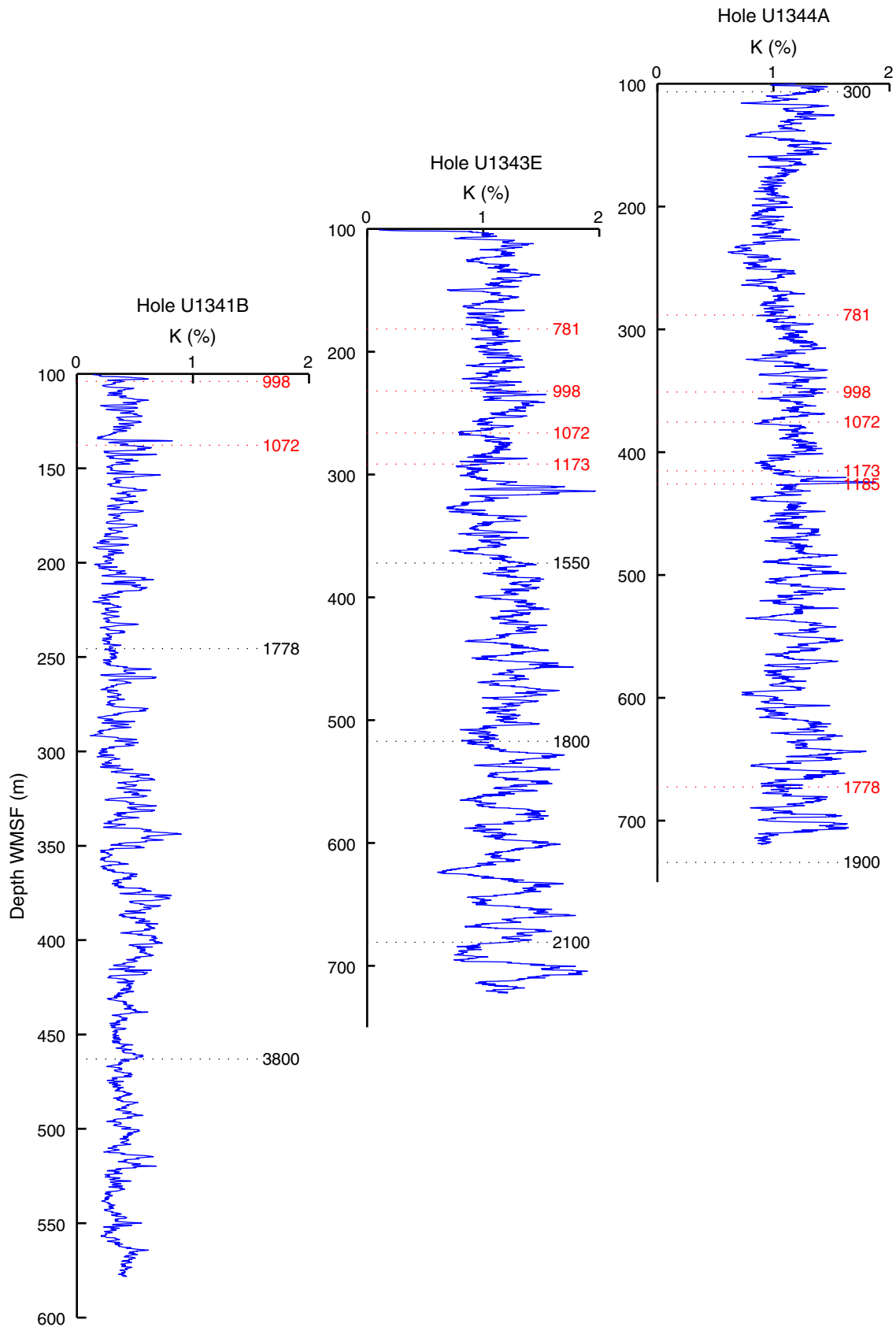




Figure F25. Variations in the ratio of natural remanent magnetization (NRM) to magnetic susceptibility (MS), or relative paleointensity, along with biostratigraphic (black) and paleomagnetic (red) age estimates in k.y. for the seven drill sites (see Tables T3, T4, T5, T6, T7, T8, T9).

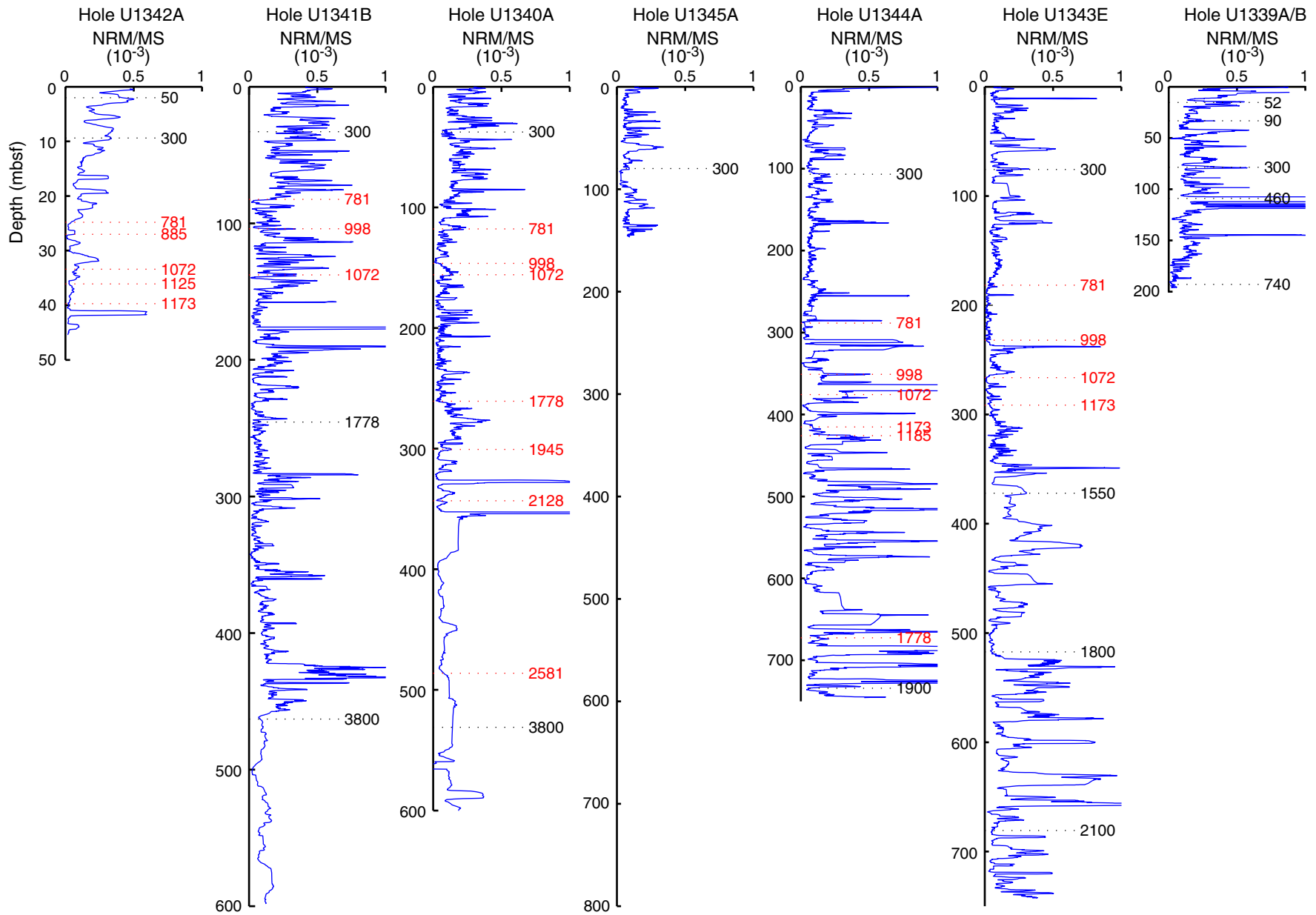


Figure F26. Changes in sea ice coverage derived from sea ice diatoms such as *Thalassiosira antarctica* spores and sea ice dinoflagellates (e.g., *Islandinium minutum*) at the seven drill sites. **A.** Sites U1342, U1341, and U1340. (Continued on next page.)

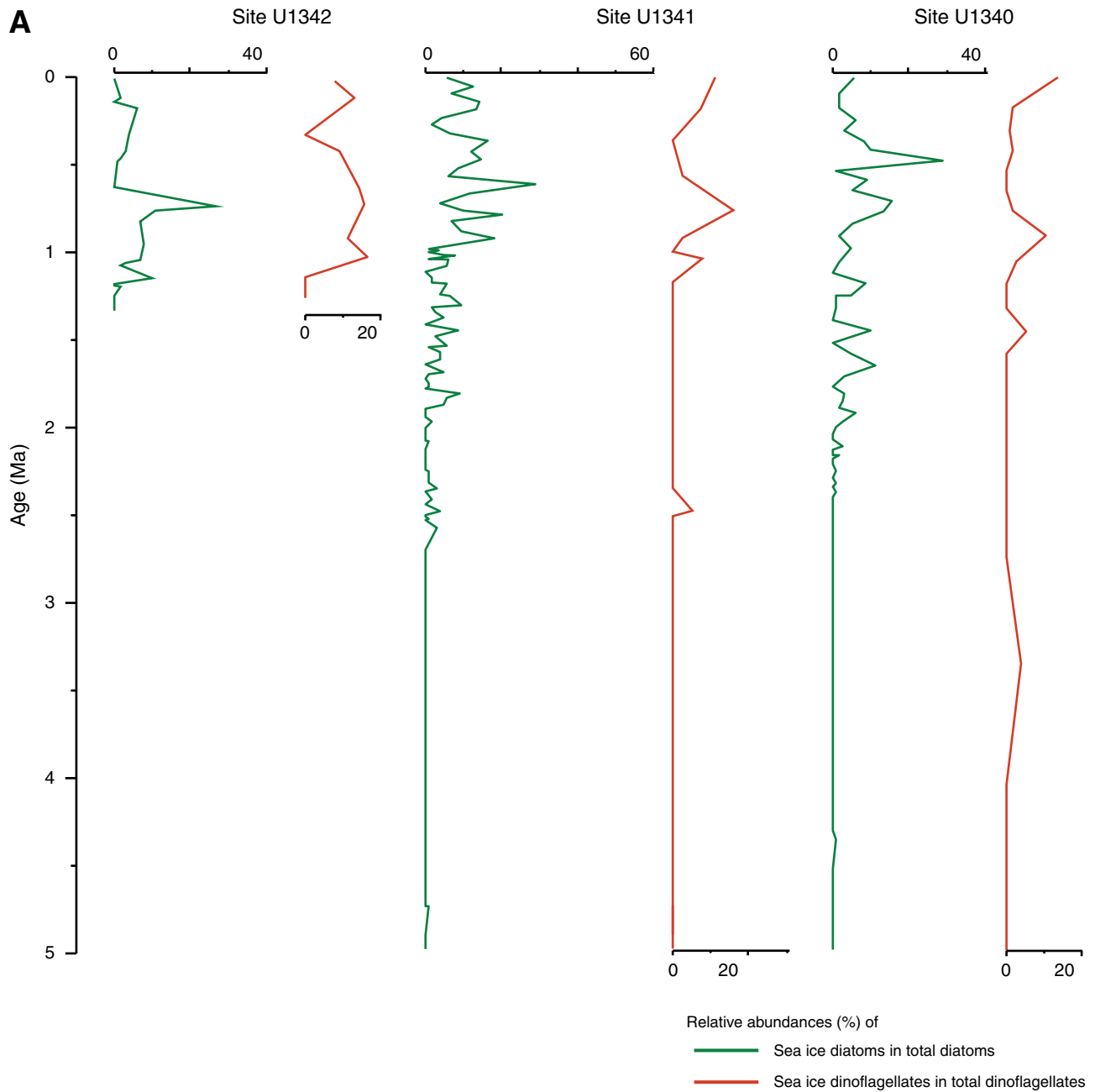


Figure F26 (continued). B. Sites U1345, U1344, U1343, and U1339.

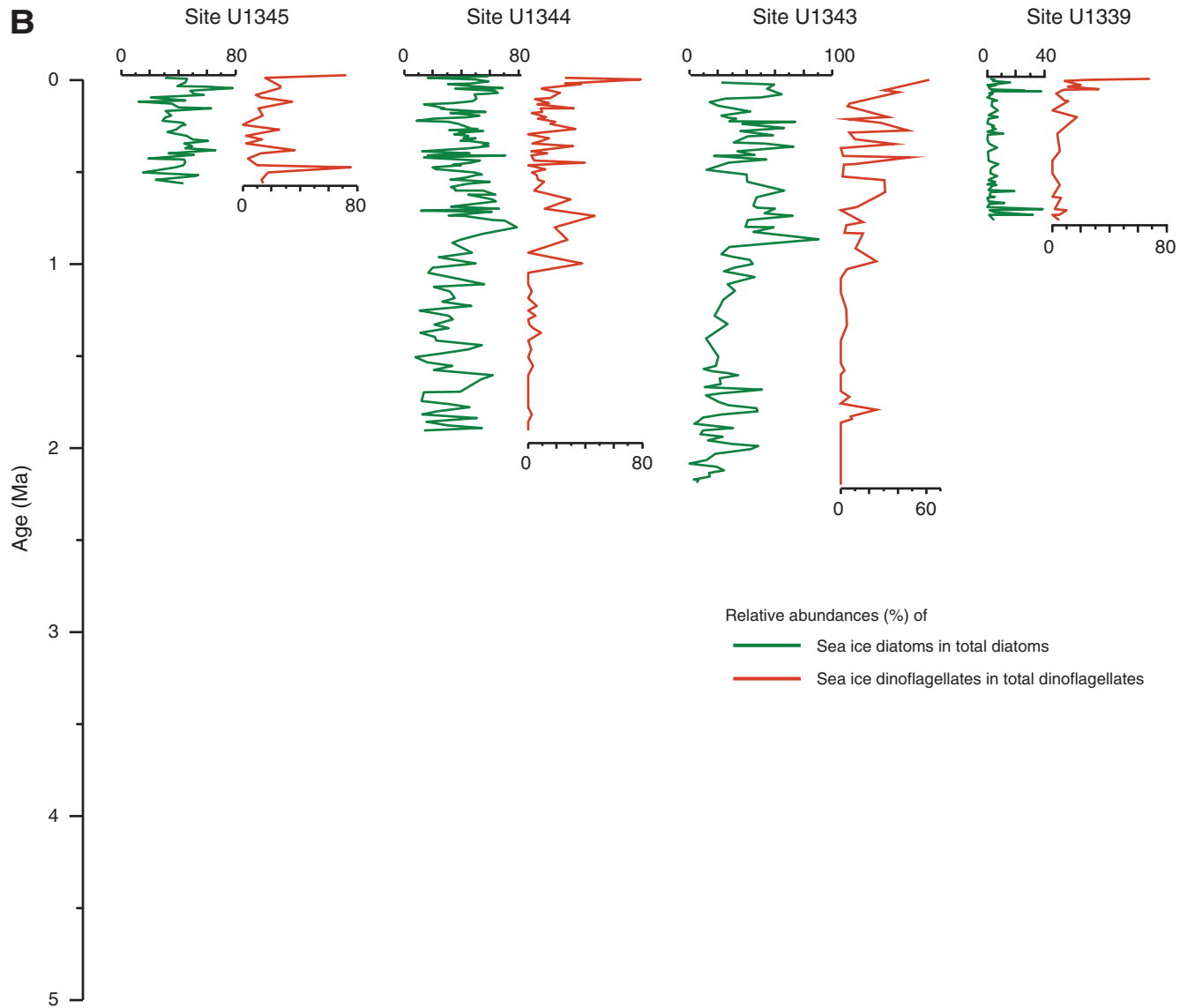




Figure F27. Changes in biological productivity and temperature at the seven drill sites, as depicted by variations in *Neodenticula* spp., *Actinocyclus* spp., *Coscinodiscus marginatus*, and heavily silicified *Stephanopyxis* spp. A. Sites U1342, U1341, and U1340. (Continued on next page.)

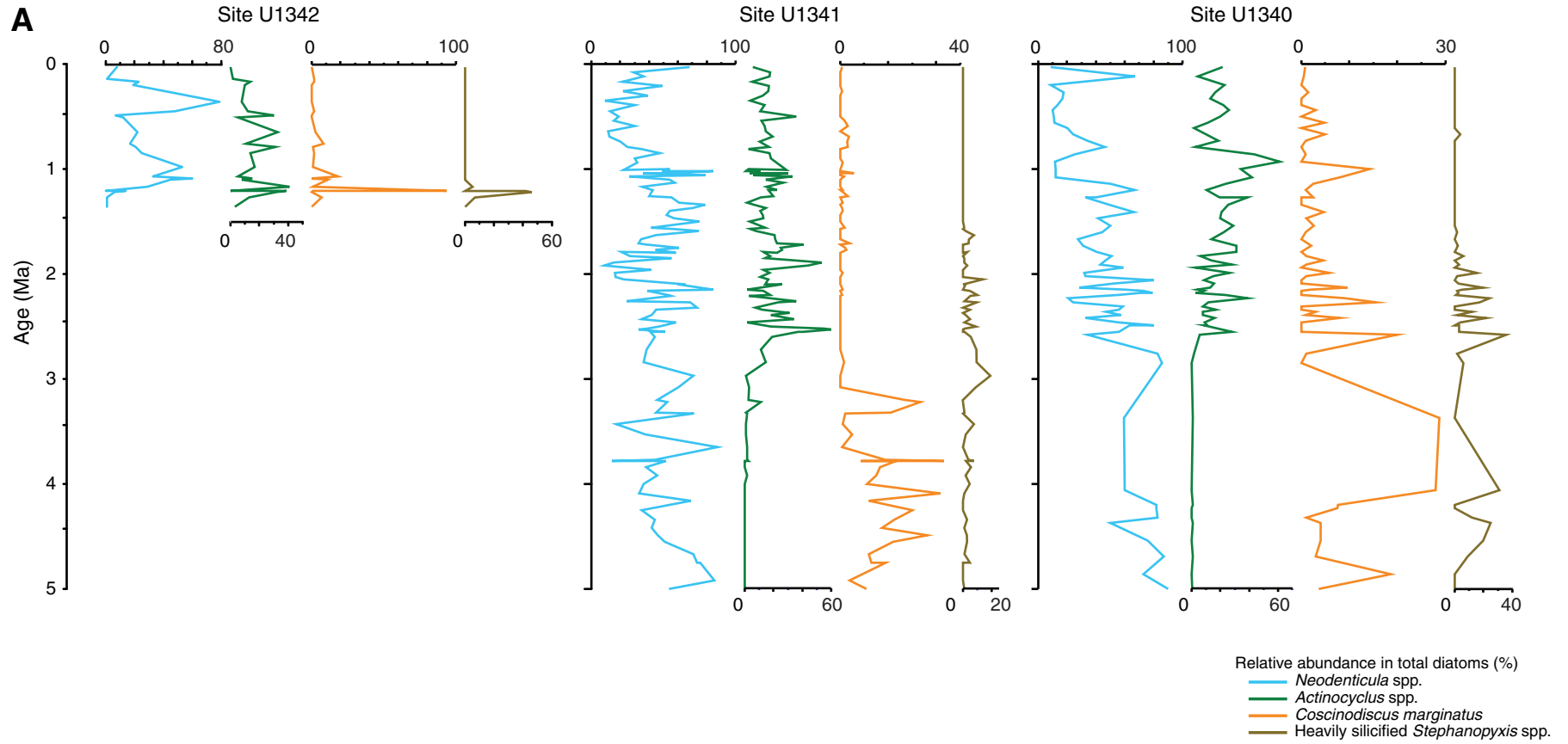




Figure F27 (continued). B. Sites U1345, U1344, U1343, and U1339.

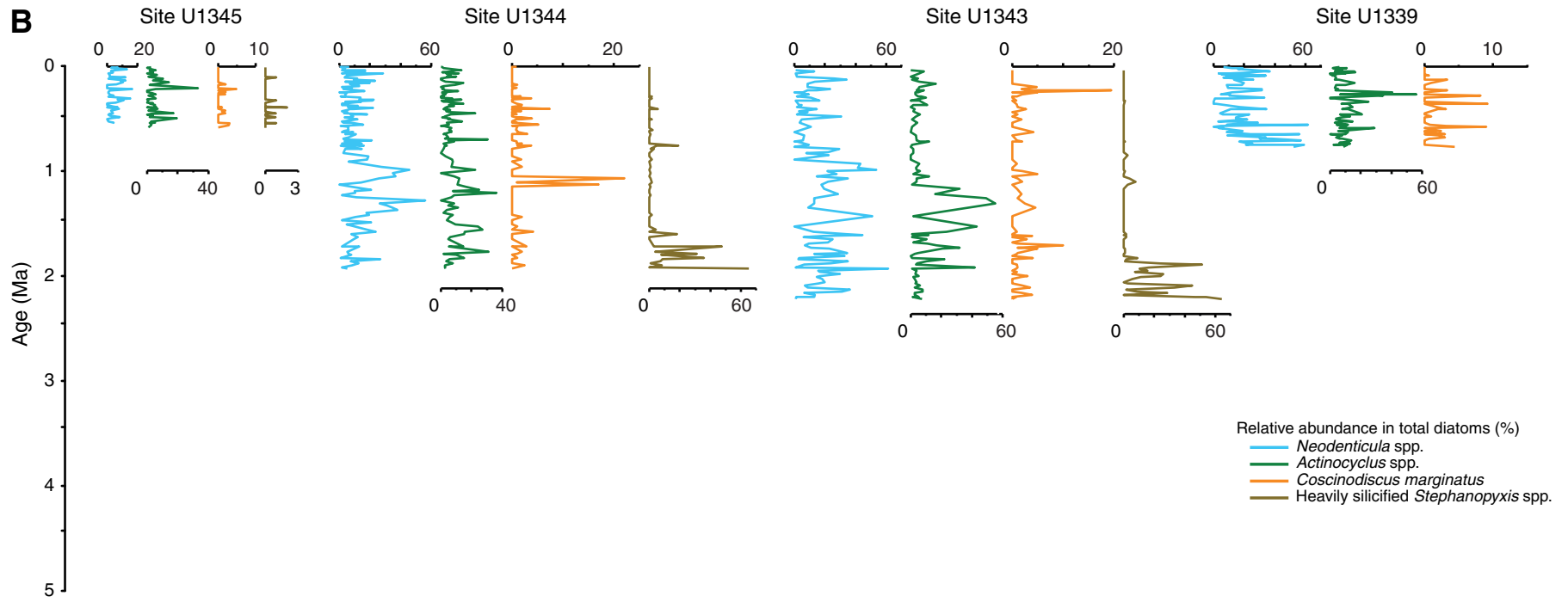


Figure F28. Changes in the relative abundance of the deep infaunal assemblage of benthic foraminifers related to low dissolved-oxygen content in bottom waters at the seven drill sites. The deep infaunal assemblage includes *Bolivina* spp., *Brizalina* cf. *spathula*, *Brizalina earlandi*, *Brizalina pygmaea*, *Bulimina* spp., *Cassidulina* spp., *Cassidulinoides tenuis*, *Fursenkoina* spp., *Globobulimina* spp., *Globocassidulina* spp., *Nonionella* spp., and *Stainforthia* aff. *fusiformis*.

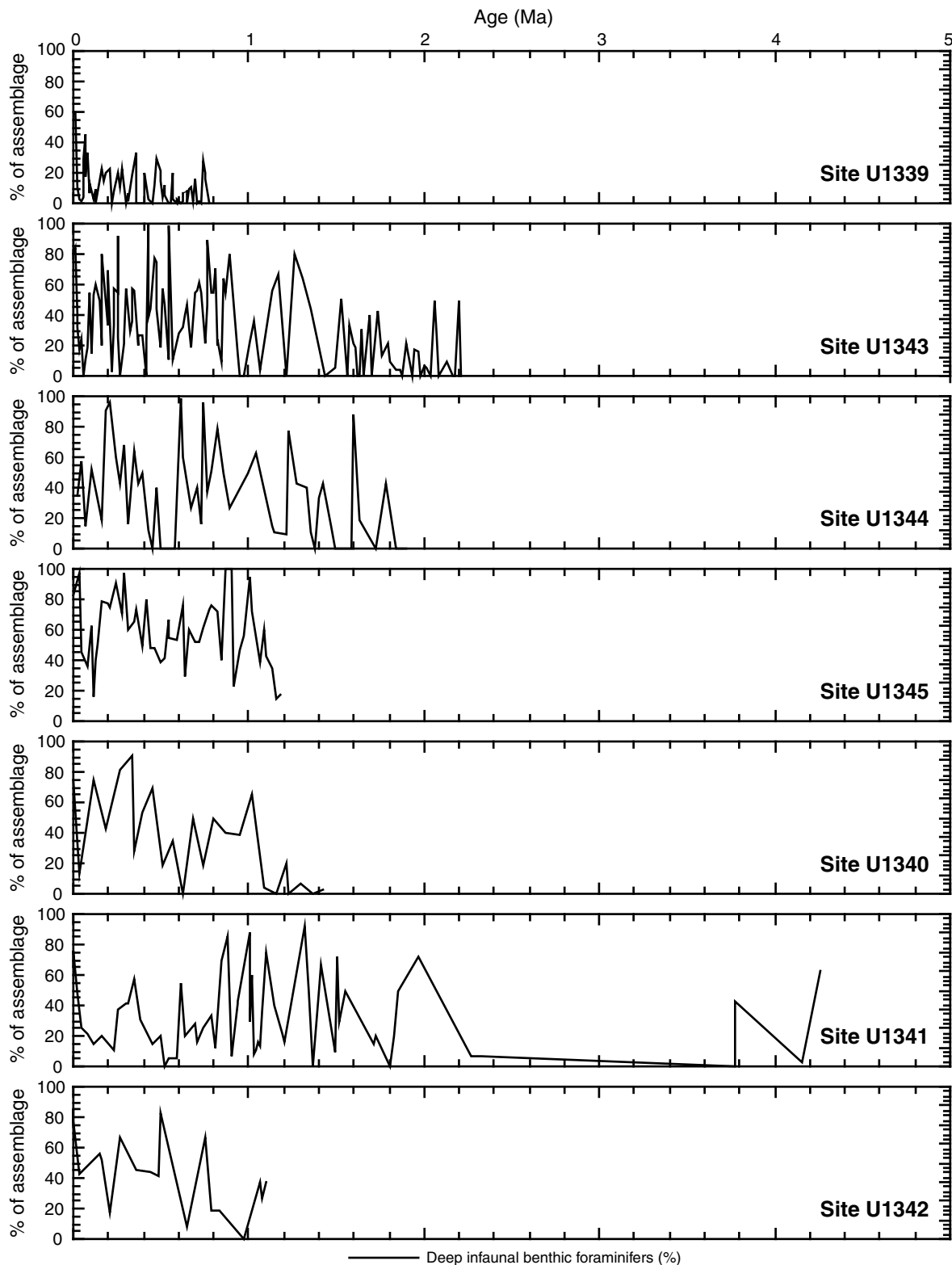




Figure F29. Changes in deep infaunal benthic foraminifers *Eggerella bradyi* and *Martinottiella communis* and intermediate water-dwelling radiolarian *Cycladophora davisiana* at Sites U1340 and U1341, indicating the bottom water ventilation history in the Bering Sea.

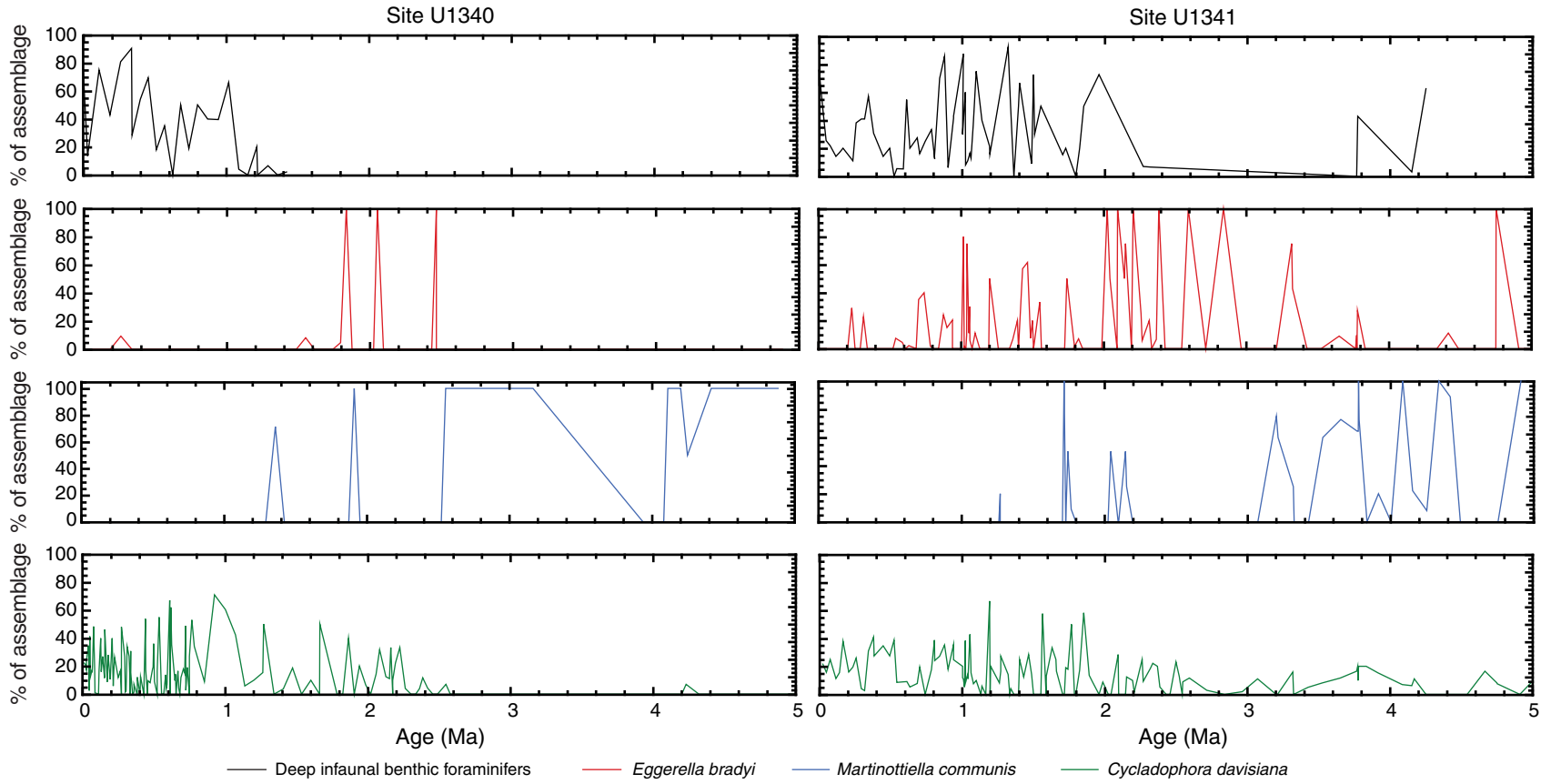




Figure F30. Depth variations in dissolved inorganic carbon (DIC), ammonium, sulfate, and sulfide, illustrating the depth of the SMTZ at Sites U1339, U1342, U1343, U1344, and U1345.

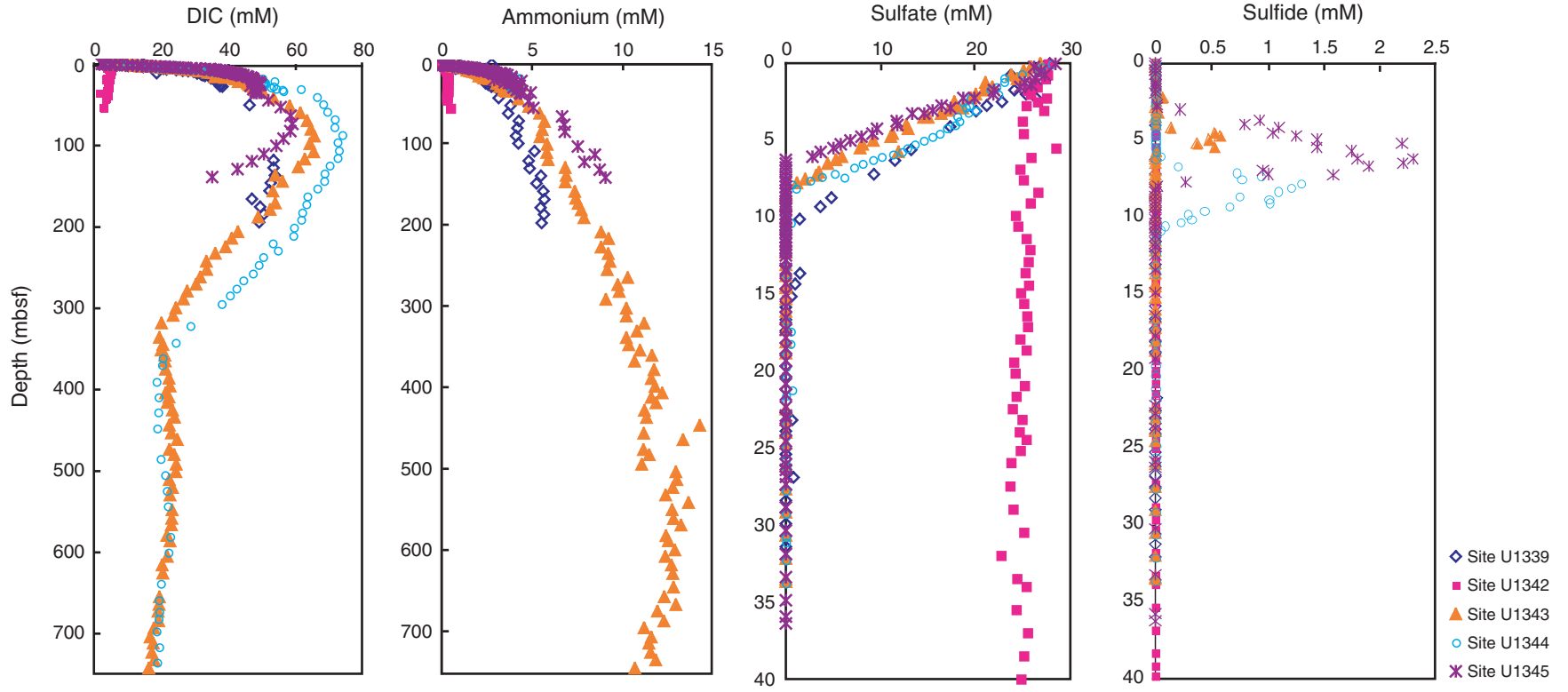


Table T1. Summary of drilled results for IODP Expedition 323 in the Bering Sea. (See table note.)

IODP site number	Water depth (mbsl)	Depth DSF (m)	Age (Ma)	Average sedimentation rate (cm/k.y.)
Umnak Plateau				
U1339	1867.5	200	0–0.8	28
Bowers Ridge				
U1340	1294.6	600	0–5	14.5
U1341	2139.5	600	0–5	14.5
U1342	818.6	45	0–1.2*	4.5
Bering slope				
U1343	1952.9	745	0–2.1	35
U1344	3173.1	745	0–1.9	45
U1345	1007.8	150	0–0.5	29

Note: * = basement rock of older age as well as a thin Miocene sandy layer just above the basement were also recovered at this site.

Table T2. Coring summary.

Hole	Latitude	Longitude	Water depth (mbsl)	Cores (N)	Cored (m)	Recovered (m)	Recovered (%)	Time on hole (h)	Time on site (days)
U1339A	54°40.2001'N	169°58.9017'W	1866.7	4	33.4	34.87	104	22.50	
U1339B	54°40.2103'N	169°58.9106'W	1867.6	22	196.0	204.45	104	29.67	
U1339C	54°40.2063'N	169°58.8852'W	1867.6	21	194.8	199.40	102	19.83	
U1339D	54°40.1891'N	169°58.8909'W	1868.1	22	200.0	206.00	103	39.58	
Site U1339 totals:				67	624.2	644.75	103	111.58	4.65
U1340A	53°24.0008'N	179°31.2973'W	1294.7	71	604.5	535.91	89	69.80	
U1340B	53°24.0002'N	179°30.9815'W	1297.1	6	53.9	55.53	103	6.95	
U1340C	53°23.8113'N	179°31.2975'W	1293.3	3	28.5	30.00	105	4.58	
U1340D	53°23.8004'N	179°31.2974'W	1293.3	3	26.3	27.23	104	6.98	
Site U1340 totals:				73	713.2	648.67	91	87.86	3.66
U1341A	54°2.0025'N	179°0.4999'E	2139.6	41	359.2	373.23	104	47.93	
U1341B	54°1.9984'N	179°0.5171'E	2139.6	71	600.0	594.98	99	90.08	
U1341C	54°2.0010'N	179°0.5390'E	2139.6	27	230.0	242.06	105	32.58	
Site U1341 totals:				139	1189.2	1210.27	102	170.59	7.11
U1342A	54°49.6987'N	176°55.0027'E	818.3	9	53.3	57.39	108	13.83	
U1342B	54°49.7004'N	176°55.0232'E	818.9	5	43.3	44.83	104	3.50	
U1342C	54°49.7017'N	176°55.0232'E	818.8	6	45.4	47.06	104	6.17	
U1342D	54°49.6987'N	176°55.0027'E	818.2	19	127.7	86.37	68	33.25	
Site U1342 totals:				39	269.7	235.70	95	56.75	2.36
U1343A	57°33.3993'N	175°48.9659'W	1950.9	22	201.5	203.86	101	24.87	
U1343B	57°33.4156'N	175°48.9951'W	1950.9	4	35.5	34.56	97	4.25	
U1343C	57°33.3982'N	175°49.0275'W	1952.6	26	234.2	231.04	99	22.92	
U1343D	57°33.3817'N	175°48.9971'W	1954.1	1	8.5	8.50	100	1.42	
U1343E	57°33.3814'N	175°48.9974'W	1956.0	82	744.3	700.27	95	106.82	
Site U1343 totals:				135	1224.0	1178.00	96.5	160.28	6.68
U1344A	59°3.0005'N	179°12.2011'W	3171.8	79	745.0	684.10	87	129.70	
U1344B	59°3.0112'N	179°12.2051'W	3173.0	1	4.44	4.80	92	2.00	
U1344C	59°3.0116'N	179°12.2052'W	3172.7	4	35.6	33.51	94	5.30	
U1344D	59°3.0224'N	179°12.2030'W	3174.1	32	286.5	286.10	100	35.50	
U1344E	59°3.0339'N	179°12.2029'W	3174.0	23	202.8	202.68	100	31.30	
Site U1344 totals:				139	1274.7	1174.80	92	203.80	8.49
U1345A	60°9.1917'N	179°28.2036'W	1007.4	16	146.9	148.24	101	16.82	
U1345B	60°9.2003'N	179°28.2127'W	1007.5	4	36.7	38.79	106	3.90	
U1345C	60°9.2097'N	179°28.2229'W	1008.8	16	148.5	152.85	103	9.00	
U1345D	60°9.2175'N	179°28.2283'W	1008.3	16	150.0	154.62	103	9.00	
U1345E	60°9.2264'N	179°28.2407'W	1007.1	16	150.0	154.15	103	14.10	
Site U1345 totals:				68	632.1	648.65	103	52.82	2.21
Expedition 323 totals:				660	5927.1	5740.84	97	843.68	35.15

Table T3. Sedimentation rates and their control points, Hole U1340A. (See table note.)

Age (Ma)	Depth (mbsf)	Control point	Sedimentation rate (cm/k.y.)
0.3	37.6	Depth of LO <i>Proboscia curvirostris</i>	13
0.781	117.9	Brunhes bottom	17
0.998	146.4	Jaramillo top	13
1.072	155.9	Jaramillo bottom	13
1.778	260.7	Olduvai top	15
1.945	300.7	Olduvai bottom	24
2.128	343.2	Reunion top	23
2.581	486.2	Gauss top	32
3.8	531.0	FO <i>Neodenticula koizumii</i>	4

Note: LO = last occurrence, FO = first occurrence.

Table T4. Sedimentation rates and their control points, Hole U1341B. (See table note.)

Age (Ma)	Depth (mbsf)	Control point	Sedimentation rate (cm/k.y.)
0.3	32.9	Depth of LO <i>Proboscia curvirostris</i>	11
0.781	82.5	Brunhes bottom	10
0.998	104.0	Jaramillo top	10
1.072	137.8	Jaramillo bottom	46
1.778	245.5	Depth of RI <i>Neodenticula seminae</i>	15
2.581	367.8	Gauss top	15
3.8	458.8	Depth of FO <i>Neodenticula koizumii</i>	8

Note: LO = last occurrence, RI = rapid increase, FO = first occurrence.

Table T5. Sedimentation rates and their control points, Site U1342. (See table note.)

Age (Ma)	Depth		Control point	Sedimentation rate (cm/k.y.)
	mbsf	CCSF-A (m)		
0.05	2.5	2.5	Average depth of LO <i>Lychnocanoma nipponica sakaii</i>	5
0.3	10.0	10.0	Average depth of LO <i>Spongodiscus</i> sp.	3
0.781	24.9	26.2	Brunhes bottom	3
0.885	27.1	28.5	Kamikatsura Excursion	2
1.072	34.0	35.6	Jaramillo bottom	4
1.125	36.1	38.3	Punaruu Excursion	5
1.173	40.1	42.5	Cobb Mountain top	9

Note: LO = last occurrence.

Table T6. Sedimentation rates and their control points, Site U1339. (See table note.)

Age (ka)	Depth CCSF-A (m)	Control point	Sedimentation rate (cm/k.y.)
52 ± 5	16.6	Average depth of LO <i>Lychnocanoma nipponica sakaii</i>	32
90 ± 10	35.5	Average depth of LO <i>Amphimelissa setosa</i>	50
300 ± 20	83.9	Average depth of LO <i>Spongodiscus</i> sp.	23
460 ± 50	118.5	Hole U1339C depth of LO <i>Stylatractus univertus</i>	22
740 ± 3	215.6	Hole U1339D depth of FO <i>Distephanus octangulatus</i> and LO <i>Dictyochoa subarctios</i>	35

Note: LO = last occurrence, FO = first occurrence.

Table T7. Sedimentation rates and their control points, Site U1343. (See table note.)

Age (Ma)	Depth		Control point	Sedimentation rate (cm/k.y.)
	mbsf	CCSF-A (m)		
0.3	79.8	87.3	Average depth of LO <i>Spongodiscus</i> sp.	29
0.781	183.6	208.0	Average depth of Brunhes bottom	25
0.998	232.0	267.6	Jaramillo top	27
1.072	266.3	302.0	Jaramillo bottom	46
1.173	291.5	327.1	Cobb Mountain top	25
1.55	372.1	407.7	LO <i>Filisphaera filifera</i>	21
1.8	517.3	552.9	LO <i>Stephanopyxis horridus</i>	58
2.1	680.8	716.4	LCO <i>Neodenticula koizumii</i>	54

Note: LO = last occurrence, LCO = last common occurrence.

Table T8. Sedimentation rates and their control points, Site U1344. (See table note.)

Age (Ma)	Depth		Control point	Sedimentation rate (cm/k.y.)
	mbsf	CCSF-A (m)		
0.3	106.6	122.8	Average depth of LO <i>Spongodiscus</i> sp.	41
0.781	284.1	332.2	Hole U1344D depth of Brunhes bottom	44
0.998	348.4	394.8	Jaramillo top	29
1.072	373.0	419.4	Jaramillo bottom	33
1.173	412.6	459.0	Cobb Mountain top	39
1.185	423.2	469.6	Cobb Mountain bottom	89
1.778	669.9	716.3	Olduvai top	42
1.9	731.43	777.9	LO <i>Ammodochium rectangulare</i>	50

Note: LO = last occurrence.

Table T9. Sedimentation rates and their control points, Site U1345. (See table note.)

Age (Ma)	Depth		Control point	Sedimentation rate (cm/k.y.)
	mbsf	CCSF-A (m)		
0.05	16.5	18.0	Average depth of LO <i>Lychnocanoma nipponica sakaii</i>	32
0.28–0.32	80.1	88.0	Average depth of LO <i>Spongodiscus</i> sp.	28

Note: LO = last occurrence.